Universität Rostock Traditio et Innovatio

# The role of bioturbation in microplastic burial in marine sediments

**Dissertation**

zur

Erlangung des akademischen Grades

doctor rerum naturalium (Dr. rer. nat.)

am Institut für Biowissenschaften

der Mathematisch-Naturwissenschaftlichen Fakultät

der Universität Rostock

**vorgelegt von**

Christopher Gebhardt

aus Rostock

Rostock, 2019

https://doi.org/10.18453/rosdok_id00002534

**Gutachter:**
PD Dr. Stefan Forster
Institut für Biowissenschaften – Meeresbiologie
Universität Rostock

Associate Professor Dr. Gary Banta
Department of Science and Environment
Universität Roskilde

**Jahr der Einreichung:** 2019
**Jahr der Verteidigung:** 2019

‘Le moindre mouvement est important pour la nature entière.
L'océan entier est affecté par un caillou.’

The least movement is of importance to all nature.
The entire ocean is affected by a pebble.

Blaise Pascal

# TABLE OF CONTENTS

LIST OF FIGURES ..... IV

LIST OF TABLES ..... VII

LIST OF ABBREVIATIONS ..... IX

LIST OF FORMULA SYMBOLS ..... XI

EXPLANATION ..... XII

SUMMARY ..... XIII

ZUSAMMENFASSUNG ..... XIV

1. INTRODUCTION ..... 1

2. MATERIALS AND METHODS ..... 10

2.1. Particle and microplastic transport induced by *H. diversicolor* ..... 10

2.1.1. Sampling ..... 10

2.1.2. Mesocosm preparation ..... 11

2.1.3. Particle transport under different feeding regimes ..... 11

2.1.4. Microplastic ingestion of *H. diversicolor* ..... 12

2.2. Sediment ingestion of *A. marina* ..... 13

2.2.1. Sampling ..... 13

2.2.2. Mesocosm preparation ..... 13

2.3. Particle and microplastic transport induced by *A. marina* ..... 14

2.3.1. Sampling ..... 14

2.3.2. Mesocosm preparation ..... 14

2.3.3. Microplastic transport ..... 15

2.4. Quantification of sediment properties ..... 16

2.5. Quantification of polychaete sediment reworking ..... 16

2.5.1. Particle tracers ..... 16

2.5.2. Calibration of particle quantification ..... 17

2.5.3. Sediment ingestion of *A. marina* ..... 18
2.5.4. Sediment and microplastic transport induced by *H. diversicolor* and *A. marina* ..... 18
2.5.4.1. Tracer addition ..... 18
2.5.4.2. Mesocosm sectioning ..... 19
2.5.4.3. Quantification of particles < 500 µm (luminophores, PE) ..... 20
2.5.4.4. Quantification of particles ≥ 500 µm (PS, PA) ..... 20
2.5.4.5. Modeling (gallery-diffusion model) ..... 21
2.6. Statistical analysis ..... 24
2.6.1. Sediment and microplastic transport induced by *H. diversicolor* ..... 24
2.6.2. Sediment ingestion of *A. marina* ..... 24
2.6.3. Sediment and microplastic transport induced by *A. marina* ..... 24
3. RESULTS ..... 26
3.1. Calibration of particle quantification ..... 26
3.2. Sediment and microplastic transport induced by *H. diversicolor* ..... 26
3.2.1. Sediment properties ..... 26
3.2.2. Visual observation ..... 27
3.2.3. Mortality and biomass change ..... 27
3.2.4. Ingestion of MP particles ..... 28
3.2.5. Particle transport ..... 29
3.2.6. Modeled particle transport ..... 34
3.3. Sediment ingestion of *A. marina* ..... 36
3.3.1. Sediment properties ..... 36
3.3.2. Visual observation ..... 36
3.3.3. Mortality and biomass change ..... 37
3.3.4. Sediment defaecation of *A. marina* ..... 37
3.4. Sediment and microplastic transport induced by *A. marina* ..... 40
3.4.1. Sediment properties ..... 40
3.4.2. Visual observation ..... 41
3.4.3. Mortality and biomass change ..... 41
3.4.4. Particle transport ..... 42
3.4.5. Grain size distribution ..... 48

4. DISCUSSION ..... 50

4.1. Particle and microplastic transport induced by *H. diversicolor* ..... 50

4.1.1. Microplastic ingestion ..... 50

4.1.2. Modeling ..... 52

4.1.3. Bioturbation of microplastics ..... 54

4.1.4. Feeding effect ..... 56

4.1.5. Particle selective transport ..... 57

4.2. Particle and microplastic transport induced by *A. marina* ..... 59

4.2.1. Sediment feeding activity ($AM_{SI}$ experiment) ..... 59

4.2.2. Sediment feeding activity (AM experiment) ..... 62

4.2.3. Bioturbation of microplastic particles ..... 63

4.3. Potential toxicity of microplastic particles ..... 67

5. SYNTHESIS: implications for the field ..... 70

REFERENCES ..... 75

APPENDIX ..... 87

# LIST OF FIGURES

Figure 1. The concept of bioturbation with focus on particle mixing and bioturbation types..... 5

Figure 2: Schematic illustration of hypothesized MP transport processes induced by *H. diversicolor*. . 8

Figure 3: Schematic illustration of known and hypothesized MP transport processes induced by *A. marina*..... 9

Figure 4: Sampling sites of sediments and specimens of *H. diversicolor* used in the experiments. ..... 10

Figure 5: Mesocosm setup of the HD experiment. ..... 11

Figure 6: Timeline of the HD experiment. ..... 12

Figure 7: Mesocosm setup of the $AM_{SI}$ experiment. ..... 13

Figure 8: Mesocosm setup of the AM experiment. ..... 15

Figure 9: Timeline of the AM experiment. ..... 16

Figure 10: Particle tracers used in the HD and AM experiment. ..... 17

Figure 11: Sectioning schematics for HD mesocosms and AM mesocosms..... 20

Figure 12: Steps of image processing carried out prior to particle quantification..... 21

Figure 13: Schematic of the transport processes considered in the gallery-diffusion model. ..... 22

Figure 14: Grain size distribution of sediment used in the HD experiment. ..... 27

Figure 15: Aggregate containing sediment particles, spinach fragments, luminophores and PE particles, agglutinated by mucus secreted by *H. diversicolor*. ..... 29

Figure 16: Luminophore and microplastic (PA, PE) profiles for controls of the HD experiment. ..... 30

Figure 17: Luminophore and microplastic (PA, PE) profiles for $F^-$ (no feeding) mesocosms of the HD experiment. ..... 31

Figure 18: Luminophore and microplastic (PA, PE) profiles for $F^+$ (feeding) mesocosms of the HD experiment. ..... 32

Figure 19: Two-dimensional MDS plot of controls and HD mesocosms for luminophore and microplastic (PA, PE) concentrations below 1 cm, 4 cm and 10 cm sediment depth. ..... 33

Figure 20: Biodiffusion (local) transport coefficients (*Db*) of all particle tracers used in the HD experiment, modeled with the gallery-diffuser model. ..... 35

Figure 21: Biotransport (non-local) coefficients (*r*) of all particle tracers used in the HD experiment, modeled with the gallery-diffuser model. ..... 35

Figure 22: Grain size distribution of sediment used in both mesocosms of the $AM_{SI}$ experiment. ..... 36

Figure 23: Mean individual rates of daily sediment defaecation, shown for all polychaetes in the $AM_{SI}$ experiment. ..... 38

Figure 24: Number of days with apparent sediment defaecation ("active days"), shown for all polychaetes in the $AM_{SI}$ experiment. ..... 38

Figure 25: Individual sediment defaecation rates and sites for both mesocosms and measurement periods of the $AM_{SI}$ experiment. ..... 39

Figure 26: Correlation of mean individual sediment defaecation rates and net biomass change (FM). 40

Figure 27: Grain size distribution of the sediment used in the AM experiment. ..... 41

Figure 28: Luminophore and microplastic particle profiles for AM control mesocosms. ..... 44

Figure 29: Luminophore and microplastic particle profiles for mesocosms AM1 - 4. ..... 45

Figure 30: Luminophore and microplastic particle profiles for mesocosms AM5 - 8. ..... 46

Figure 31: Two-dimensional MDS plot of controls and AM mesocosms for luminophore and microplastic (PS, PA) concentrations below 2 cm and 8 cm sediment depth. ..... 48

Figure 32: Median grain size for all AM mesocosms after experiment termination, grouped as controls, STI (short time interval: runtime ≤134 d) and LTI (long time interval: runtime 239/240 d)..... 49

Figure 33: Mean error, representing fit of the gallery-diffuser model to obtained particle distributions in the HD experiment. ..... 52

Figure 34: Local transport coefficients (*Db*) of the HD experiment, shown for PE particles and modeled for different biodiffusive mixing depths (1 cm, 2 cm, 4 cm). ..... 53

Figure 35: Non-local transport coefficients (*r*) of the HD experiment, shown for PE particles and modeled for different biodiffusive mixing depths (1 cm, 2 cm, 4 cm). ..... 54

Figure 36: Correlation of mortality determined for individual mesocosms and modeled bioturbation coefficients. ..... 56

Figure 37: Correlation of tail shaft relocation frequency and mean defaecation rate and biomass change. ..... 61

Figure A1: Linear regression of particle mass and particle number, shown for PS particles used in the AM experiment. ..... 89

Figure A2: Linear regression of particle mass and particle number, shown for PA particles used in the AM and HD experiment. ..... 90

Figure A3: Linear regression of particle mass and particle number, shown for luminophores used in the AM, HD and $HD_I$ experiment. ..... 90

# LIST OF TABLES

Table 1: Characteristics of all particle tracers used. ..... 18

Table 2: Tracer quantities added to each mesocosm of the HD and AM experiment. ..... 19

Table 3: Linear regression and confidence interval coefficients for mass–number relationships of all particle tracer types. ..... 26

Table 4: Total biomasses (g FM) added and recovered from each HD mesocosm. ..... 28

Table 5: Maximum penetration depth (MPD) of all particle types used in the HD experiment. ..... 34

Table 6: Individual biomass (FM) of all polychaetes added to the $AM_{SI}$ experiment. ..... 37

Table 7: Individual and total biomasses added and recovered from each AM mesocosm. ..... 42

Table 8: Maximum penetration depths (MPD) of all particle types used in the AM experiment. ..... 47

Table 9: Mean individual sediment reworking shown as individual sediment ingestion rate derived from particle concentration profiles. ..... 63

Table A1: Camera settings used for sample imaging. ..... 89

Table A2: Individual biomass (FM) of all polychaetes added to the HD experiment. ..... 91

Table A3: Recovery rates (% of total amount of added tracers) for all particles types and mesocosms of the HD experiment. ..... 91

Table A4: Depth-dependent particle tracer concentrations determined for the first control mesocosm (C1) of the HD experiment. ..... 92

Table A5: Depth-dependent particle tracer concentrations determined for the second control mesocosm (C2) of the HD experiment. ..... 92

Table A6: Depth-dependent particle tracer concentrations determined for the third control mesocosm (C3) of the HD experiment. ..... 93

Table A7: Depth-dependent particle tracer concentrations determined for the HD1 mesocosm. ..... 93

Table A8: Depth-dependent particle tracer concentrations determined for the HD2 mesocosm. ..... 94

Table A9: Depth-dependent particle tracer concentrations determined for the HD3 mesocosm. ..... 94

Table A10: Depth-dependent particle tracer concentrations determined for the HD4 mesocosm. ..... 95

Table A11: Depth-dependent particle tracer concentrations determined for the HD5 mesocosm. ..... 95

Table A12: Depth-dependent particle tracer concentrations determined for the HD6 mesocosm. ..... 96

Table A13: PERMANOVA results comparing particle tracer depth distribution using the factors particle type (luminophores, PE, PA), treatment (controls, $F^-$, $F^+$) and sediment depth. ..... 96

Table A14: Recovery rates (% of total amount of added tracers) for all particles types and mesocosms of the AM experiment. ..... 97

Table A15: Depth-dependent particle tracer concentrations determined for the first control mesocosm (C1) of the AM experiment. ..... 97

Table A16: Depth-dependent particle tracer concentrations determined for the second control mesocosm (C2) of the AM experiment. ..... 98

Table A17: Depth-dependent particle tracer concentrations determined for the third control mesocosm (C3) of the AM experiment. ..... 98

Table A18: Depth-dependent particle tracer concentrations determined for the AM1 mesocosm. ..... 99

Table A19: Depth-dependent particle tracer concentrations determined for the AM2 mesocosm. ..... 99

Table A20: Depth-dependent particle tracer concentrations determined for the AM3 mesocosm. .... 100

Table A21: Depth-dependent particle tracer concentrations determined for the AM4 mesocosm. .... 100

Table A22: Depth-dependent particle tracer concentrations determined for the AM5 mesocosm. .... 101

Table A23: Depth-dependent particle tracer concentrations determined for the AM6 mesocosm. .... 101

Table A24: Depth-dependent particle tracer concentrations determined for the AM7 mesocosm. .... 102

Table A25: Depth-dependent particle tracer concentrations determined for the AM8 mesocosm. .... 102

# LIST OF ABBREVIATIONS

| | |
|---|---|
| AFDM | ash-free dry mass |
| AM | *Arenicola marina* |
| $AM_{SI}$ | sediment ingestion - *Arenicola marina* experiment |
| ANOVA | analysis of variance |
| BPA | bisphenol A |
| C | carbon |
| $d_0$ | day 0 (start) of the experiment |
| DM | dry mass |
| $F^-$ | no food addition - *Hediste diversicolor* experiment |
| $F^+$ | food addition - *Hediste diversicolor* experiment |
| FM | fresh mass |
| HB | high bioturbation - *Arenicola marina* experiment |
| HD | *Hediste diversicolor* |
| $HD_I$ | ingestion treatment - *Hediste diversicolor* experiment |
| ind. | individual |
| LB | low bioturbation - *Arenicola marina* experiment |
| LFL | lower feeding layer - *Arenicola marina* experiment |
| LOI | loss on ignition |
| LTI | long term interval - *Arenicola marina* experiment |
| MDS | multidimensional scaling |
| MP | microplastic |
| MPD | maximum penetration depth |
| N | nitrogen |
| NaCl | sodium chloride |
| NP | nonylphenol |
| OM | organic matter |
| p | significance level |
| PA | polyamide |
| PAH | polycyclic aromatic hydrocarbons |
| PBDE | polybrominated diphenyl ether |
| PCB | polychlorinated biphenyls |
| PE | polyethylene |
| POC | particulate organic carbon |
| POP | persistent organic pollutant |

| | |
|---|---|
| PS | polystyrene |
| SD | standard deviation |
| sed. | sediment |
| STI | short term interval - *Arenicola marina* experiment |
| TOC | total organic carbon |
| UFL | upper feeding layer - *Arenicola marina* experiment |
| UV | ultraviolet |

# LIST OF FORMULA SYMBOLS

| | | |
|---|---|---|
| $C$ | | particle concentration |
| $\delta$ | | delta |
| $D$ | ($m^2\ s^{-1}$) | diffusion coefficient |
| $Db$ | ($cm^2\ yr^{-1}$) | local bioturbation coefficient |
| $\eta$ | ($N\ s\ m^{-2}$) | dynamical viscosity |
| $k_B$ | ($J\ K^{-1}$) | Boltzmann constant |
| $\mu$ | ($s\ kg^{-1}$) | particle mobility |
| $r$ | ($yr^{-1}$) | non-local bioturbation coefficient |
| $t$ | | time |
| $T$ | (K) | absolute temperature |
| $W$ | ($kg\ m^2\ s^{-3}$) | Watt |
| $x$ | | sediment depth |
| $x_1$ | | lower limit of tracer redistribution |
| $x_2$ | | upper limit of tracer redistribution |
| $x_3$ | | lower limit of tracer redistribution |

# EXPLANATION

Considerable parts of the present thesis are already published in the scientific journal cited below. In this publication I am the first and responsible author, having done most of the data compilation, all of the data evaluation and most of the writing of the publication draft.

Concept and experimental design of all experiments described in this thesis was developed in cooperation with Stefan Forster. Help in mesocosm sampling and determination of particle tracer concentrations was obtained from by Melina Dressler-Allame and Lenke Tödter (AM experiment) and Michael Beckers (HD experiment, $HD_I$ experiment), respectively. Polychaete biomass determination in the HD experiment was done by Michael Beckers. Obtained data of the HD experiment were used by Michael Beckers in the context of the Master's thesis "Bioturbation von Plastikpartikeln durch *Hediste diversicolor* (O.F. Müller, 1776)", (2017). Compilation and evaluation of remaining data, statistical analysis and bioturbation coefficient modeling of all experiments shown in this thesis were my own work. This PhD thesis has been written and arranged without further external assistance.

Contents referring to particle burial induced by the feeding activity of *Arenicola marina* (AM experiment) are published in the journal Environmental Pollution:

Gebhardt, C. and Forster, S. (2018): Size-selective feeding of *Arenicola marina* promotes long-term burial of microplastic particles in marine sediments. Environmental Pollution 242, 1777-1786.

Sections taken from the original publication are denoted with "…" within the text and a proceeding footnote.

# SUMMARY

Though marine sediments are acknowledged to represent a sink for microplastic particles, investigations on the further fate of once deposited particles have received relatively little interest so far. In interaction with sediment-dwelling organisms, these particles might be subjected to further transport, leading to a burial of microplastics in the wake of bioturbation. The exact potential for microplastic burial might differ with species, based on ecological traits and bioturbation type, rendering certain taxa possible key species for effective microplastic burial. To investigate the influence of different bioturbation types on benthic microplastic transport, two mesocosm laboratory experiments were conducted using differently sized particle tracers (luminophores, polystyrene (PS), polyamide (PA) and polyethylene (PE) particles). Two benthic polychaetes – the gallery-diffusor *Hediste diversicolor* and the conveyor belt-feeder *Arenicola marina* – were chosen for investigation. Particle reworking activity of *H. diversicolor* was stimulated by food addition to assess potential effects of food availability on particle transport.

At abundances of 200 individuals $m^{-2}$, particle burial mediated by *H. diversicolor* was observed to extend down to sediment depths of 14 cm, with biodiffusive transport rates (*Db*) of 1.09 $cm^2$ $yr^{-1}$ (luminophores). Microplastic showed slightly lower local transport, exhibiting *Db*s of 0.81 $cm^2$ $yr^{-1}$ (PA) and 0.57 $cm^2$ $yr^{-1}$ (PE). Non-local transport (*r*) was low for all particle types, with slightly increased values for PA (0.95 $yr^{-1}$) and PE (1.27 $yr^{-1}$) compared to luminophores (0.69 $yr^{-1}$). Differences in particle transport between luminophores and microplastic were small and not statistically significant, which is ascribed to high variability in sediment reworking. A slight increase of local transport due to food addition was observed, which was not significant, either.

Bioturbation of the conveyor belt-feeder *A. marina* resulted in considerable particle burial in all mesocosms to maximum burial depths of 20 cm. Vertical transport rates were similar for all particle types, reaching up to ~ 1 mm $d^{-1}$. Sediment feeding activity was found to be variable, with minimum values of 1.03 ml $day^{-1}$ $ind.^{-1}$ and maximum values of 16.21 ml $day^{-1}$ $ind.^{-1}$. While low sediment feeding activities generated particle distributions resembling diffusion-analogous transport, particle accumulations in sediment depths between 8 and 14 cm were found for high sediment ingestion rates. Particles were retained within these depths, indicating particle discrimination due to size-selective feeding. In accordance with these results, a general increase in medium grain size in all feeding layers was observed after experiment termination.

These findings demonstrate the differential potential for microplastic burial by species representing different bioturbation types, resulting in varying burial depths and velocities. Maximal microplastic burial depths observed in both experiments emphasize the role of marine sediments as sinks for these particles, rendering them less accessible for other marine organisms, but eventually promoting their long-term conservation within these systems.

# ZUSAMMENFASSUNG

Auch wenn marine Sedimente als Senke für Mikroplastikpartikel gelten, ist das weitere Verhalten einmal abgelagerter Partikel weitgehend unbekannt. Die Interaktion mit sedimentbewohnenden Organismen kann einen weiteren Transport bewirken und möglicherweise zu einer Vergrabung als Folge von Bioturbationsprozessen führen. Basierend auf ökologischen Eigenschaften und jeweiligem Bioturbationstyp kann das Potential zur Vergrabung von Mikroplastik dabei zwischen einzelnen Arten variieren und einzelne Taxa als Schlüsselarten für eine effektive Vergrabung auszeichnen. Um den Einfluss verschiedener Bioturbationstypen auf den benthischen Mikroplastiktransport zu untersuchen, wurden zwei Mesokosmos-Experimente unter Verwendung von Partikeltracern verschiedener Größe (Luminophoren, Polystyrol (PS), Polyamid (PA) und Polyethylen (PE) durchgeführt. Zwei benthische Polychaeten – der „gallery-diffusor" *Hediste diversicolor* und der „conveyor belt-feeder" *Arenicola marina* – wurden für die experimentelle Arbeit ausgewählt. Die Partikelvermischungsaktivität von *H. diversicolor* wurde durch Nahrungszugabe stimuliert, um einen möglichen Einfluss der Nahrungsverfügbarkeit auf den Partikeltransport zu untersuchen.

Für Besiedlungsdichten von 200 Individuen $m^{-2}$ reichte der von *H. diversicolor* vermittelte Partikeltransport bis in Sedimenttiefen von 14 cm, die für Luminophoren ermittelten Biodiffusionskoeffizienten (*Db*) betrugen dabei 1.09 $cm^2$ $Jahr^{-1}$. Das verwendete Mikroplastik zeigte einen leicht erhöhten diffusionsanalogen Transport mit *Db*-Werten von 0.81 $cm^2$ $Jahr^{-1}$ (PA) und 0.57 $cm^2$ $Jahr^{-1}$ (PE). Für alle Partikeltypen wurde lediglich geringer advektiver Partikeltransport (*r*) festgestellt, wobei Mikroplastik in Kontrast zu Luminophoren (0.69 $Jahr^{-1}$) stärkeren Transport zeigte (PA: 0.95 $Jahr^{-1}$; PE: 1.27 $Jahr^{-1}$). Die unterschiedlichen Transportraten für Luminophoren und Mikroplastik waren gering und nicht statistisch signifikant, was auf die hohe Variabilität der beobachteten Bioturbationsraten zurückgeführt werden kann. Der diffusionsanaloge Partikeltransport konnte durch Nahrungszugabe leicht erhöht werden, auch hier waren die ermittelten Unterschiede nicht statistisch signifikant.

Die Bioturbationsaktivität von *A. marina* führte zu einer deutlichen Partikelvergrabung in allen Mesokosmen in Tiefen von bis zu 20 cm. Der Abwärtstransport verlief für alle Partikeltypen vergleichbar schnell und erreichte Geschwindigkeiten von bis zu 1 mm $Tag^{-1}$. Die Sedimentaufnahme zeigte große Variation und betrug minimal 1.03 ml $Tag^{-1}$ $Ind.^{-1}$, maximal 16.21 ml $Tag^{-1}$ $Ind.^{-1}$. Während geringe Fraßaktivität diffusionsanaloge Partikelverteilungen im Sediment erzeugte, wurden für erhöhte Aktivität Partikelakkumulationen in Sedimenttiefen zwischen 8 und 14 cm festgestellt. Die Partikel wurden in diesen Horizonten zurückgehalten, was einen partikelgrößenabhängigen Fraß von Sediment nahelegt. In Einklang mit dieser Beobachtung wurde eine generelle Erhöhung der mittleren Korngröße in allen Fraßschichten nach Experimentende festgestellt. Ausschlaggebender Prozess für die Vergrabung von Partikeln war die Bedeckung mit als Kot abgesetztem Sediment an der Sedimentoberfläche; der Partikeltransport über den Sandstrang spielte nur eine untergeordnete Rolle.

Diese Ergebnisse zeigen, dass sich der durch Makrofauna vermittelte Transport von Mikroplastik in Abhängigkeit vom jeweiligen Bioturbationstyp mit Hinsicht auf Vergrabungstiefe und Vergrabungsgeschwindigkeit deutlich unterscheiden kann. Die in beiden Experimenten beobachteten maximalen Eindringtiefen unterstreichen die Rolle mariner Sedimente als Senken für Mikroplastik, was mit einer verringerten Verfügbarkeit dieser Partikel für andere marine Organismen, jedoch einer gleichzeitigen langfristigen Konservierung in diesen Ökosystemen einhergehen kann.

# 1. INTRODUCTION

Plastic has an impact on our modern life as profound as hardly any other man-made product. Featuring a multitude of desirable properties, the usages of plastic products in everyday life are manifold. Plastic is extraordinary durable, bio-inert, exhibits low specific weights and is, above all, cheap to produce (Andrady, 2011; Andrady and Neal, 2009). This set of features often leads to the preferred use of plastic in numerous aspects of everyday life, both in personal and commercial applications. For instance, plastic is used for the production of construction materials, household goods, clothing and especially packaging. Due to the ever-expanding demand for plastics, worldwide production has grown from 1.7 million tons annually in the 1950s to 348 million t annually today with a net increase in plastic production of 43 % in the last decade alone (PlasticsEurope, 2018). Based on its longevity and low-cost production, the net global plastic production is growing alongside the amounts of plastic waste generated annually. While the share of plastic in municipal waste by mass rose by one order of magnitude within the last five decades in many countries of the western hemisphere, at present, plastic contributes 73% to all waste produced globally (Hoornweg, D., Bhada-Tata, P., 2012). Besides recycling and combustion (Geyer et al., 2017), deposition to landfills is still a major pathway for post-consumer plastic disposal. In 2012, 38% of all plastic waste generated in Europe was deposited in landfills (PlasticsEurope, 2018).

As a consequence of still growing plastic production rates and partially inadequate recycling strategies, the contamination of many natural habitats with solid plastic waste has been recognized as an emerging environmental hazard for decades. Due to its ubiquitous distribution around the globe, its suspicious appearance and prolonged degradation rates, plastic has been suggested as a potential biostratigraphic marker to indicate the onset of the so-called Anthropocene (Corcoran et al., 2014; Zalasiewicz et al., 2016). The impacts of plastic pollution are particularly recognizable in the marine realm, which is, based on strong terrestrial inputs, one of the great global distribution and accumulation sites for plastic. Once transported to seas and oceans, plastic is often subjected to wind or current-induced transport (Kukulka et al., 2012; Maximenko et al., 2012) and tends to accumulate at beaches or within the great oceanic gyres (Browne et al., 2011; Law et al., 2010). Marine litter in the size range of centimeters to decimeters (known as macrolitter) is known to pose many potential hazards to marine biota, including entanglement (Laist, 1997) or gut blockage (Plotkin and Amos, 1988) and is even discussed to represent a potential vector for the spreading of invasive species (Gregory, 2009; Miralles et al., 2018). Whereas many potential threats of macro- and mesolitter to marine life are known since the 1980s (Laist, 1987), the occurrence and impacts of much smaller plastic particles, so-called microplastics, have become subject to substantial research in the last decade only, even though this particle type has been identified in marine waters already in the 1970s (Carpenter et al., 1972). Microplastics (hereafter referred to as MPs), mostly defined as particles ≤ 5 mm in diameter (Arthur et al., 2009) and classified into two categories, originate from a multitude

of sources. Primary MPs were manufactured in the actual size in which they are found in the environment. This is common for MPs used for industrial or domestic applications, e.g. virgin plastic pellets for further plastic production and modification (Pruter, 1987), abrasives for usages in industry or personal hygiene products (Duis and Coors, 2016; Fendall and Sewell, 2009) or synthetic microfibers which are released from clothing (Browne et al., 2011). Secondary MPs originate from fragmentation of larger litter objects (Barnes et al., 2009), a process mainly mediated by photodegradation under UV radiation (Handy and Shaw, 2007; Suhrhoff and Scholz-Böttcher, 2016) and mechanical abrasion (Gewert et al., 2015). Owing to their small size and longevity, MPs bear great potential for long-distance transport and were found to be ubiquitous in marine systems such as beaches, coastal shelf sediments (Van Cauwenberghe et al., 2013), surface waters (Song et al., 2014) and even remote habitats like deep sea sediments (Fischer et al., 2015; Woodall et al., 2014) or the Arctic shelf ice (Obbard et al., 2014). Hot spots of extraordinary high MP concentrations are commonly identified adjacent to heavily anthropogenic influenced sites like harbors or metropolitan areas, reaching abundances up to several thousand MP items per liter seawater (Norén, 2008) or kilogram sediment (Matsuguma et al., 2017), respectively.

Besides long-distance transport, the small particle sizes of MPs can facilitate ingestion by numerous marine vertebrate and invertebrate taxa. To date, MPs have been identified in marine mammals such as baleen whales (Fossi et al., 2012) or seals (Bravo Rebolledo et al., 2013), pelagic and demersal fish (Lusher et al., 2013), plankton species (Cole et al., 2013) and benthic invertebrates like crustaceans (Devriese et al., 2015; Welden and Cowie, 2016) or bivalves (Mathalon and Hill, 2014; Van Cauwenberghe et al., 2015a). Numerous hazardous effects of MP ingestion by marine taxa have been hypothesized in the recent past, of which several were verified for marine invertebrates. This record ranges from animals representing transport vectors for MPs by adhesion to body appendages (Lehtiniemi et al., 2018; Watts et al., 2014) or trophic transfer via predatory feeding (Farrell and Nelson, 2013; Setälä et al., 2014) to effects directly affecting health and fitness of organisms in question. MPs are known to impair feeding activity in polychaetes and cladocerans (Besseling et al., 2013; Ogonowski et al., 2016), to hamper growth and fecundity in rotifers (Jeong et al., 2016) and to trigger inflammatory responses (Ribeiro et al., 2017) or oxidative stress (Jeong et al., 2016) upon uptake. Once ingested, translocation of MP particles into body tissues adjoining the digestive tract was shown for two bivalve species (Browne et al., 2008; Ribeiro et al., 2017), which might have considerable effect on residence times of ingested MPs in marine organisms. Besides physical effects of MP ingestion, MP particles are known to act as vectors for persistent organic pollutants (POPs) such as polychlorinated biphenyls (PCBs) or polycyclic aromatic hydrocarbons (PAHs) (Hirai et al., 2011; Mato et al., 2001) which might raise additional harmful effects on health and fitness of marine species. The steadily progressing fragmentation of MPs into smaller pieces down to size ranges referred to as nanoplastics (Gigault et al., 2016; Ter Halle et al., 2017) might further promote their distribution as well as their potential ingestion or translocation within marine taxa. Due

to their inherent or already verified impact on marine life, a precise understanding of MP behavior in the marine realm is crucial for a proper assessment of the ecological risks of these particles, including the identification of major transport pathways and net accumulation zones.

Particle density as well as wind or current-induced drifting play pivotal roles in MP transport (Kowalski et al., 2016; Kukulka et al., 2012; Ryan, 2015) and both are acknowledged to facilitate their long-distance transport and occurrence even in apparently pristine ecosystems (Baztan et al., 2014; Fischer et al., 2015). Whereas larger plastic items tend to accumulate in large oceanic gyres (Law et al., 2010; Lebreton et al., 2012) or at shorelines (Ballent et al., 2013; Ivar do Sul et al., 2009), the majority of plastic debris and especially MP is subjected to vertical export to deeper water layers or the seafloor over time. The occurrence of low-density polymers in marine sediments that technically are supposed to float suggests that plastic and MP sedimentation is not governed by specific density alone. Density-altering processes as biofouling of surfaces (Kooi et al., 2017; Ye and Andrady, 1991), integration into marine aggregates (Long et al., 2017, 2015) or zooplankton faecal pellets (Cole et al., 2016) are known to promote vertical export of MPs. The mean residence time of a MP particle in surface waters before its transition to sedimentation is estimated with the comparatively short mean time span of three years (Koelmans et al., 2017). Based on these experimental data, modeling results and high MP loads found in seafloor habitats around the globe (Bergmann et al., 2017), marine sediments are identified as a major sink for MP particles. Little is known about the fate of once deposited particles as the journey of a MP particle might not necessarily end at the sediment water interface. Bottom currents and tidal forces might redistribute deposited MPs (Ballent et al., 2013) and furthermore, constant sedimentation can lead to slow but steady burial of MPs into marine sediments (Castañeda et al., 2014; Matsuguma et al., 2017). The interaction of MPs with sediment-dwelling organisms has received very little attention up to now but might be another important factor with respect to the redistribution of MPs at the sea floor. Given the fact that ~ 70% of the Earth's surface are covered with oceans and that soft-bottom habitats represent the utmost majority of the ocean bottoms, the organisms residing within these sediments can be considered to represent the largest faunal assemblage on Earth, constituting high biodiversity and profoundly affecting ecosystem processes (Snelgrove, 1998).

Fauna-induced relocation of MP particles might lead to enhanced vertical transport of deposited MPs, namely in the context of bioturbation. Defined as "all transport processes carried out by animals that directly or indirectly affect sediment matrices" (Kristensen et al., 2012), bioturbation-induced transport impacts both solids (particle reworking) and solutes (ventilation) (Figure 1), having profound effects on sediment geochemistry, matter exchange across sediment water interfaces and thus, ecological functioning of marine sediments. Particle reworking includes horizontal and/or vertical translocation of sediment particles as a consequence of animal movements, burrowing, burrow maintenance and ingestion or deposition of particles. Those biomixing activities can modify physical sediment parameters such as surface topography by the formation of mounds or pits (Retraubun,

Dawson, and Evans 1996; Valdemarsen et al. 2011), and sediment granulometry and porosity as a consequence of size-selective particle uptake (Cadée, 1976; Self and Jumars, 1988). Burial of freshly deposited organic material to deeper sub- or anoxic zones can delay or completely inhibit organic matter degradation and associated nutrient remineralization (Blair et al., 1996; Gerino et al., 1998; Josefson et al., 2012). Conversely, the lifting of buried material back to the sediment-water interface can stimulate remineralization processes, sometimes up to one order of magnitude (Kristensen and Holmer, 2001). Burrow ventilation often leads to exchange processes with adjacent pore waters and a net release of associated solutes, such as ammonia, phosphate or hydrogen sulfide from the sediment (Kristensen et al., 2011; Papaspyrou et al., 2010). Ventilation of burrows allows oxygen to penetrate into otherwise anoxic sediment zones, stimulating organic matter degradation by microbial activity (Andersen and Kristensen, 1988; Banta et al., 1999). The effects of burrow construction, which can increase the sediment-water interface area by factors up to three (Davey, 1994) as well as the stimulation of microbial activity as a consequence of ventilation often lead to solute transport rates that exceed molecular diffusion by far, a phenomenon called bioirrigation in this context (Aller, 1980; Volkenborn et al., 2016). The extent of biomixing and bioirrigation is comprised by a set of numerous processes, often in complex interaction with each other. Hence, the precise magnitude of bioturbation activity is affected by species composition, biomass and abundance, burrow morphology (i.e. open- vs. blind-ended, maximum burrowing depth), feeding mode or patterns of ventilation (Welsh, 2003). Due to this spatial and temporal complexity, particle reworking activity is often classified into sub-processes and described with respect to a diffusion-analogous ("local", *Db*) and advective ("non-local", *r*) transport (Hedman et al., 2011; Kristensen et al., 2012) In this context, non-local transport can be distinguished from local processes by larger transport step lengths and the lack of isotropy (Meysman et al., 2003). To determine particle mixing, often the vertical distribution of inert (e.g. luminophores; Maire et al., 2010) or reactive particle tracers (e.g. radioactive isotopes, chlorophyll; Gerino et al., 1998; Lecroart et al., 2010) is quantified. Fitting of obtained particle distribution values into the framework of deterministic bioturbation models allows the description of *Db* and *r*. If bioturbation performance is regarded with respect to the extent of local and non-local transport, macrofauna can be attributed to one of four major functional bioturbation categories (François et al., 1997; Kristensen et al., 2012; Figure 1). Within the biodiffusor group, particle redistribution is mainly accomplished by local transport, whereas particle transport in conveyor belt-feeding and regenerator-type fauna is dominated more by non-local mechanisms, rendering the latter potential key organisms for a fast or deep particle burial.

Though MPs widely occur in benthic habitats, very little is known about MP redistribution as a consequence of infaunal bioturbation activity. The assumption that MPs are affected by bioturbation in the same manner as regular sediment particles appears plausible, as artificial plastic particles were already used as conservative tracers in both in situ and laboratory experiments to assess horizontal (Wheatcroft, 1991) and vertical (Valdemarsen et al., 2011) sediment reworking rates. Näkki et al.

(2017) recently demonstrated burial of MPs into the upper 5 sediment centimeters for a Baltic Sea community mainly comprised of biodiffusors, generating a diffusion-analogous vertical particle distribution. While these findings indicate that MPs are not limited to the sediment-water interface and can migrate into deeper sediment layers, potentially buried MP particles might be missed by recent standard monitoring techniques, which often only sample the upper sediment centimeters (Blumenröder et al., 2017; Nor and Obbard, 2014; Reed et al., 2018). As the global mean depth for biomixing of sediment strata is estimated to be around 6 – 10 cm (Boudreau, 1994; Teal et al., 2008), burial of MPs into considerable sediment depths might be a phenomenon relevant for most soft-sediment habitats around the globe. Furthermore, non-local transport might contribute to vertical MP export by bypassing upper well-mixed sediment layers (Blair et al., 1996; Levin et al., 1997) and depositing MP particles at deeper sediment strata. Hence, the effect of bioturbation on MP distribution possibly constitutes a process that to date is not well represented within our current state of knowledge on MP transport and accumulation in benthic ecosystems. Consequently, a substantial amount of MPs in the marine realm might not be considered by attempts to estimate global benthic MP contamination. The potential burial of MPs mediated by bioturbation is further emphasizing the role of marine sediments as sinks for MPs and might result in additional conservational effects on these already hardly degradable materials, enhancing their longevity in the marine realm even further.

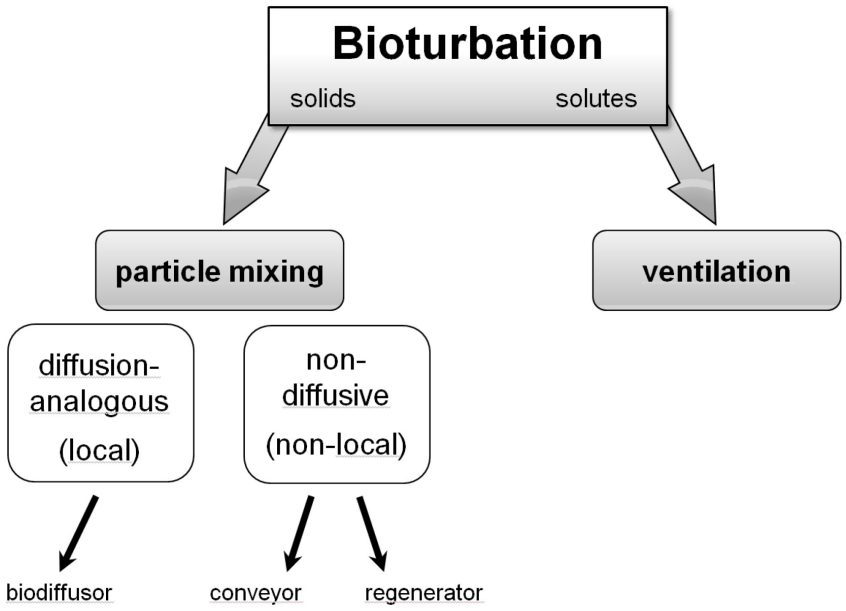


**Figure 1. The concept of bioturbation with focus on particle mixing and bioturbation types.** Adapted from Kristensen et al. (2012).

Despite the existing evidence that MPs are quantitatively and qualitatively buried in a similar fashion to ambient sediment grains, mechanics of MP burial, especially with regard to particle

densities or sizes contrasting surrounding sediment particles have not been investigated yet in terms of bioturbation. Most plastic polymers are less dense and often differently sized (i.e. considerably smaller) than the surrounding sediment which might induce a differential behavior in randomized, diffusion-analogous mixing, leading to separation effects, as there are known for other mixed substrates (Hong et al., 2001; Möbius et al., 2001). Additionally, MP particles in situ exhibit rapid biofouling leading to the formation of complex biofilm communities within several weeks (Ye and Andrady, 1991), which are similar to natural occurring particles with respect to community composition (Harrison et al., 2014; Lobelle and Cunliffe, 2011). Surface-associated prokaryote and eukaryote assemblages represent common food sources for a multitude of deposit-feeding taxa (Andresen and Kristensen, 2002; Lopez and Levinton, 1987) and biofilm formation is hypothesized to facilitate ingestion of MP particles, which has already been shown for several pelagic copepod species (Vroom et al., 2017). Due to smaller density and distinct biofilms, MPs resemble rather organic-rich particles, such as detritus or marine aggregates, than sediment particles. As organic-rich, less dense particles are often ingested preferentially over sediment grains (Self and Jumars, 1988; Taghon, 1982), the physical properties of MPs might further facilitate their potential to be ingested by macrofauna and therefore, their potential for non-local transport.

Against the background of the manifold unknowns in benthic MP transport, the purpose of this study was to determine the effects of bioturbation on MP redistribution and burial in marine sediments under the aspects of different bioturbation types (i.e. organisms with different potentials for local and non-local sediment reworking) and differently sized MP particles. Additionally, reworking rates of MPs and ambient sediment particles (i.e. luminophores) were compared to assess possible differences in particle transport due to varying particle densities. Based on experimental results, the identification of key bioturbation modes and species that promote particular fast or deep burial of MPs was intended. Contrasting transport coefficients for MPs with *Db* and *r* values assessed for established particles tracers (luminophores) might furthermore allow evaluating the MP burial potential of other species and communities from already existing bioturbation data.

As many polychaetes are known to be strong bioturbators and often to facilitate non-local transport, two polychaete species were chosen to address these questions. The ragworm *Hediste diversicolor* (O.F. Müller, 1776) is widespread in many brackish habitats along North American and European coasts and can constitute a major faunal element in many estuaries, reaching maximum abundances of several 1000 individuals $m^{-2}$ (Arndt, 1989; Davey and Watson, 1995). The polychaete is known for the construction of complex burrow networks, which can extend down to 20 cm depth into the sediment (Davey, 1994). *H. diversicolor* burrows tend to be composed of multi-branched structures in shallow sediment strata with several connections to the sediment surface (the so-called gallery) and parts of vertical orientation, reaching into deeper sediment strata (Davey, 1994; Scaps, 2002; Figure 2). Owing to this distinctive burrow morphology, *H. diversicolor* is classified as a gallery-diffusor, performing both local and non-local mixing processes. Local mixing is limited to

gallery and surface layers, representing the sum of activities of which feeding by dragging food particles into the burrow may be the dominant one (Figure 2A), either carried out actively (catching food with the jaws) or passively (particle adhesion to the abdomen or parapodia). Additionally, movement, burrow construction and maintenance (Figure 2B) contribute to the generation of diffusion-analogous mixture patterns within upper sediment layers and the incorporation of particles into the burrow walls (François et al., 2002; Hedman et al., 2011). Non-local particle displacement mainly occurs along vertical burrow sections by gravity-driven particle transport, leading to the formation of particle accumulation zones in larger depths (Duport et al., 2006; Hedman et al., 2011; Figure 2D). Based on its specific bioturbation behavior, *H. diversicolor* was chosen to investigate effects of MP transport via both local and non-local mixing. In a mesocsom experiment (HD experiment), the differential mixing between MPs of varying size as well as between MPs and luminophores of the same size was assessed. As sediment reworking activity of *H. diversicolor* can be stimulated by food addition (Nogaro et al., 2007), the impacts of varying food availability on vertical MP transport rates were investigated in the HD experiment as well. Sediment reworking activity for all particle tracers and food regimes was quantified in terms of *Db* and *r* by using the gallery-diffuser model introduced by François et al. (2002). In this context, an overall bioturbation of MPs both by local and non-local mixing was hypothesized, though different mixing values for particles of varying size were expected, as larger particles might be harder to introduce into the burrows by polychaetes. Food addition was expected to stimulate sediment reworking activity and to amplify potential effects of particle size and density on depth transport. Potential effects of particle size and density on depth transport were expected to intensify by stimulation of sediment reworking activity with food addition. To further verify if ingestion and defaecation might constitute another pathway of MP transport, a second mesocosm experiment ($HD_I$ experiment) was conducted. After ingestion, we expected the deposition of MPs sufficiently small for ingestion back at the sediment surface (Gunnarsson et al., 1999; Figure 2C), causing no net burial of MPs.

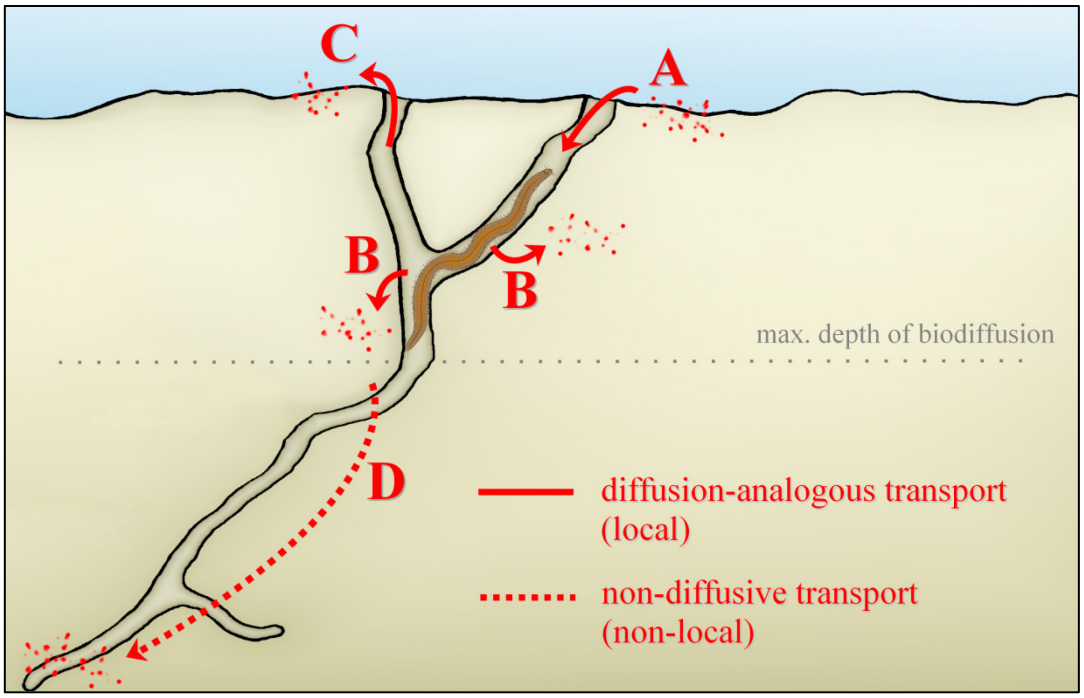


**Figure 2: Schematic illustration of hypothesized MP transport processes induced by *H. diversicolor*.** **A**: Introduction to burrows by feeding activity; **B**: Burial into sediment above maximum biodiffusion depth or integration into burrow walls; **C**: defaecation of ingested MPs at the sediment surface; **D**: transport beneath maximum biodiffusion depth. For further explanations see text.

The other organism studied, the lugworm *Arenicola marina* (Linnaeus, 1758) represents one of the most abundant members of European mudflat communities, with maximum abundances up to 100 ind. $m^{-2}$ (Beukema and De Vlas, 1979). Inhabiting characteristic J or U shaped burrows, *A. marina* can have profound effect on sediment properties due to their ventilation and feeding activity. [1]"The polychaete is known to alter sediment porosity (Volkenborn et al., 2007), enhance sediment oxygenation and organic matter decomposition (Banta et al., 1999) and to rework substantial amounts of sediment (Cadée, 1976). Owing to the characteristic architecture of its burrow, consisting of feeding funnel, feeding picket and tailshaft (Figure 3), this upward conveyor belt feeder generates both downward and upward particle transport. The interaction of *A. marina* with MPs has been subjected to substantial research and it was shown that MP particle are able to descend via the feeding funnel (Valdemarsen et al., 2011; Figure 3A), can be ingested (Green et al., 2016; Van Cauwenberghe et al., 2015; Figure 3B) and are defaecated again at the sediment surface (Van Cauwenberghe et al., 2015; Figure 3C). However, *A. marina* is known to feed selectively on particles by discriminating particles larger than ~1 mm in diameter (Baumfalk, 1979), which often leads to the formation of a coarse particle and shell debris layer at the base of headshaft and feeding pocket ("graded bedding"; (Baumfalk, 1979; Cadée, 1976). Since *A. marina* inhabits deep burrows reaching up to 20-40 cm sediment depth (Krüger, 1971), the selective feeding of particles smaller than 1 mm may provide a

[1] The denoted passage is cited according to Gebhardt & Forster (2018).

possible pathway for a fast non-local burial of larger MP particles via feeding funnel transport and their accumulation in considerable depths due to non-ingestion (Figure 3D).” To test this hypothesis, a long-term mesocosm bioturbation experiment (AM experiment) was conducted. Two differently sized MP particle types were used to test for size-depending mixing effects and to identify a hypothetical particle diameter threshold that still allows for MP ingestion. Additionally, by the simultaneous use of luminophores it was intended to reveal possible effects of variable density on particle transport and ingestion. In this context, the ingestion and subsequent defaecation of luminophores was hypothesized, whereas at least for the larger MP type evidence of particle retention within the feeding pocket was expected. Polychaete faeces could not be removed for determination of sediment reworking activity, since no tracer particles should be lost or moved in this experiment. Therefore, sediment defaecation rates and hence, bioturbation activity was studied in a second mesocosm setup ($AM_{SI}$ experiment) with experimental conditions similar to the AM setup.

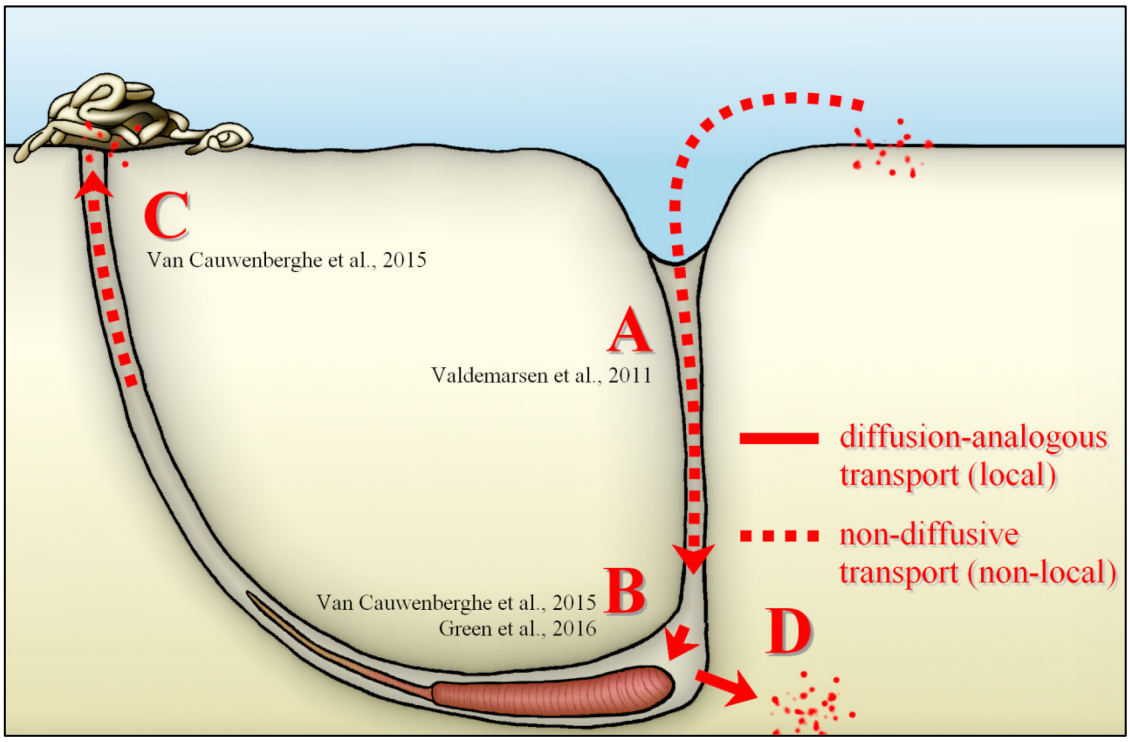


**Figure 3: Schematic illustration of known and hypothesized MP transport processes induced by *A. marina*.** **A**: Burial via feeding funnel transport; **B**: Particle ingestion; **C**: deposition of ingested particles in faecal casts; **D**: Accumulation of rejected MPs at the bottom of the feeding pocket. Cited references indicate existing evidence for transport processes in question (**A**-**C**). For further explanations see text.

# 2. MATERIALS AND METHODS

## 2.1. Particle and microplastic transport induced by *H. diversicolor*

### 2.1.1. Sampling

Sediment, polychaetes and water were collected in March 2017 at Schnatermann beach, located at the eastern shore of the Breitling, a lagoon-type opening of the Warnow Estuary near Rostock, Germany (water temperature: 6.1°C, salinity: 8.4; 54.1728°N, 12.1420°E; Figure 4). Sediment was sieved through 1000 µm mesh to remove macrofauna, coarse sediment and shell debris. Sediment parameters were determined from homogenized sediment as described in section 2.4.

Approximately 90 specimens of *H. diversicolor* were collected upon sediment sieving and kept in aerated glass aquaria (20 x 25 x 20 cm), filled with several cm of sediment and habitat water (15°C) prior to their use in the experiment.

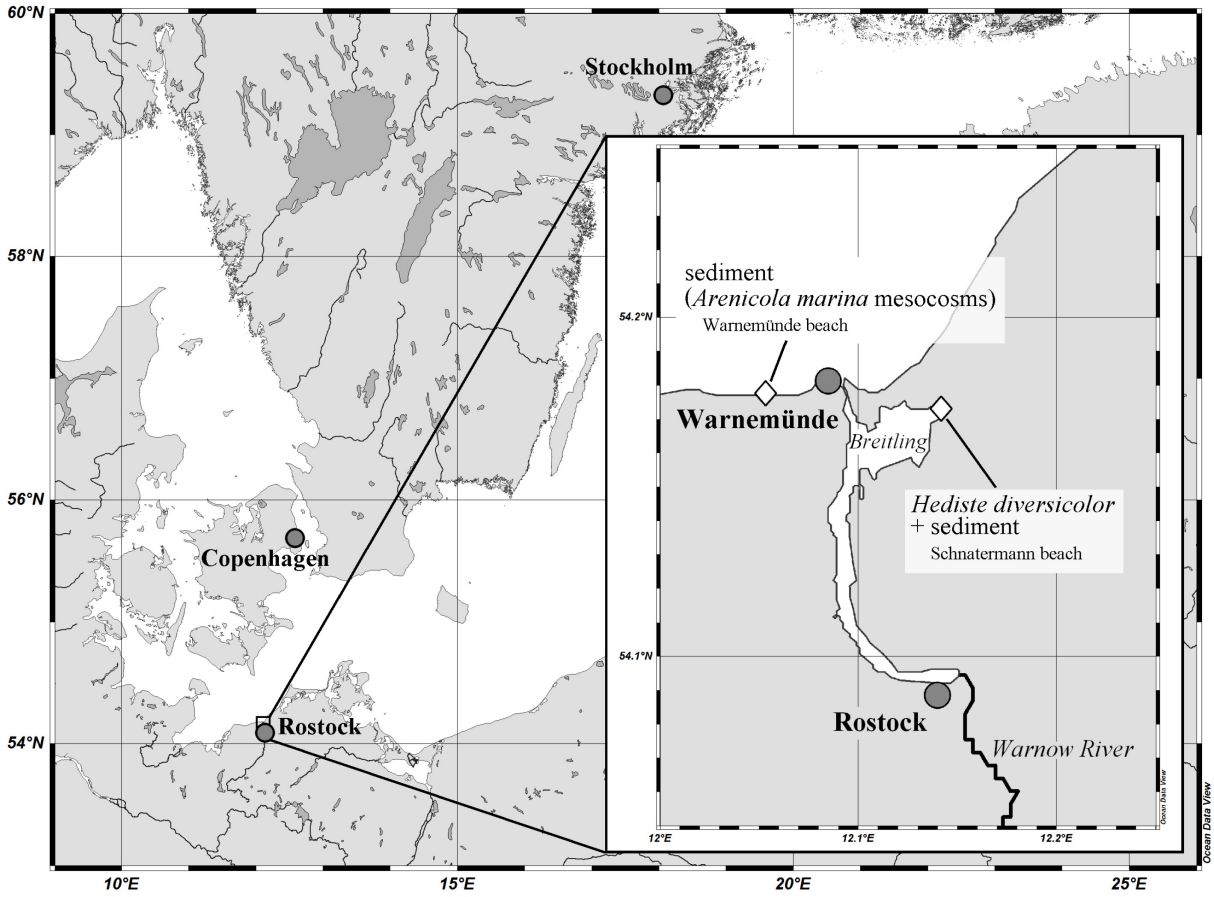


**Figure 4: Sampling sites of sediments and specimens of *H. diversicolor* used in the experiments.**

### 2.1.2. Mesocosm preparation

Nine glass aquaria (20 x 25 x 20 cm, volume 10 L) were used as mesocosms and filled with 16 cm of homogenized sediment, overlaid by several L of habitat water which was adjusted to a salinity of 12. Mesocosms were equipped with aeration and were kept in a temperature-controlled chamber with an ambient temperature adjusted to 15°C for a stabilization period of 13 d (two mesocosms) and 27 d (seven mesocosms), respectively. A 12h light/dark cycle was simulated by using two aquaria lamps (Nano light, 11 W, Dennerle, Münchweiler, Germany). Aeration was switched off for three days to induce anoxic conditions in all mesocosms to remove meiofauna and juvenile stages of macrofauna which might not have been captured during sediment sieving. 10 specimens (~ 4.0 g fresh mass (FM)) of *H. diversicolor* were introduced to six mesocosms (HD1 – HD6), respectively; corresponding to an abundance of 200 ind. $m^{-2}$. The remaining three mesocosms served as azoic control setups (C1 – C3; Figure 5). Prior to weighting, polychaetes were kept in habitat water-filled plastic bowls overnight for gut clearance. Added polychaetes were allowed to establish burrows in the sediment and acclimatize for 7 – 9 days (Figure 6). Polychaetes resting motionless on the sediment surface during acclimatization were removed and replaced by specimens of similar mass.

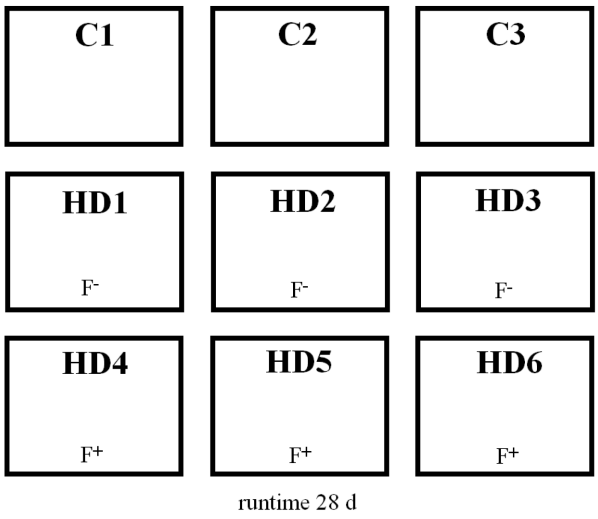


**Figure 5: Mesocosm setup of the HD experiment.** **C**: control mesocosms; **HD**: mesocosms with added *H. diversicolor*; **F$^-$**: no food addition; **F$^+$**: weekly addition of 0.7 g (WW) of spinach (see section 2.1.3).

### 2.1.3. Particle transport under different feeding regimes

Addition of particle tracers to mesocosms is described in section 2.5.4.1. Subsequent to tracer addition, mesocosms were incubated for 28 days under conditions described above. HD mesocosms were divided into two treatments, consisting of three replicates each. In the non-feeding treatment (HD1 – 3, $F^-$) no additional food was given over the course of the experiment, whereas polychaetes of the feeding treatment (HD 4 – 6, $F^+$) were fed with 0.7 g (FW) spinach weekly, equating the addition

of 289 mg C and 35 mg N each feeding event (C/N ratio: 8.25). Spinach C and N content were determined with a C/N analyzer (CE instruments NC 2500).

A partial water exchange was carried out twice a week in all mesocosms by removing 250 ml of water and replacing it with fresh habitat water using a syringe while carefully avoiding sediment resuspension. Water losses caused by evaporation were adjusted by adding deionized water, salinity was determined after every water exchange. Specimens of *H. diversicolor* lying on the sediment surface and not being able to rebury into the sediment within 12 h were removed and not replaced.

Upon experiment termination, mesocosms were sectioned as described in section 2.5.4.2 and residence depth of recovered polychaetes was noted. Polychaetes retrieved alive were stored in water-filled plastic boxes overnight for gut clearance before determination of fresh mass (FM), dry mass (DM) and ash-free dry mass (AFDM) as described by van der Meer *et al.* (2005).

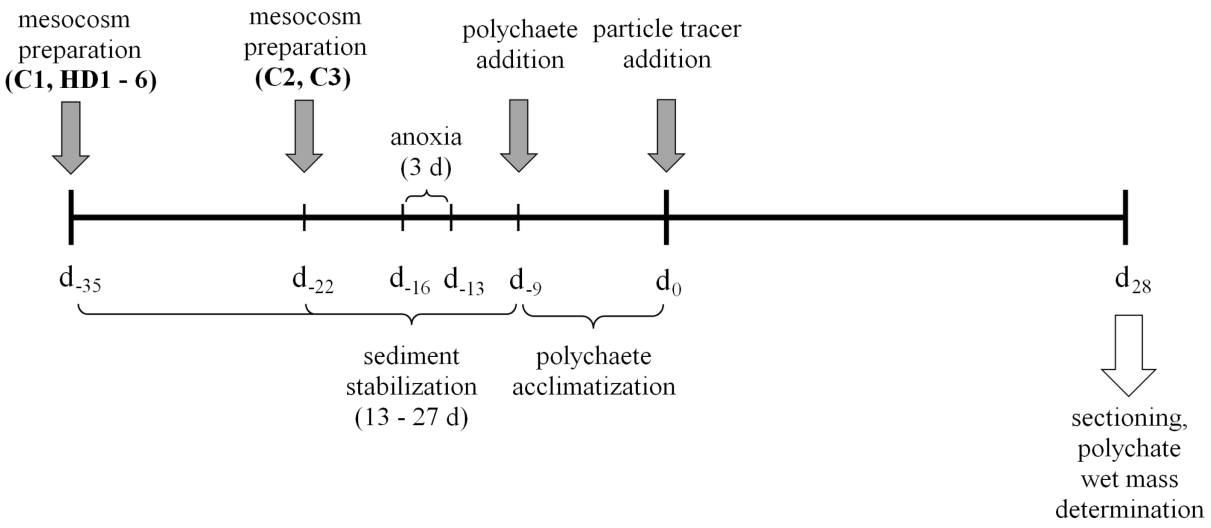


**Figure 6: Timeline of the HD experiment.** Tracer addition ($d_0$) indicates start of the experiment.

### 2.1.4. Microplastic ingestion of *H. diversicolor*

To screen for potential ingestion of MP particles by polychaetes, a mesocosm was prepared as described in section 2.1.2 (salinity 12, storage at 15 °C), hereafter referred to as the *H. diversicolor* ingestion ($HD_I$) setup. Food was added as described above, addition of particle tracers is described in section 2.5.4.1. After two weeks of incubation, visible faecal pellets and samples of mucus lining were collected from the sediment surface with a syringe. Samples were stored in plastic tubes at – 18°C until screening for present PE particles under UV light with a dissection microscope.

## 2.2. Sediment ingestion of *A. marina*

### 2.2.1. Sampling

Sediment was collected in January 2016 at Warnemünde beach north of Rostock, Germany (water temperature: 10.5°, salinity: 13; 54.1777°N, 12.0536°E; Figure 4) and was sieved through 1000 µm mesh to remove macrofauna and shell debris. The sediment was homogenized and stored in sealed barrels at room temperature. Homogenized sediment was taken from both mesocosms and used for determination of sediment parameters (see section 2.4).

[1]"Specimens of *A. marina* were obtained as bait worms from a local fishing supplier (Angelcenter Bastian, Rostock, Germany) in December 2016 and were kept in plastic bowls filled to a height of 10 cm with sediment for two weeks (10°C, salinity 30). Polychaetes originated from the Dutch Wadden Sea (A. Ullrich, Feb. 2016, pers. comm.) and were collected 1 – 2 d prior to their purchase."

### 2.2.2. Mesocosm preparation

Homogenized sediment was filled into two plastic boxes that served as mesocosms (43 x 28 x 25 cm; 50 x 30 x 15 cm, respectively) up to a height of 12 cm. Sediment was covered with habitat water, aeration was added and boxes were stored in a dark, temperature-controlled water tank (volume ca. 650 L) for constant incubation temperature during the experiment. Mesocosm sediment area was separated by pushing acrylate boards (thickness ~1 cm) vertically into the sediment, generating nine compartments in total ($AM_{SI}$ 1 – 9) with areas of 182 – 476 $cm^2$ (Figure 7).

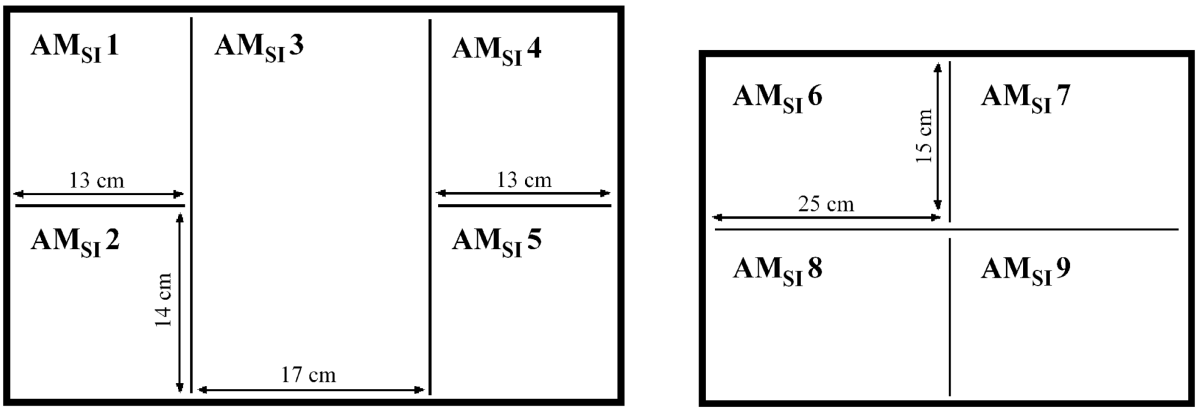


**Figure 7: Mesocosm setup of the $AM_{SI}$ experiment.** Top view on both mesocosms showing compartments.

Spacing between acrylate walls was set to ~0.5 cm to ensure water exchange between adjacent compartments but to prevent polychaetes from leaving their assigned area. After three weeks of

[1] The denoted passage is cited according to Gebhardt & Forster (2018).

sediment stabilization, one polychaete was added to each compartment. Prior to addition, fresh mass of polychaetes was determined. Individuals that dug not into the sediment within ~30 min or were lying motionless on the sediment surface during the following acclimatization period of two days were replaced by new polychaetes. Mesocosms were incubated for seven weeks (10°C, salinity 30) in the dark without feeding.

## 2.3. Particle and microplastic transport induced by *A. marina*

### 2.3.1. Sampling

Sampling of sediment was done in November 2015 and January 2016 at Warnemünde Beach, Rostock, Germany (water temperature: 10.5°, salinity: 13; 54.1777°N, 12.0536°E; Figure 4). [1]"Sediment was sieved through 1000 µm mesh to remove macrofauna and shell debris. Prior to its use, sediment was stored in sealed barrels at room temperature. Sediment from both sampling dates was mixed to assure equal sediment properties. Sediment characteristics were determined as described in section 2.4 before the start of the experiment.

Polychaetes were obtained as bait worms from a local fishing supplier (Angelcenter Bastian, Rostock, Germany) in February 2016 and were kept in plastic bowls filled to a height of 10 cm with sediment overnight (10°C, salinity 30). Polychaetes originated from the Dutch Wadden Sea (A. Ullrich, Feb. 2016, pers. comm.) and were collected 1 – 2 d prior to their purchase."

### 2.3.2. Mesocosm preparation

The mesocosm setup consisted of 11 10 L buckets (diameter 25 cm), made out of food graded polypropylene which were filled with homogenized sediment to a height of 20 cm and overlaid by ~1.5 L of ambient Baltic Sea water (original salinity ~10) that was adjusted to a salinity of 30. Mesocosms were equipped with aeration and stored in a dark, temperature-controlled water tank (10°C, volume ~650 L) for 14 d for sediment stabilization. Two individuals of *A. marina* were added to eight mesocosms (AM1 – 8), respectively, equating an abundance of 40 ind. $m^{-2}$. Remaining mesocosms served as azoic control treatments (C1 – 3; Figure 8). C1 was incubated alongside with AM cores; C2 and C3 were prepared several months later with sediment of the same origin (collected in January 2016) and incubated under similar conditions (10°C, salinity 30).

All mesocosms were incubated in the dark and without the addition of any food over the whole duration of the experiment. Total polychaete biomass was determined as individual fresh mass prior to introducing individuals into the mesocosms. After addition, polychaetes were allowed to acclimatize for another 14 days. Polychaetes that dug not into the sediment within 24 h were replaced with individuals of similar mass.

[1] The denoted passage is cited according to Gebhardt & Forster (2018).

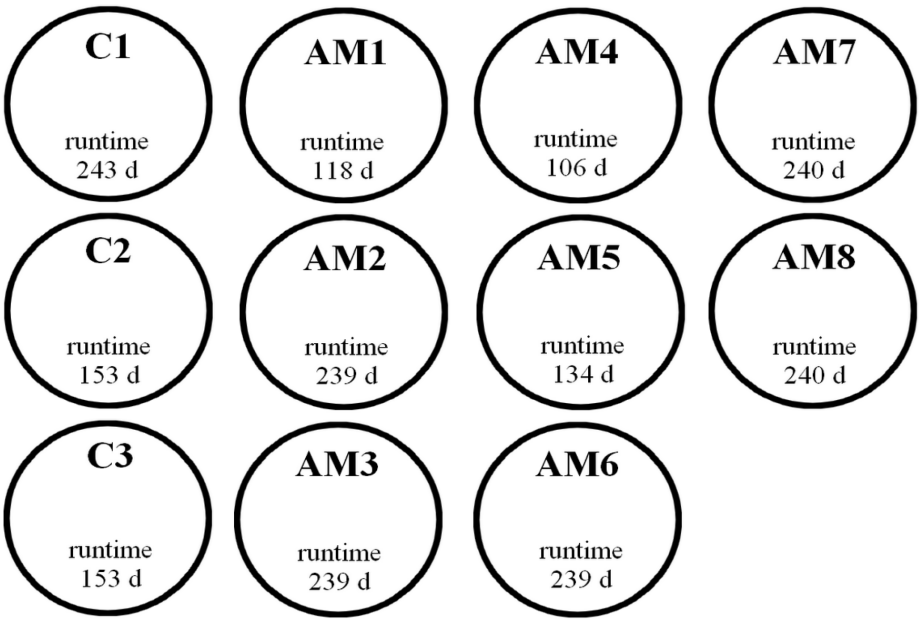


**Figure 8: Mesocosm setup of the AM experiment.** C: controls; AM: mesocosms with added *A. marina*.

### 2.3.3. Microplastic transport

Addition of particle tracers to mesocosms is described in section 2.5.4.1. During incubation, water temperature and salinity were controlled weekly; salinity was adjusted if necessary by addition of ambient Baltic Sea water to compensate for evaporation losses. AM mesocosms were checked daily for any freshly produced faecal casts. Occurring casts were smoothened with a stainless steel spoon to mimic horizontal redistribution of sediment grains by wave action and tidal flows. Incubation time for each mesocosm ranged between 106 and 243 d (Figure 9).

With respect to incubation time mesocosms were classified into two groups (STI: short time interval, runtime ≤ 134 d; LTI: long time interval, runtime ≥ 239 d). Upon experiment termination, mesocosms were sectioned as described in section 2.5.4.2. Polychaetes retrieved alive were kept in habitat water overnight for gut clearance. Grain size distribution of sediment surface layers (0 – 2 cm) and feeding layers (AM mesocosms) or lowermost sediment layers (18 – 20 cm, controls) was determined as described in section 2.4. Collected worms were stored at – 18°C until determination of FM, DM and AFDM.

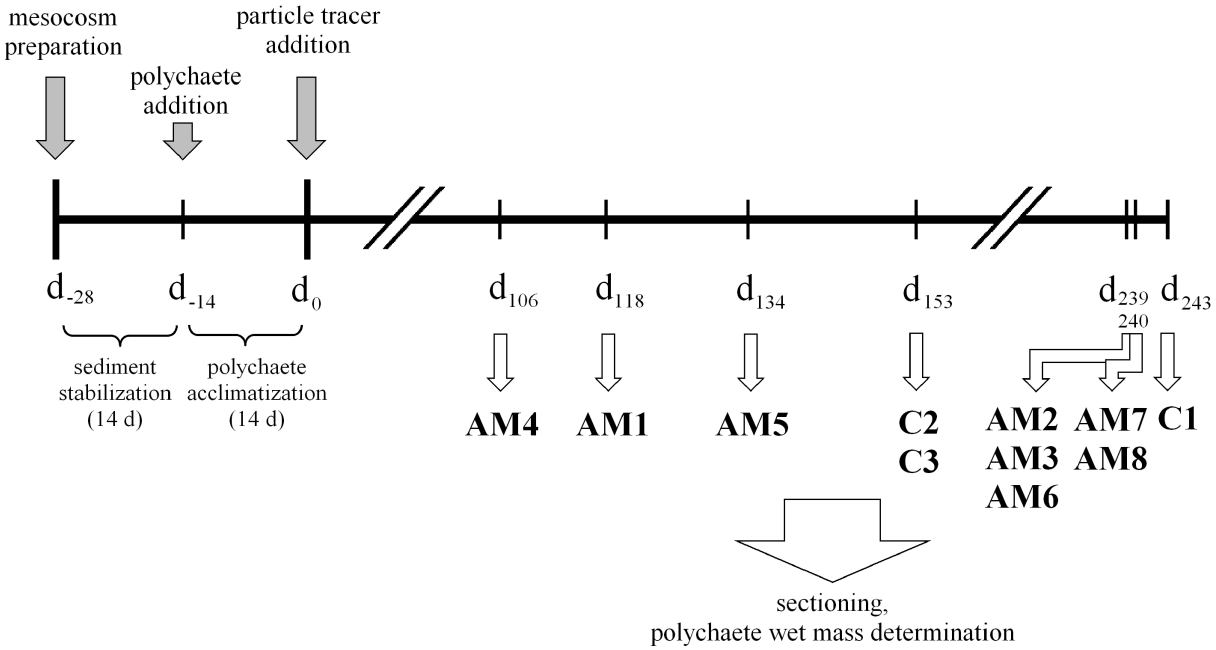


**Figure 9: Timeline of the AM experiment.** Tracer addition ($d_0$) indicates start of the experiment.

## 2.4. Quantification of sediment properties

Grain size distribution, sorting and porosity of sediment samples were determined according to Folk & Ward (1957). Organic matter content was assessed as loss on ignition (LOI, 500°C for 12 h; (Bale and Kenny, 2005)); particular organic carbon POC content was derived from LOI as described in Leipe et al. (2011).

## 2.5. Quantification of polychaete sediment reworking

### 2.5.1. Particle tracers

To investigate burial and accumulation effects of larger MP particles in sediments, particles with a diameter of 1 mm (polystyrene (PS) BASF, Ludwigshafen, Germany) and 0.5 mm, respectively (polyamide (PA) Monofil-Technik GmbH, Hennef/Sieg, Germany), Figure 10A, B), were used. PS particles were extruded and cut to final size at the IPF Dresden, Germany prior to the experiments. Burial of sediment grain-sized microplastic particles was assessed by using polyethylene (PE; Copsheric, Santa Barbara, CA, USA) particles (diameter 125 – 150 µm, Figure 10C), covered with ultraviolet (UV)-fluorescent dye to facilitate particle recovery. All MP particles used exhibited a particle density > 1 g $cm^{-3}$ to assure sedimentation and potential mixing into the sediment. To quantify possible differential mixing patterns of plastic particles and ambient sediment grains due to differences in particle size and density, luminophores with a diameter of 130 µm (Partrac Ltd., Glasgow, UK; Figure 10D) were used as an additional particle tracer type (Mahaut and Graf, 1987; Maire et al.,

2010). Luminophores represent natural sediment particles, covered with UV-fluorescent dye. Further information characterizing the particle tracers used is given in Table 1.

### 2.5.2. Calibration of particle quantification

To quantify particle tracers from sediment samples, particle number-mass ratios for luminophores, PA and PS particles were determined. Several particle samples (luminophores: n = 148; PA: n = 142; PS: n = 140) of different masses (luminophores: up to 2.3 mg; PA: up to 27 mg; PS: up to 700 mg) were weighted using a micro balance (Sartorius Pro 11, readability 0.001 mg). Subsequently, samples were photographed and particles were counted manually on the images taken using the cell counter plugin implemented in the image processing software ImageJ (Rasband, 2014). Information on the specific particle number-mass ratio of PE particles was provided by the manufacturer.

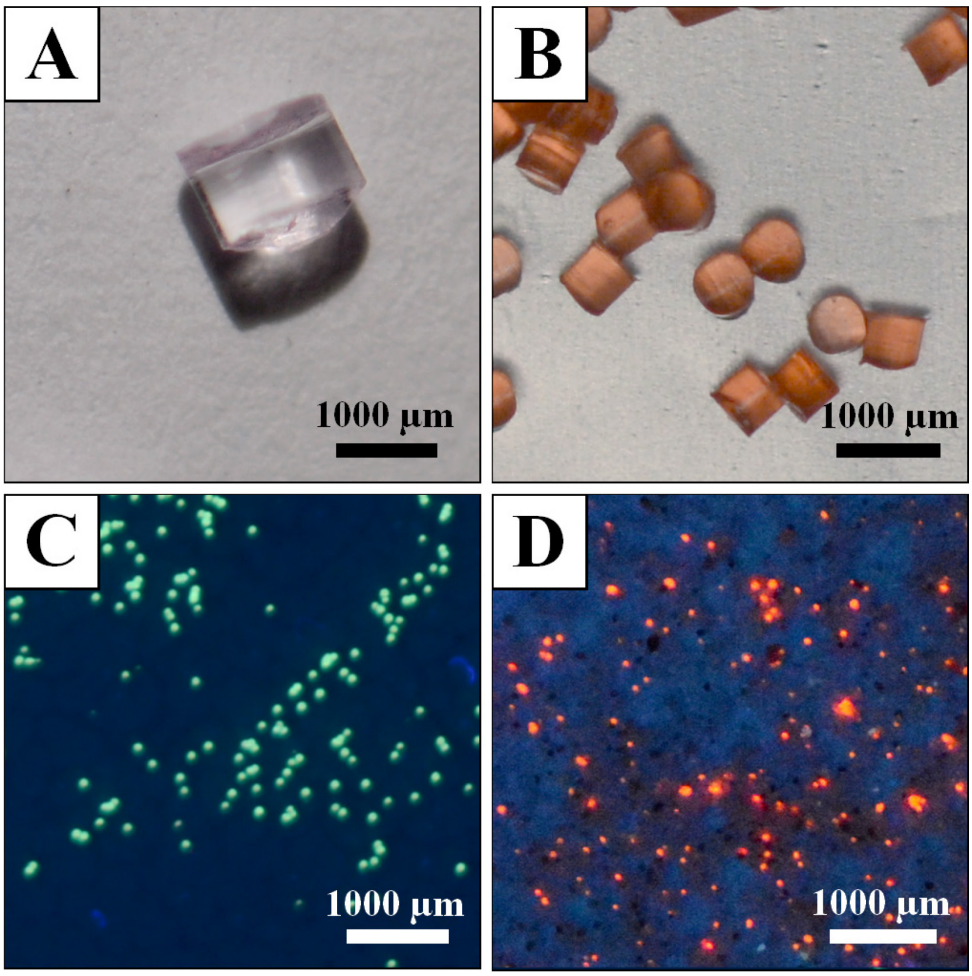


**Figure 10: Particle tracers used in the HD and AM experiment.** A: polystyrene (PS); B: polyamide (PA); C: polyethylene (PE; under UV light); D: luminophores (under UV light).

**Table 1: Characteristics of all particle tracers used.**

| particle type | product name | diameter (µm) | density (g $cm^{-3}$) | fluorescent |
|---|---|---|---|---|
| luminophores | Partrac tracer JK 146 magenta | 130 | 2.65 | yes |
| polyethylene (PE) | Cospheric UVPMS-BG-1.025 | 125 – 150 | 1.03 | yes |
| polyamide (PA) | Trofil® PA 6 | 500 | 1.14 | no |
| polystyrene (PS) | BASF PS 143 E | 1000 | 1.04 | no |

### 2.5.3. Sediment ingestion of *A. marina*

During mesocosm incubation, polychaete sediment ingestion was determined for 16 and 17 consecutive days, respectively. One day before the beginning of both measuring periods, occurring faecal casts were smoothened to sediment surface level using a stainless steel spoon. Position and quantity of freshly produced casts was noted every 24 h. Casts were gently removed with a syringe before dry mass of the collected sediment was determined. Volume of sediment samples was calculated based upon sediment dry mass.

Mesocosm water temperature and salinity were monitored daily; latter was adjusted with deionized water if necessary. At the end of the experiment polychaete DM and AFDM was determined after keeping individuals in habitat water overnight for gut clearance.

### 2.5.4. Sediment and microplastic transport induced by *H. diversicolor* and *A. marina*

#### *2.5.4.1. Tracer addition*

Prior to addition to mesocosms, PS and PA particles were incubated one (HD experiment) – four (AM experiment) weeks in habitat water to stimulate biofilm formation, ensuring a decrease in surficial hydrophobicity and buoyancy (Lobelle and Cunliffe, 2011; Stolte et al., 2015). Due to their small diameter, PE particles were suspended in 0.1w% polysorbate 80 solution according to the protocol "Preparing Tween Solutions" (Cospheric, 2014) for improved dispersion in sea water. At the start of the HD, $HD_I$ and AM experiment, suspensions of luminophores, PE and PA particles in ca. 15 ml sea water were applied to the sediment surface of each mesocosm using a syringe. In the AM experiment, PS particles were added by submerging a small PS-filled container into the overlying water of each mesocosm and carefully pouring the particles down onto the sediment surface. Tracer quantities added to the mesocosms of the HD, $HD_I$ and AM experiment are shown in Table 2.

**Table 2: Tracer quantities added to each mesocosm of the HD and AM experiment.** Shown particle concentrations depict the MP load integrated over the total mesocosm sediment mass.

| | HD/HD$_I$ experiment | | | AM experiment | | |
|---|---|---|---|---|---|---|
| | mass (g) | number (n) | concentration (part kg$^{-1}$ sed.$^{-1}$ DM) | mass (g) | number (n) | concentration (part kg$^{-1}$ sed.$^{-1}$ DM) |
| luminophores | 8.0 | 4 855 760 | 522 479 | 13.0 | 7 890 610 | 582 777 |
| PE | 2.0 | 161 112 | 14 577 | - | - | - |
| PA[1] | 1.3 | 10 011 | 905 | 10.0 | 77 008 | 5 688 |
| PS | - | - | - | 20.0 | 10 782 | 796 |

[1] No PA particles were added to the HD$_I$ experiment.

#### *2.5.4.2. Mesocosm sectioning*

[1]"Before sectioning, overlying water was removed carefully to avoid sediment resuspension. Mesocosms were further dried for 7 – 19 h with a 100 W heat lamp since this method proved effective to remove last remnants of overlying water but rendered polychaetes to stay alive until sediment sectioning." Sediment of each mesocosm was sliced into 16 layers with 1 cm thickness (HD experiment) or 10 layers with 2 cm thickness (AM experiment, Figure 11). Sectioning was carried out by using plastic scoops with according depth markings. Scoops were inserted into the sediment up to the marking position, surrounding sediment was carefully removed with another scoop and a stainless steel spoon. This procedure was repeated until all sediment from a depth layer was collected. For HD mesocosms, additional depth markings were drawn on the aquaria walls to aid sectioning. Precision of this method was ± 1 mm for the thickness of the removed sediment layers. Collected sediment was dried, thoroughly homogenized and stored in plastic boxes under darkness at room temperature until analysis. Polychaetes retrieved during sectioning were carefully removed, cleaned from adhering sediment and stored at – 18°C for biomass determination. Sediment layers in which polychaetes of the AM experiment were found were assumed to represent their respective feeding layers.

[1] The denoted passage is cited according to Gebhardt & Forster (2018).

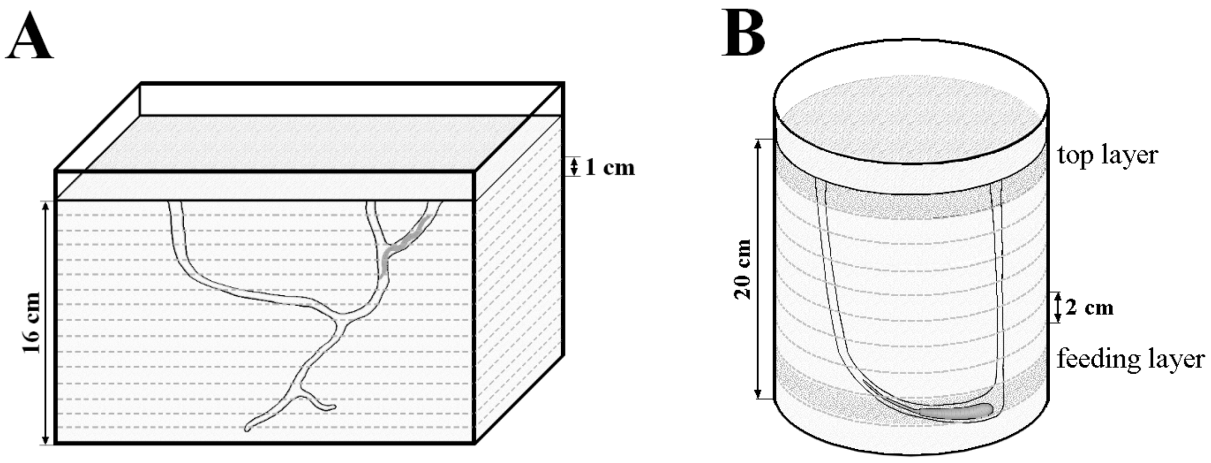


**Figure 11: Sectioning schematics for HD mesocosms (A) and AM mesocosms (B).** In B, uppermost and feeding sediment layers, from which sediment for grain size determination was taken, are highlighted.

#### *2.5.4.3. Quantification of particles < 500 µm (luminophores, PE)*

For fluorescent particle quantification, subsamples (volume 1.5 ml) were taken from every homogenized sediment layer (HD experiment: three replicates; AM experiment: five replicates). Sediment samples were photographed with a single-lens reflex camera (NIKON D7100, AF-S NIKKOR 60 mm 1:2.8 G lens) under UV light (emission maxima of the UV lamp used both at 254 and 365 nm). Camera settings used for imaging are shown in the Appendix (Table A1). Images were processed with the software ImageJ (Rasband, 2014), processing was done by splitting images into color channels, using single channels for further particle quantification (luminophores: red channel; PE particles: green channel) and subsequent binary thresholding of the image (Figure 12).

#### *2.5.4.4. Quantification of particles ≥ 500 µm (PS, PA)*

All sediment layers were sieved through 1000 µm and 500 µm meshes for quantification of larger MP particles. Lower MP concentrations were assessed by photographing MP-containing sieves and determining particle counts manually on the images taken using the cell counter plugin implemented in ImageJ. MP in quantities too large to count adequately on-sieve was extracted from the sediment by density separation as described in Thompson *et al.* (2004). The sieved sediment residue was transferred into 1 L of saturated NaCl solution, vigorously shaken and allowed to settle for 5 min. The supernatant was sieved through 1000 µm and 500 µm meshes. This separation step was repeated twice, recovered MP was dried and weighted (Sartorius BA 210 S: readability 0.1 mg). Particle numbers were calculated based on plastic dry mass. 500 µm sieves were photographed after density separation to screen for PA particles potentially stuck in the meshwork. Present particles were counted on images taken using the ImageJ cell counter plugin.

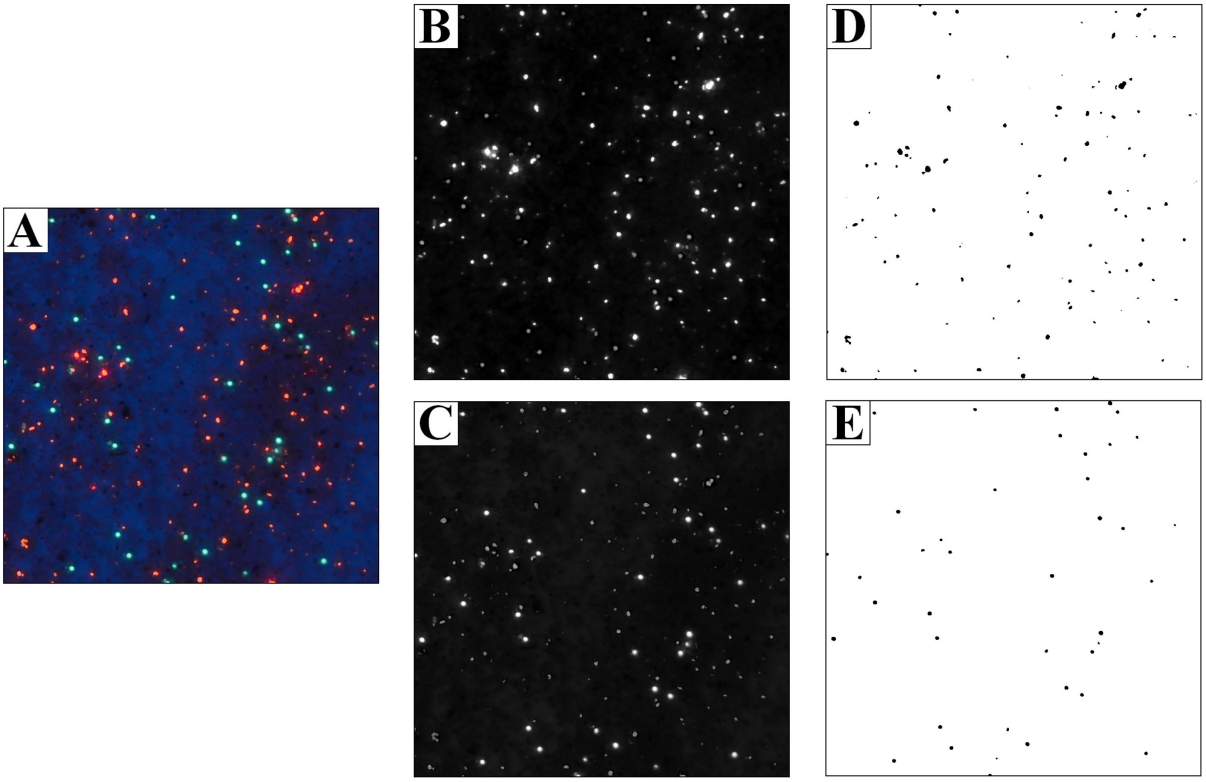


**Figure 12: Steps of image processing carried out prior to particle quantification.** **A:** original image with luminophores (red) and PE particles (green); **B:** isolated red color channel; **C:** isolated green color channel; **D** and **E:** binary images, solely showing luminophores (D) or PE particles (E).

#### *2.5.4.5. Modeling (gallery-diffusion model)*

To describe the macrofauna-induced particle transport into the sediment, the one-dimensional gallery-diffusion model (Duport et al., 2007; François et al., 1997) was applied. Based on the generic diagenetic equation expressed by Berner (1980), this model describes sediment reworking as a function of both diffusion-analogous (local) and non-diffusive (non-local) particle translocation processes (Figure 13).

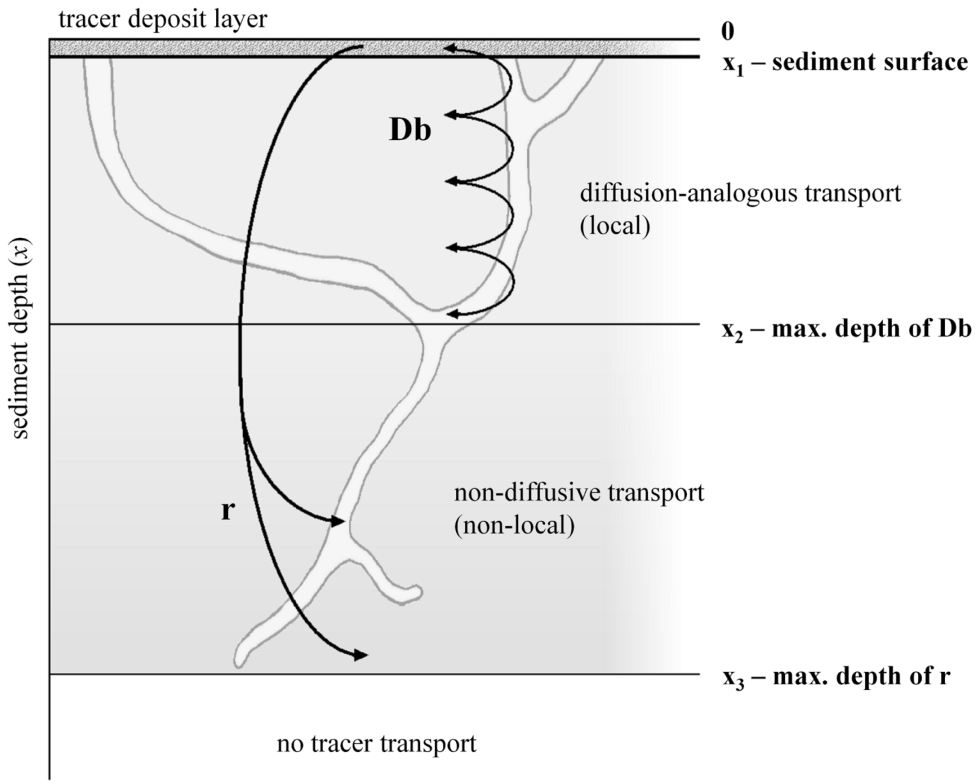


**Figure 13: Schematic of the biological transport processes considered in the gallery-diffusion model.**

Thus, sediment reworking can be characterized by the application of two transport coefficients:

$$\frac{\delta C}{\delta t} = Db\frac{\delta^2 C}{\delta x^2} + R\big(C(x,t)\big) \tag{1}$$

The biodiffusion coefficient *Db* describes the transport of a quantity of tracer *C(x,t)* at sediment depth *x* and time *t* as a random, omnidirectional process over short spatial scales, as it is found in regions of intense burrowing activity. *Db* is derived from the kinetic theory of gases, where the diffusion coefficient *D* of a particle is introduced to describe its diffusivity. *D* is directly linked to the Boltzmann constant $k_B$, the absolute temperature *T* and the particle's mobility $\mu$ – the ratio of the particle's drift velocity to an applied force (Einstein-Smoluchowski relation (Einstein, 1905; von Smoluchowski, 1906)):

$$D = \mu\, k_B\, T \tag{2}$$

For spherical particles with a radius *r* and the dynamical viscosity $\eta$ of the surrounding medium, this relation results in the Stokes-Einstein equation:

$$D = \frac{k_B T}{6 \pi \eta r} \tag{3}$$

Within the framework of the gallery diffuser model, the rapid vertical translocation of particles across large distances from upper to lower sediment layers *R(x,t)* is described by the non-local biotransport coefficient *r*, which was originally exemplified by François *et al.* (2002). According to Duport *et al.* (2007) this displacement term can alternatively expressed as

$$R(C(x,t) = \begin{cases} -rC(x,t) \; if \; x \in [0; x_1] & (4.1) \\ \frac{r}{x_3 - x_2} \int_0^{x_1} C(x,t) dx \; if \; x \in [x_2; x_3] & (4.2) \\ 0 \; if \; x > x_3 & (4.3) \end{cases}$$

where $x_2$ and $x_3$ define the upper and lower limits of the tracer redistribution, $x$ and $x_1$ are depth variables and $r$ represents the biotransport coefficient, denoted as the percentage of tracer that left the initial [*0*, $x_1$] deposit and was translocated in the [$x_2$, $x_3$] sediment layer. Equation (4.1) describes the tracer removal from the 0 – $x_1$ deposit layer; Equation (4.2) depicts the redistribution of tracers between $x_2$ and $x_3$. Equation (4.3) indicates that no tracer movement occurs below $x_3$. The model's initial conditions are described as followed:

$$C(x,0) = \begin{cases} C_0 \; if \; x \in [0; x_1] \\ 0 \; else \end{cases} \tag{5}$$

All tracers are contained within the initial particle layer [0; $x_1$] at time $t$ = 0. Additionally, a zero-flux Neuman boundary condition was formulated:

$$\frac{\delta C}{\delta x}(0,t) = \lim_{x \to +\infty} \frac{\delta C}{\delta x}(x,t) = 0 \tag{6}$$

The lower limit of *Db* was assumed with a sediment depth of 2 cm as a conservative estimate for modeling purposes (Hedman et al., 2011; Murray et al., 2017, see section 4.1.2). Both *Db* and *r* were determined by minimizing the weighted sum of squared differences between observed and calculated tracer concentrations of all sediment depths (François et al., 2002).

## 2.6. Statistical analysis

IBM SPSS Statistics (version 25) and PRIMER-e PRIMER v.6 were used for statistical analysis. The Shapiro-Wilk test was used to test for normal distribution of all data. Statistical differences were accepted as significant at $p < 0.05$, all results are shown as mean ± standard deviation (SD).

### 2.6.1. Sediment and microplastic transport induced by *H. diversicolor*

Influences of feeding regime (control, $F^-$, $F^+$), mean estimated depth of biodiffusivity (1 cm, 2 cm, 4 cm) particle type (luminophores, PE, PA) on *Db* and *r* were assessed using the Games-Howell test. Furthermore, the Games-Howell test was applied to test the influence of feeding regime and particle tracer type on particle maximum penetration depth (MPD) and absolute and cumulative (below sediment depths of 1 cm, 2 cm and 10 cm) particle tracer concentrations. The effect of feeding regime ($F^-$, $F^+$) on polychaete mortality and biomasses (FW) was tested using Student's t test.

MDS was performed with PRIMER v.6 to indicate differences in tracer quantities below sediment surface levels and sediment depths of 10 cm in all mesocosms. A three-way permutational multivariate analysis of variance (PERMANOVA, (Anderson, 2017)) was carried out with the add-on package PERMANOVA+ for PRIMER v.6 to compare the effects of feeding regime (control, $F^-$, $F^+$), particle type (luminophores, PE, PA) and sediment depth on particle concentrations in all sediment layers. Homogeneity of dispersions of all factors was tested with the PERMDISP test.

### 2.6.2. Sediment ingestion of *A. marina*

The non-parametric Mann-Whitney-U test was applied to test for differences in sediment ingestion of single polychaetes between the two time periods analyzed as well as for differences in sediment reworking activity between the respective mesocosms. Differences in polychaete biomasses upon experimental start and termination as well as net biomass changes between the two mesocosms were assessed using Student's t test. Correlation between polychaete sediment reworking activity (measured as individual sediment ingestion and number of active days during the experiment) with individual biomass was tested by calculating Pearson's correlation coefficient or at lack of normal distribution, Spearman's rank correlation coefficient.

### 2.6.3. Sediment and microplastic transport induced by *A. marina*

[1]"Differences in vertical particle transport between controls and AM mesocosms and between different incubation times were tested using the non-parametric Mann-Whitney U test. To assess differences in burial rates between particle tracer types (luminophores, PA, PS), the Games-Howell test was applied in post hoc analysis. Differences in grain sizes within groups of long or short

[1] The denoted passage is cited according to Gebhardt & Forster (2018).

incubation times were assessed by using the post hoc Tukey-HSD test. To test the influence of incubation time and sediment depth on median sediment grain size, a two-way ANOVA and a post-hoc Tukey HSD test were carried out. The influence of incubation time and sediment ingestion on median grain size and biomass change was determined by using a two-way ANOVA as well.

Multidimensional scaling (MDS), performed with PRIMER v.6, was used as an ordination method to reveal differences in particle tracer concentrations below sediment surface levels and sediment depths of 8 cm in all mesocosms. Prior to scaling, particle concentration data were square root transformed to ensure data normal distribution."

# 3. RESULTS

## 3.1. Calibration of particle quantification

A highly linear relationship between particle mass and number was determined for MP particles (PS, PA), corresponding well to MP particles regular in shape in size as they were produced by polymer extrusion (Table 3; Appendix, Figures A1, A2). In contrast, luminophore sample masses and numbers showed much higher variation, representing a mixture of differently sized sediment grains (Table 3; Appendix, Figure A3). Based on regression data, MP quantities added to mesocosms (Table 3) exhibited very little variation (HD: PA 10 011 ± 52 particles; AM: PS: 10 782 ± 20 particles, PA: 77 008 ± 400 particles), whereas added luminophore masses could differ up to 6.8% from the mean regression value (HD: ± 331 520 particles; AM: ± 538 720 particles; Table 3).

**Table 3: Linear regression and confidence interval coefficients for mass–number relationships of all particle tracer types.**

| particle type | regression equation | $R^2$ | 95% confidence interval equation | variance (particles $g^{-1}$) |
|---|---|---|---|---|
| | | | upper<br>lower | |
| luminophores | y = 606.97x | 0.57 | y = 648.41x<br>y = 565.53x | ± 41 440 |
| PS | y = 0.54x | 0.99 | y = 0.54x<br>y = 0.54x | ± 1 |
| PA | y = 7.66x | 0.99 | y = 7.70x<br>y = 7.61x | ± 40 |

## 3.2. Sediment and microplastic transport induced by *H. diversicolor*

### 3.2.1. Sediment properties

With respect to the median grain size of 184 µm and a sorting of 0.78 (Folk and Ward, 1957) the sediment used in the HD experiment can be classified as moderately sorted fine sand, dominated by the 250 – 125 µm size fraction (Figure 14). Organic matter content was 0.46 ± 0.02% DM (n = 5); POC content was thus determined as 0.18 ± 0.01% DM (n = 5), thus. Mean porosity was 0.36 ± 0.004.

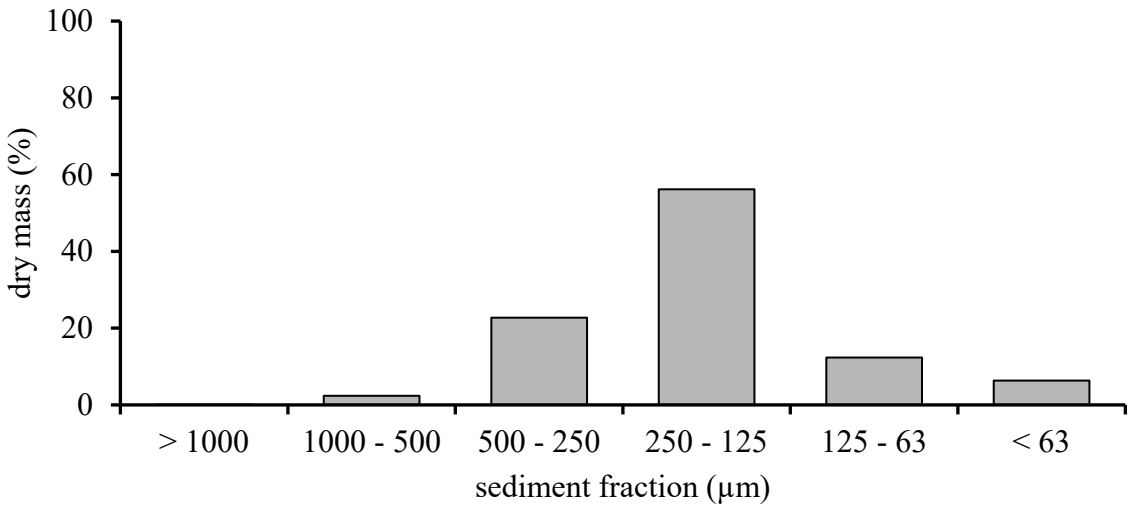


**Figure 14: Grain size distribution of sediment used in the HD experiment.**

### 3.2.2. Visual observation

A thin yellowish-brown layer covering the sediment was observed after several days of incubation in all mesocosms, with an underlying layer of yellow oxidized sediment extending to a depth of 0.5 – 1 cm. Sediment at lower depths was found to have a dark grayish color, indicating anoxic or suboxic conditions. Besides burrow openings established by *H. diversicolor* specimens introduced to the mesocosms, numerous smaller burrow structures with diameters of ~ 1 mm reaching to maximum sediment depths of 1 – 2 cm were noted at the aquaria walls in all mesocosms. These structures can be ascribed to the activity of meiofauna or juvenile stages of polychaetes, indicating that sieving and mesocosm anoxia were not sufficient to remove all fauna. In the majority of mesocosms, several polychaetes that left their burrows during experimental incubation were found, not being able to dig back into the sediment.

Polychaetes were frequently observed to display typical searching behavior by prospecting the sediment surface for food, leaving mucus-lined trails in star-like patterns around most burrow openings. Immobilization of all tracer types at contact with mucus was observable, resulting in the formation of numerous mucus-particle pellets, accompanied by an increasing patchy distribution of tracers at the sediment surface with progressing time. Polychaetes showed an immediate and strong reaction to water exchanges or food addition, resulting in phases of intense searching behavior. Feeding and feeding-mediated particle transport was frequently noted: particles adhering to spinach pieces or polychaetes themselves were moved upon prospecting the sediment surface for food and frequently dragged into the burrows.

### 3.2.3. Mortality and biomass change

During experimental incubation, several polychaetes, most of them with a conspicuously green coloring were found to be lying on the sediment surface, showing only slight movements. Specimens

that were not able to bury back into the sediment within 12 h were removed and not replaced (18 individuals in total, equating a mortality of 30%). Losses by mortality emerged in every mesocosm except HD1 and reached up to 60% of the originally added number of specimens (HD4; Table 4). No statistical difference in mortality between the $F^-$ and $F^+$ group was determined (t test). Further polychaetes died during mesocosm drying in HD1 and HD2 due to long exposition to the heat lamp, these losses were not counted in mortality as depicted in Table 4, though.

All mesocosms with polychaete mortality exhibited a net loss of biomass between 0.7 g and 3.0 g (FM) upon experiment termination, with highest loss coinciding with the highest mortality observed in HD4. In HD1, nearly no net biomass change was detected (Table 4). Biomasses between feeding groups $F^-$ and $F^+$ did not differ significantly either at experiment start or termination (t test).

**Table 4: Total biomasses (g FM) added and recovered from each HD mesocosm.** Net biomass change is shown as difference between experiment start and termination.

| mesocosm | initial biomass (g FM) | terminal biomass (g FM) | net biomass change (g FM) | mortality (ind.) |
|---|---|---|---|---|
| HD1 | 3.95 | 3.97 | 0.02 | - |
| HD2 | 3.84 | 2.63 | - 1.21 | 3 |
| HD3 | 4.10 | 3.41 | - 0.69 | 2 |
| HD4 | 3.75 | 0.73 | - 3.02 | 6 |
| HD5 | 3.85 | 2.46 | - 1.39 | 3 |
| HD6 | 4.17 | 2.74 | - 1.43 | 4 |

### 3.2.4. Ingestion of MP particles

In all six sediment samples taken in total from the $HD_I$ setup, numerous luminophores and PE particles were abundant under UV light, but no structures resembling faecal pellets or similar products of defaecation were found. As no evidence of particle agglutination in faeces was observed, the frequent occurrence of spinach fragments in different stages of decomposition cannot be unambiguously linked to a possible ingestion and defaecation activity by *H. diversicolor*. However, agglutination of spinach fibers, sediment grains and particle tracers with mucus lining produced by polychaetes was observed in one case, illustrating the potential of mucus trails for immobilization of differently sized particles at the sediment water interface and integration into larger aggregates (Figure **15**).

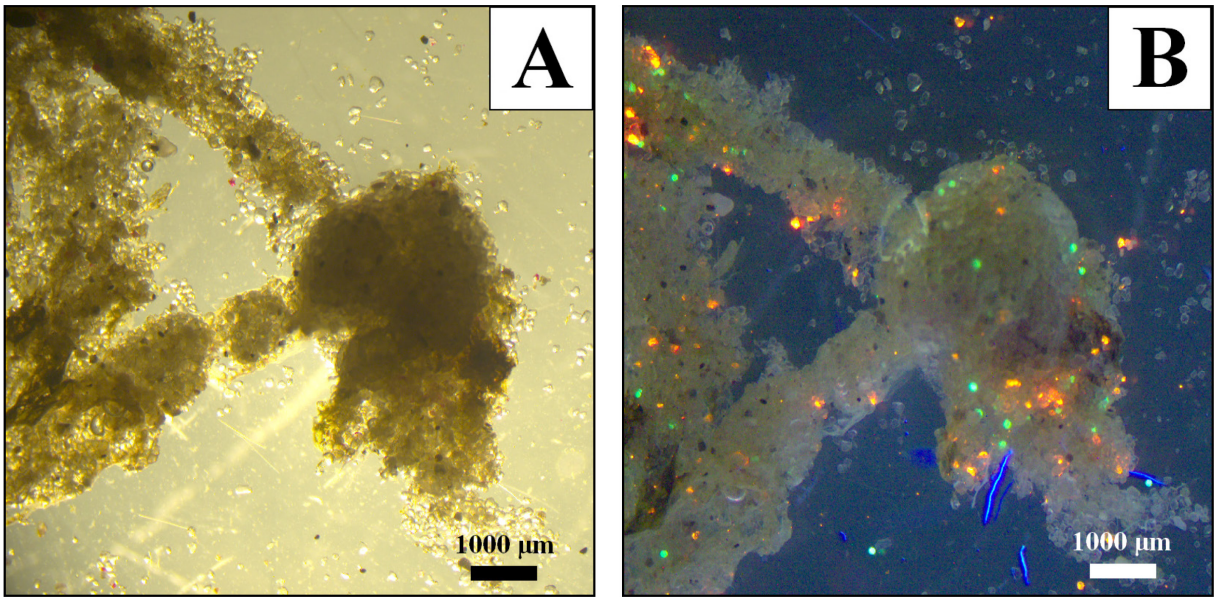


**Figure 15: Aggregate containing sediment particles, spinach fragments, luminophores (red) and PE particles (green), agglutinated by mucus secreted by *H. diversicolor*.** Detail of a sediment sample taken from the $HD_I$ setup, photographed under visible light (A) and UV light (B).

### 3.2.5. Particle transport

Overall particle recovery rates were 95.81 ± 6.05% for luminophores (n = 9), 97.11 ± 4.19% for PE (n = 9 and 96.06% ± for PA particles (n = 9; Appendix, Table A3). In control mesocosms, a mean particle quantity of 98.82 ± 0.52% (luminophores, n = 3), 99.63 ± 0.16% (PE, n = 3) and 95.42 ± 0.65% (PA, n = 3) remained in the sediment surface layer. A small vertical particle export occurred in all control mesocosms down to 16 cm sediment depth with uniform particle concentrations in all subsurface layers (Figure 16). Subsurface PA concentrations were increased in all layers (0.31 ± 0.03%, n=15) compared to luminophores (0.08 ± 0.02%, n = 15) and PE particles (0.02 ± 0.02%, n = 15). Maximum penetration depth of particles (MPD), defined as depth of 99% tracer recovery was highest for PA particles (Table 5) and differed significantly from MPD of PE particles ($p < 0.01$; Games Howell test), but not from luminophores.

Polychaete treatments exhibited stronger vertical particle export than controls with surface layer concentrations of 78.88 ± 11.82% (n = 6) for luminophores, 79.25 ± 9.72% (n = 6) for PE and 78.27 ± 8.58 (n = 6) for PA particles. Below surface level, concentrations of all particle tracers decreased exponentially and reached background concentrations as observed in controls at sediment depths around 10 cm in all mesocosms. Slight subsurface peaks in particle concentrations were determined in several mesocosms within the depth range of 4 – 6 cm with maximum peak concentrations of ~ 10% of total particle quantities added (Figure 17, Figure 18). With respect to controls, luminophores and PE showed generally deeper MPDs (Table 5), this difference was only significant for PE particles in the $F^-$ treatment, though ($p < 0.05$; Games Howell test).

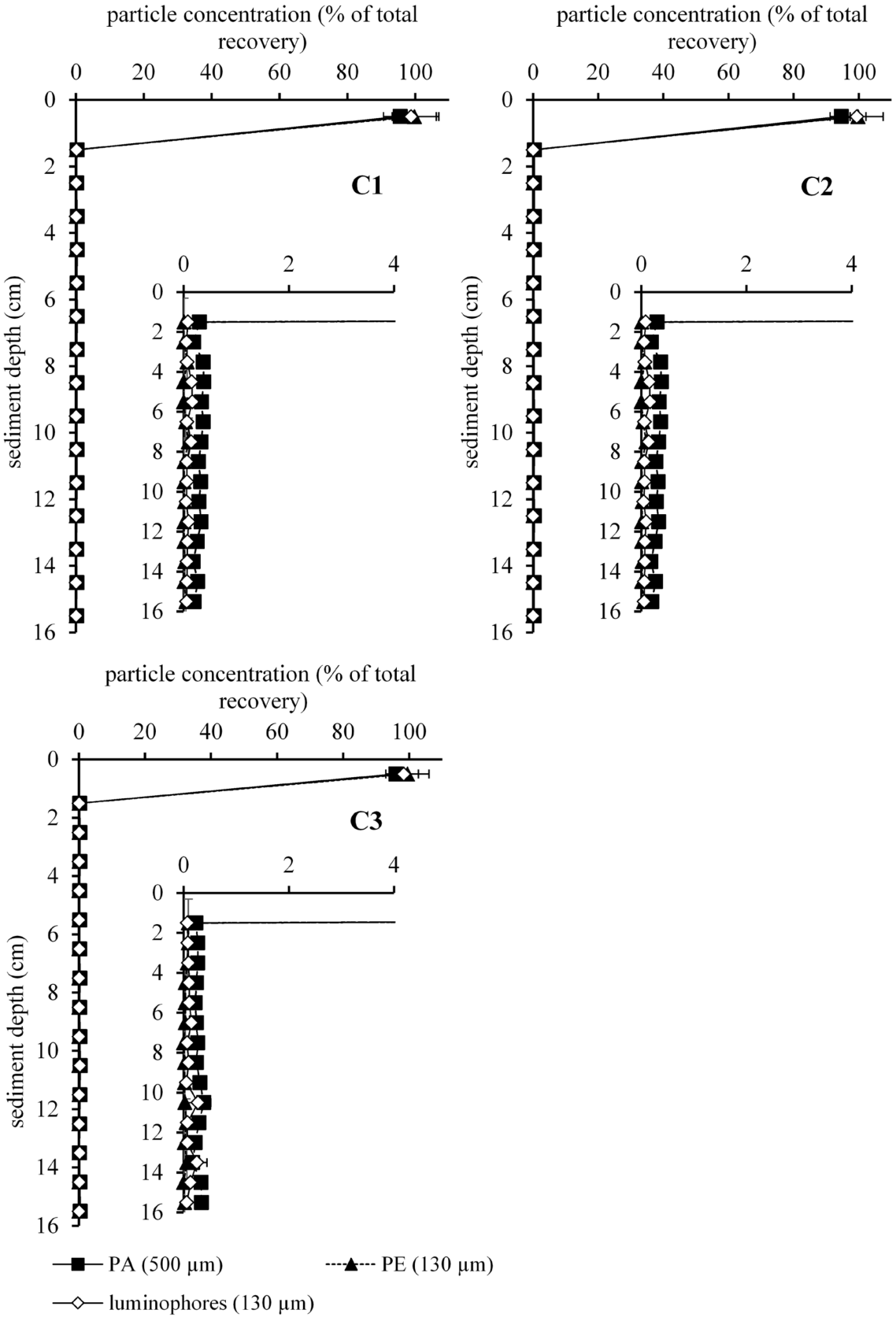


**Figure 16: Luminophore and microplastic (PA, PE) profiles for controls of the HD experiment.** Error bars represent analytical replicates for luminophore concentration determination (mean ± SD; n = 3). Inserts depict low concentration range (0 – 4%).

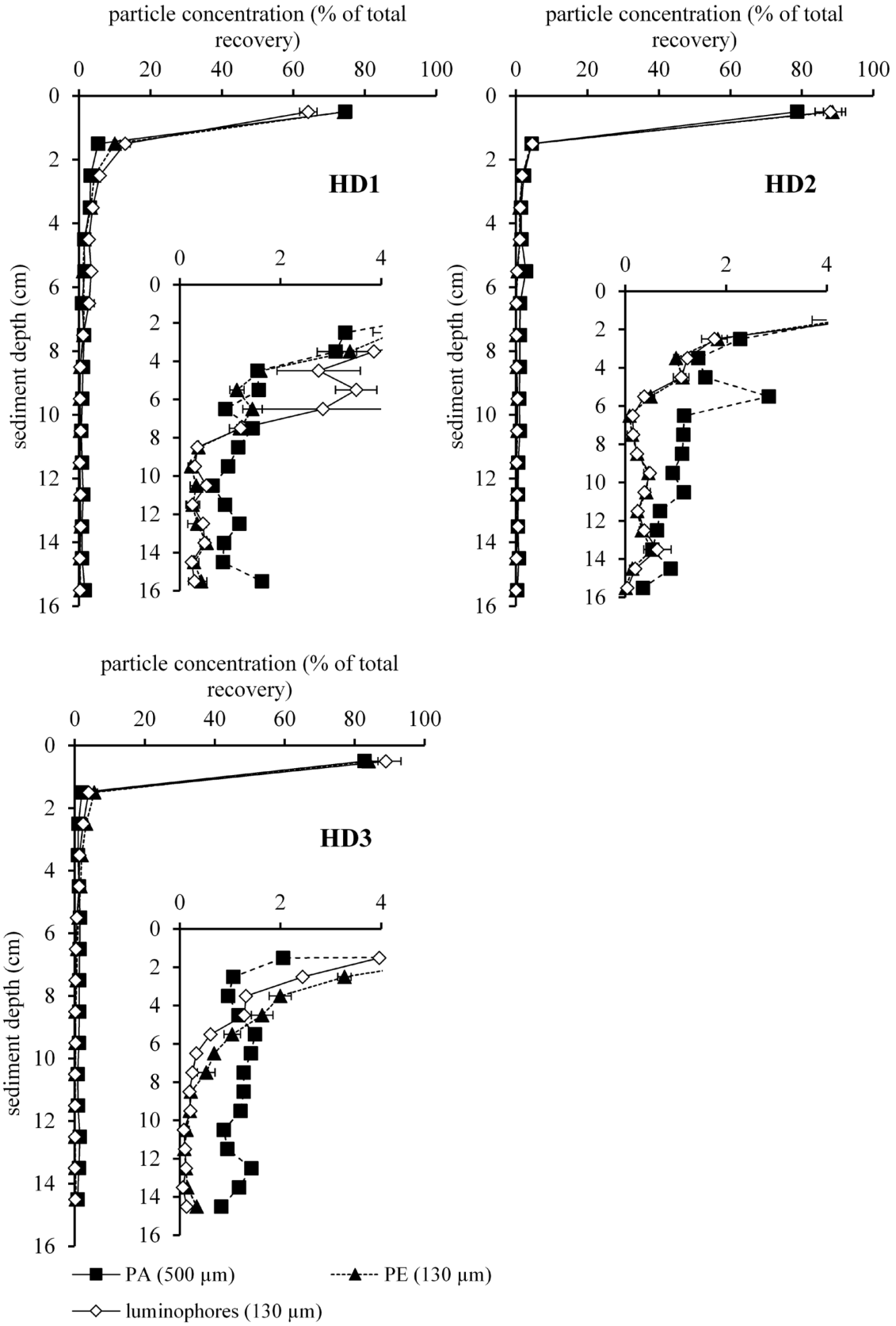


**Figure 17: Luminophore and microplastic (PA, PE) profiles for $F^-$ (no feeding) mesocosms of the HD experiment.** Error bars represent analytical replicates for luminophore concentration determination (mean ± SD; n = 3). Inserts depict low concentration range (0 – 4%).

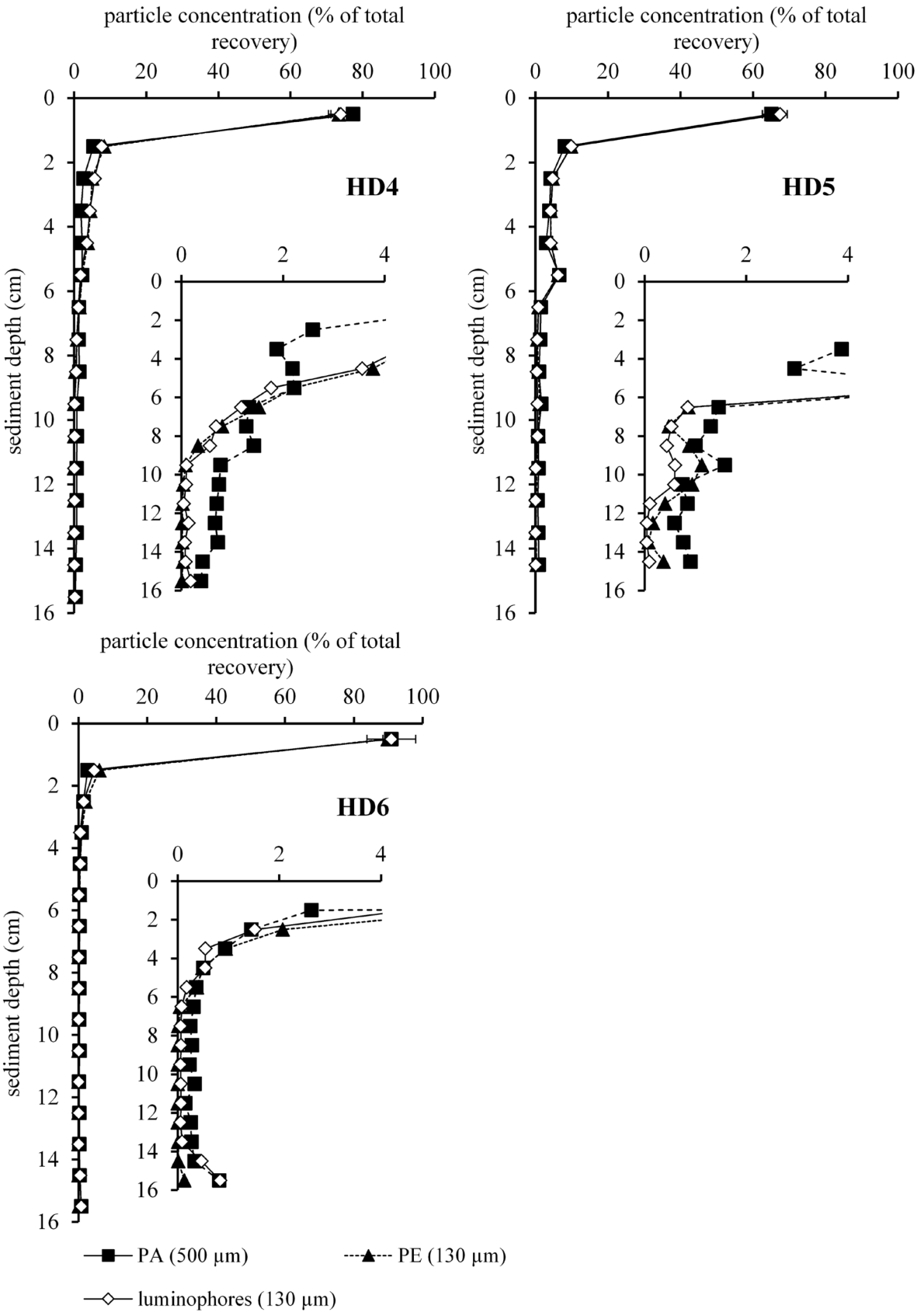


**Figure 18: Luminophore and microplastic (PA, PE) profiles for $F^+$ (feeding) mesocosms of the HD experiment.** Error bars represent analytical replicates for luminophore concentration determination (mean ± SD; n = 3). Inserts depict low concentration range (0 – 4%).

Particle quantities were not significantly different between control, $F^-$ and $F^+$ treatments for luminophores at any depth. For PE particles significant differences were detected only between controls and $F^+$ treatment in the 1 – 2 cm layer ($p < 0.05$; Games Howell test) and between control and $F^-$ treatment in the 4 – 5 cm layer ($p < 0.05$). Particle distribution of PA particles was significantly different between control and $F^-$ treatment in several depth layers (0 – 1 cm, 4 – 5 cm, 6 – 10 cm, 11 – 12 cm and 14 – 15 cm; $p < 0.05$). As a measure for particle export from the surface level and the zone of biodiffusive mixing to deeper sediment layers, cumulative particle concentrations below sediment depths of 1 cm, 4 cm and 10 cm were determined. Again, significant differences were only found between control and $F^-$ treatments for PA particles below all three depths thresholds ($p < 0.05$; Games Howell test). Despite only few significant differences in particle distribution between treatments were found, the MDS analysis conducted with respect to the amount of tracers exported below depths of 1 cm, 4 cm and 10 cm indicated a rough distinction of control and HD mesocosms (Figure 19). However, due to high variances of depth-dependent particle distribution within the polychaete treatments, no clear distinction between both feeding groups could be made.

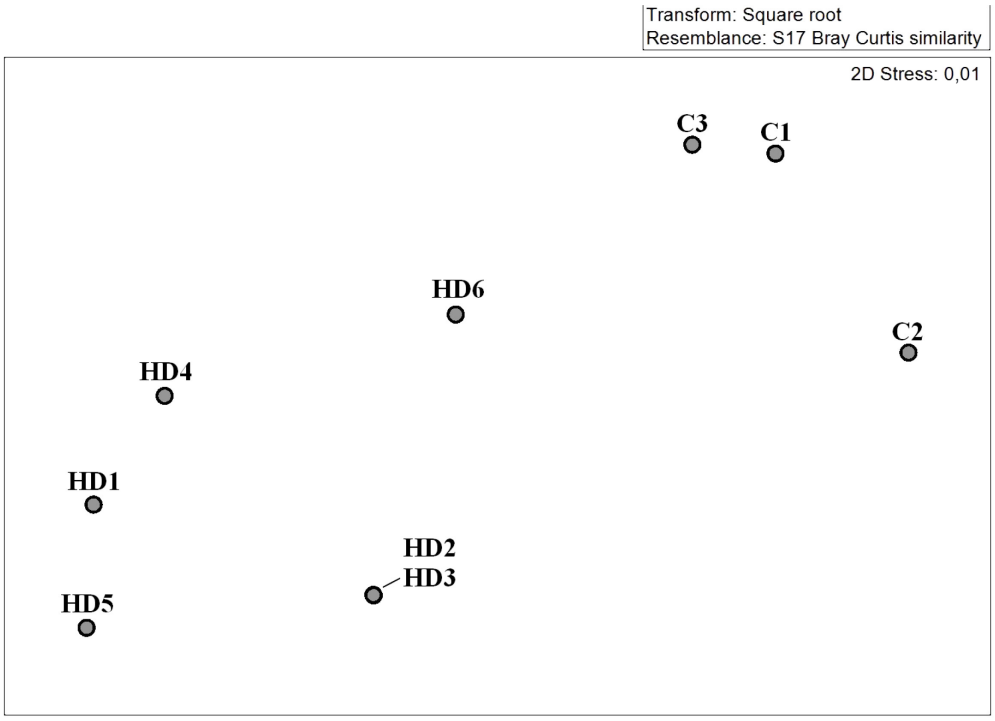


**Figure 19: Two-dimensional MDS plot of controls and HD mesocosms for luminophore and microplastic (PA, PE) concentrations below 1 cm, 4 cm and 10 cm sediment depth.**

PERMANOVA revealed significant effects of the factors particle type, treatment and depth on particle distribution in every depth layer ($p < 0.01$). Interactions occurred between particle type and treatment, particle type and depth as well as between treatment and depth, but not between all three factors together (Appendix, Table A13). PERMDISP test indicated significant differences in

dispersion homogeneity for all three factors ($p < 0.01$). Differences in particle-dependent mixing were evident in control mesocosms, where PA concentrations significantly exceeded luminophore and PE concentrations in most depth layers ($p < 0.05$, Games Howell test). In the $F^-$ treatment, PA concentrations were significantly increased in some sediment layers below 8 cm depth (8 – 10 cm, 11 – 12 cm, 14 – 15 cm; $p < 0.01$, Games Howell test). In the $F^+$ treatment, no differential mixing of particles at any depth was detected.

**Table 5: Maximum penetration depth (MPD) of all particle types used in the HD experiment.** MPD is defined as the depth of 99% recovery of each tracer, respectively.

| mesocosm | luminophores (cm) | PE (cm) | PA (cm) |
|---|---|---|---|
| C1 | 5 | 1 | 12 |
| C2 | 1 | 1 | 13 |
| C3 | 9 | 1 | 13 |
| HD1 | 14 | 14 | 16 |
| HD2 | 13 | 12 | 15 |
| HD3 | 8 | 10 | 14 |
| HD4 | 9 | 8 | 14 |
| HD5 | 10 | 12 | 14 |
| HD6 | 15 | 5 | 15 |

### 3.2.6. Modeled particle transport

As a depth of 2 cm served as a conservative estimate for maximal depth of biodiffusive mixing (see section 4.1.2), this depth threshold was used for modeling of particle concentration data. In control mesocosms, very little biodiffusive particle transport occurred, with *Db* values determined close to zero for luminophores ($0.03 \pm 0.05$ cm$^2$ yr$^{-1}$, $n = 3$) and PE particles ($0.03 \pm 0.06$ cm$^2$ yr$^{-1}$, $n = 3$) No biodiffusive transport of PA particles at all was found. Small non-local transports (r) were detected for all particle types and were more distinct for luminophores ($0.19 \pm 0.21$ yr$^{-1}$, $n = 3$) and PA particles ($0.59 \pm 0.05$ yr$^{-1}$, $n = 3$) than for PE ($0.07 \pm 0.1$ yr$^{-1}$, $n = 3$, Figure 20, Figure 21).

Modeled particle distributions for polychaete treatments resulted in higher local and non-local transport for all particle types compared to controls. Concerning *Db*, highest transports were determined for luminophores, lowest for PA particles (luminophores: $1.51 \pm 1.28$ cm$^2$ yr$^{-1}$; PE: $1.19 \pm 1.28$ cm$^2$ yr$^{-1}$; PA: $0.97 \pm 1.07$ cm$^2$ yr$^{-1}$, $n = 6$), while for *r* this pattern was reversed (luminophores: $0.54 \pm 0.40$ yr$^{-1}$; PE: $0.85 \pm 0.77$ yr$^{-1}$; PA: $1.28 \pm 1.10$ yr$^{-1}$ $n = 6$, Figure 20, Figure 21).

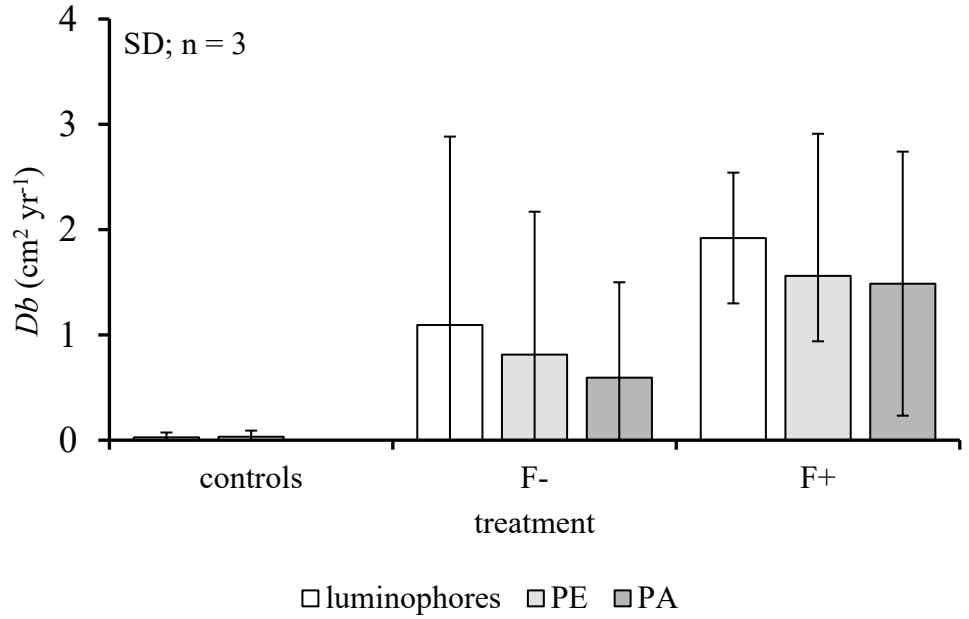


**Figure 20: Biodiffusion (local) transport coefficients (*Db*) of all particle tracers used in the HD experiment, modeled with the gallery-diffuser model.** $F^-$: no feeding group (HD1 - HD3), $F^+$: feeding group (HD4 - HD6).

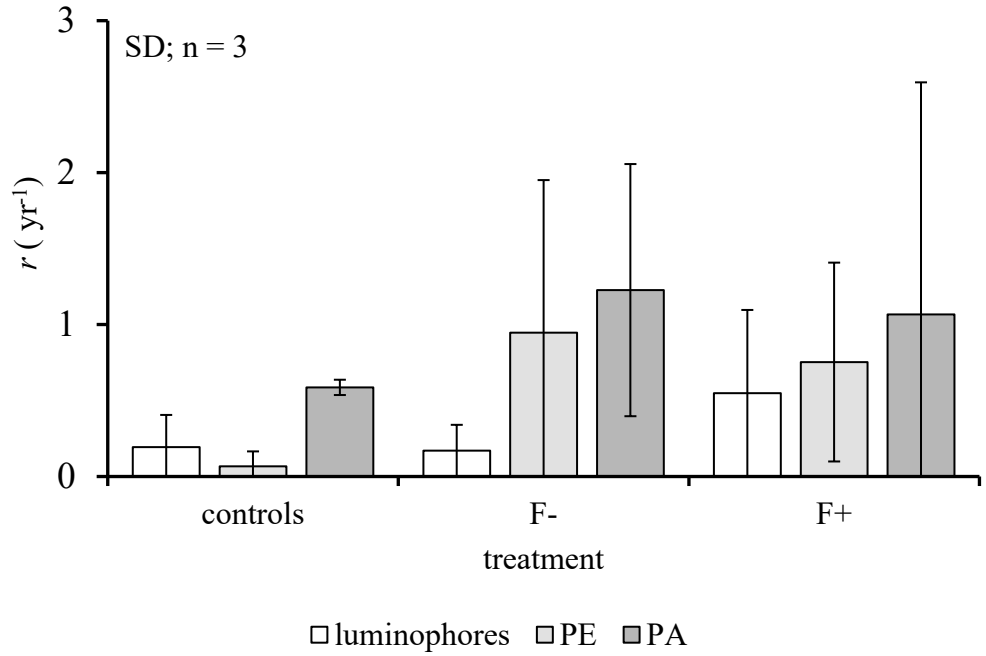


**Figure 21: Biotransport (non-local) coefficients (*r*) of all particle tracers used in the HD experiment, modeled with the gallery-diffuser model.** $F^-$: no feeding group (HD1 - HD3), $F^+$: feeding group (HD4 - HD6).

Due to high variability of modeled transport coefficients, *Db* and *r* values did not differ significantly between control, $F^-$ and $F^+$ treatments. Within the treatments no significant influence of

particle type with respect to intensity of biodiffusive mixing was found. Non-local mixing of PA particles was significantly higher compared to PE in controls ($p < 0.05$), within $F^-$ and $F^+$ treatments no significant differences in particle-dependent non-local transport were found.

## 3.3. Sediment ingestion of *A. marina*

### 3.3.1. Sediment properties

Median grain size of sediment used in both $AM_{SI}$ mesocosms was 258 µm and 273 µm, respectively, dominated by the 500 – 250 µm sediment fraction (64.63% and 63.25%, Figure 22.). Sorting was determined with 0.78 (0.61), hence the sediment was classified as moderately sorted medium sand (Folk and Ward, 1957). Mean porosity was 0.35 ± 0.003 (0.36 ± 0.005, n = 3), mean organic matter content was 0.26 ± 0.02% DM (0.32 ± 0.01% DM, n = 3). POC content was derived from OM content with 0.1 ± 0.01% DM (0.13 ± 0.002% DM, n = 3).

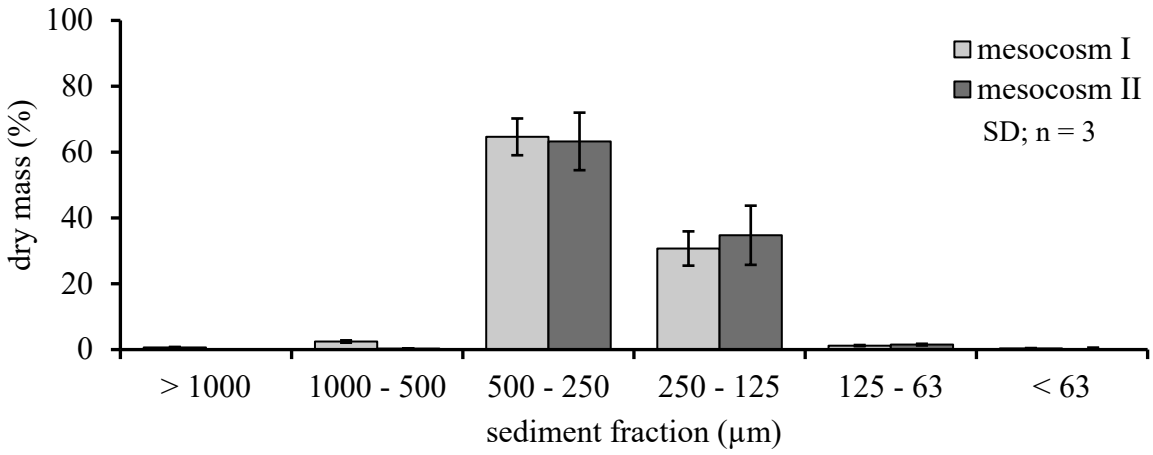


**Figure 22: Grain size distribution of sediment used in both mesocosms of the $AM_{SI}$ experiment.**

### 3.3.2. Visual observation

Faeces production began 1 – 2 d after polychaete introduction in all mesocosms, but was found to be very variable with time and among individuals. Faeces production occurred with a mean rate of ~ 1 cast $d^{-1}$. Individual sediment defaecation was generally composed of phases with elevated activity that lasted 4 – 7 d and phases of similar duration with very little or no apparent sediment defaecation. Additionally, frequent relocation of sites of faecal cast deposition was observable for the majority of polychaetes, indicating a constant re-establishment of burrow structures (i.e. the tail shaft). Alongside tail shaft relocation, fresh deposition of multiple faecal casts at different positions was observed in

some compartments, suggesting frequent movement of polychaetes between newly established and older burrow structures. Faeces were of the same color as surficial sediment (yellowish-brown).

### 3.3.3. Mortality and biomass change

Upon experiment termination, one polychaete ($AM_{SI}5$) could not be recovered and might already have died before the start of the second measuring period, equating an overall mortality of 11%. A net loss of biomass was determined for two individuals ($AM_{SI}7$, $AM_{SI}9$), the remaining specimens showed a mean biomass gain of 0.87 ± 0.57 g (FM, n = 6; Table 6). Total biomasses of both mesocosms differed not significantly from each other, neither at start or end of the experiment. Net biomass change as well did not show significant differences between both mesocosms.

**Table 6: Individual biomass (FM) of all polychaetes added to the $AM_{SI}$ experiment.** Net biomass change per compartment is shown as difference between experiment start and termination. Biomass change for $AM_{SI}5$ could not be determined due to mortality.

| compartment | initial biomass (g FM) | terminal biomass (g FM) | net biomass change (g FM) | mortality (ind.) |
|---|---|---|---|---|
| $AM_{SI}1$ | 2.58 | 3.52 | 0.94 | - |
| $AM_{SI}2$ | 1.81 | 2.43 | 0.63 | - |
| $AM_{SI}3$ | 1.41 | 2.92 | 1.52 | - |
| $AM_{SI}4$ | 2.55 | 2.94 | 0.39 | - |
| $AM_{SI}5$ | 2.25 | | | 1 |
| $AM_{SI}6$ | 1.40 | 1.58 | 0.18 | - |
| $AM_{SI}7$ | 3.26 | 2.79 | -0.47 | - |
| $AM_{SI}8$ | 2.04 | 3.57 | 1.53 | - |
| $AM_{SI}9$ | 2.27 | 2.11 | -0.16 | - |

### 3.3.4. Sediment defaecation of *A. marina*

Sediment defaecation rates showed high variances for single specimens as well as among different polychaetes (Figure 23). Minimum defaecated sediment volume was 0.08 ml $d^{-1}$ ($AM_{SI}9$), maximum volume was 15.34 ml $d^{-1}$ ($AM_{SI}4$). Sediment defaecation rates did not differ significantly between both mesocosms.

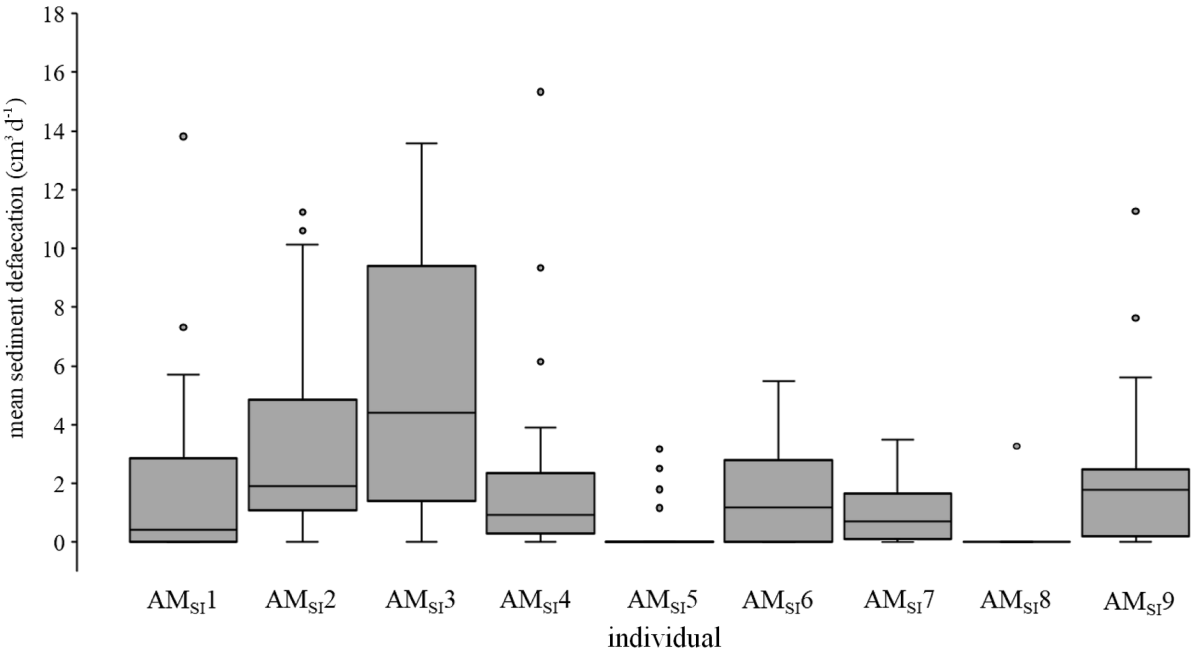


**Figure 23: Mean individual rates of daily sediment defaecation, shown for all polychaetes in the $AM_{SI}$ experiment.**

During the two measuring periods (33 d in total) defaecation occurred on average on 20 d (minimum: 1 d: $AM_{SI}8$; maximum: 33 d, $AM_{SI}3$; Figure 24).

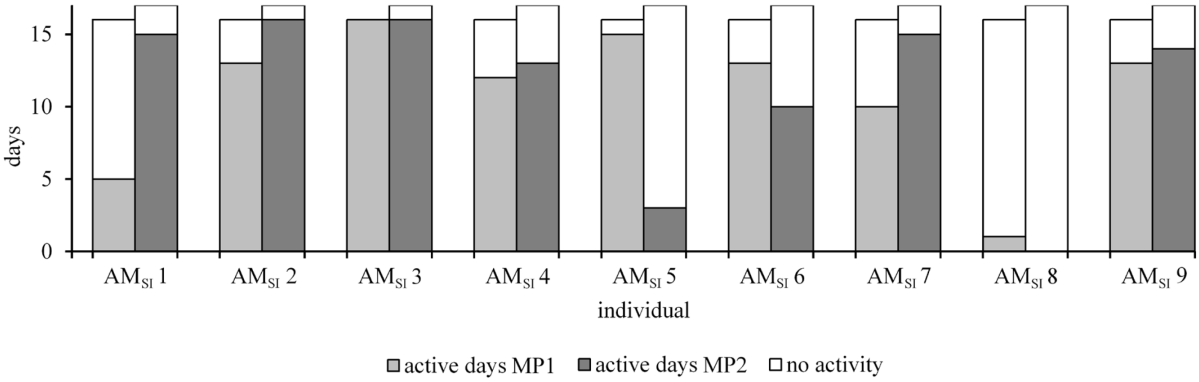


**Figure 24: Number of days with apparent sediment defaecation ("active days"), shown for all polychaetes in the $AM_{SI}$ experiment.** MP1: measurement period 1; MP2: measurement period 2.

Seven polychaetes (77% of total added individuals) showed a relocation of the faeces deposition site, with a minimum rate of a single relocation ($AM_{SI}6$) and a maximum of 30 relocations ($AM_{SI}2$). New burrow openings were established in intervals of 4 – 7 d. In cases of relocation, new burrow openings were often used alongside already existing openings, indicating a frequent movement of polychaetes and the use of several burrow tailshafts for defaecation (Figure 25).

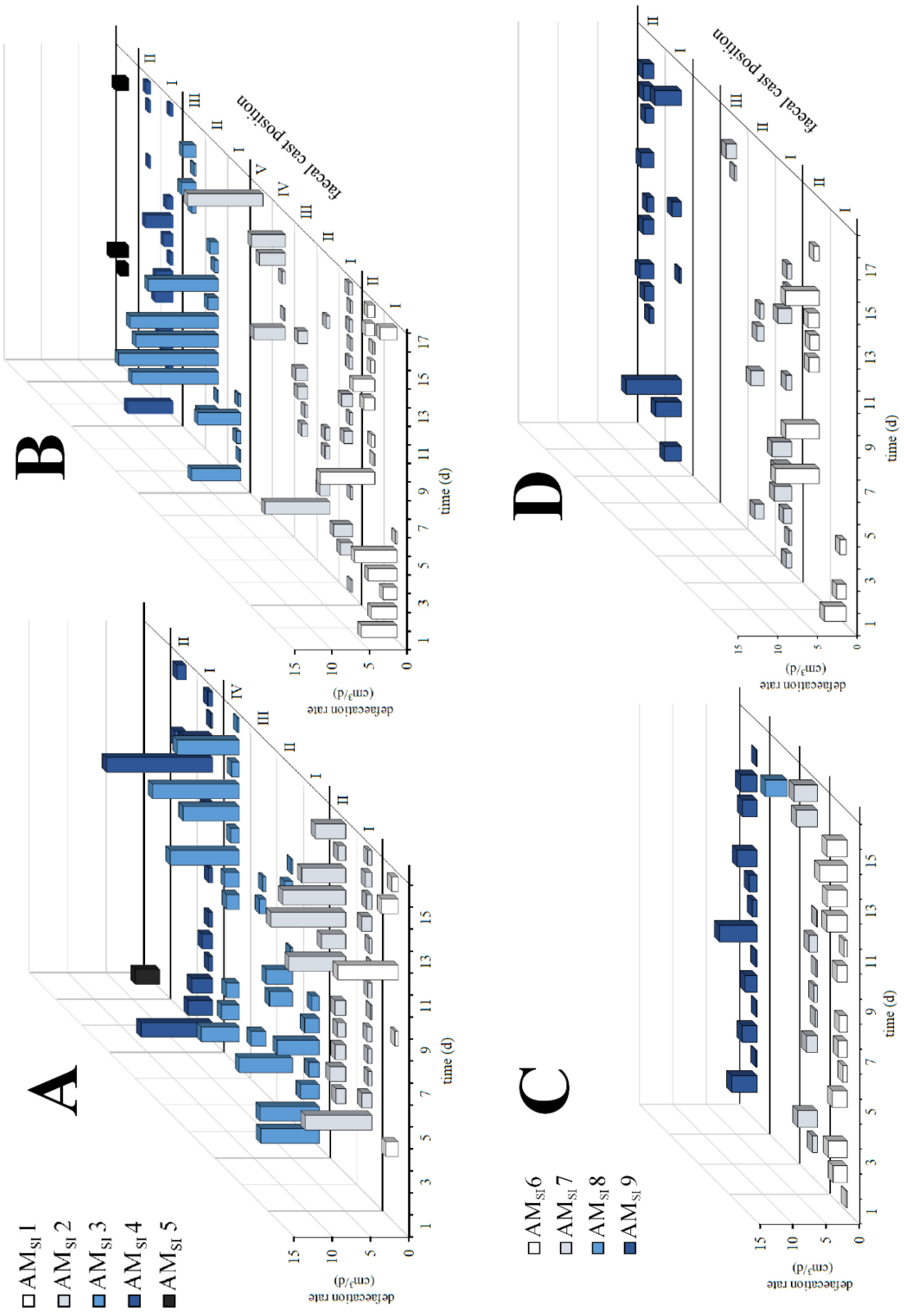


**Figure 25: Individual sediment defaecation rates and sites for both mesocosms and measurement periods of the AMSI experiment.** A, B: mesocosm 1 (AMSI 1 – 5); C, D: mesocosm 2 (AMSI 6 – 9). A, C: measurement period 1; B, D: measurement period 2. Roman numerals depict individual sites of faeces deposition. Sites with same numbers are not identical in different measurement periods.

Mean individual sediment defaecation rate correlated negatively with individual biomass either at experiment start and end (-0.485 and -0.138, respectively, Pearson's correlation), but was not significant, though. Mean sediment defaecation rate and individual biomass change showed a slight positive, but not significant correlation (Figure 26A), which was found to be significant when only days of active defaecation were considered for defaecation rate determination (0.810, $p < 0.05$, Pearson's correlation; Figure 26B). Furthermore, sediment deposition correlated significantly with number of days of active defaecation (0.912, $p < 0.01$; Spearman rank correlation).

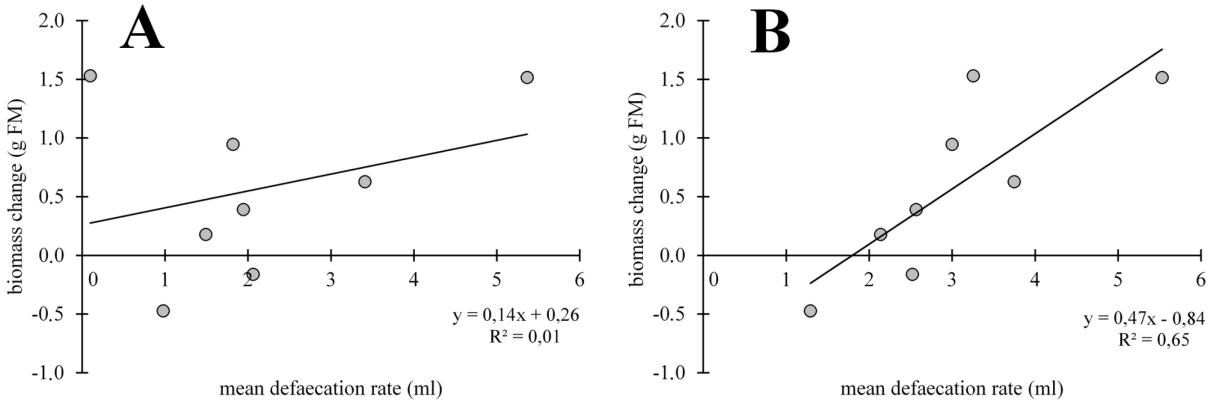


**Figure 26: Correlation of mean individual sediment defaecation rates and net biomass change (FM).** For mean defaecation rate determination, the total time range of the $AM_{SI}$ experiment (A) was considered as well as only the number of days of active sediment defaecation (B).

## 3.4. Sediment and microplastic transport induced by *A. marina*

### 3.4.1. Sediment properties

With a median grain size of 186 mm and sorting of 0.46 the homogenized sediment was classified as well sorted, fine sand. Medium to fine sand within the grain size range of 125 – 250 µm was the dominant sediment fraction (Figure 27), mean sediment porosity was determined with 0.038 ± 0.004 (n = 5). Organic matter content was 0.41 ± 0.02% DM (n = 5) and POC content was determined with 0.16 ± 0.01% DM (n = 5).

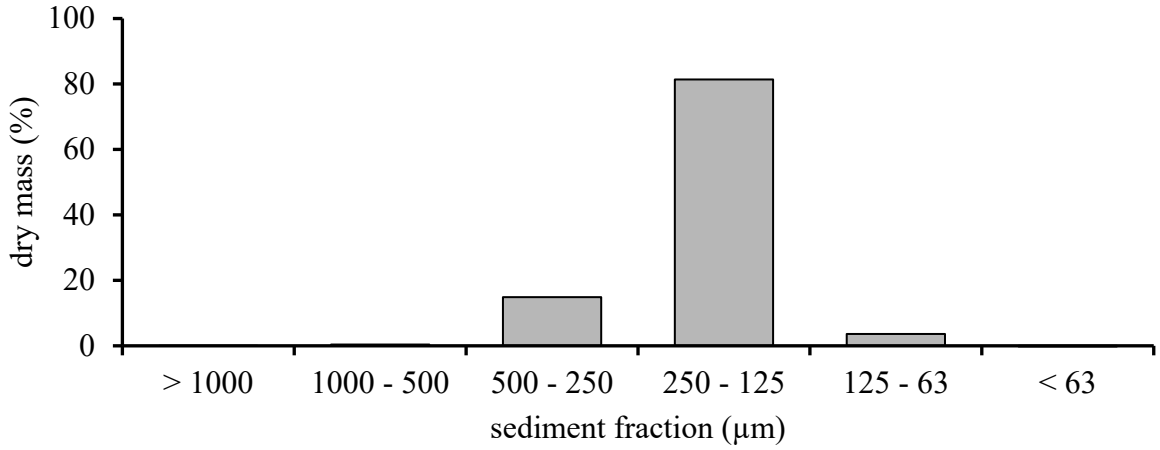


**Figure 27: Grain size distribution of the sediment used in the AM experiment.**

### 3.4.2. Visual observation

[1]"Faeces cast production started 1 - 2 days after polychaete introduction in all mesocosms. Variation with time was high, with a general production rate of 1 cast individual$^{-1}$ day$^{-1}$, but longer phases of inactivity (up to 7 days) could be observed in mesocosms AM1 and AM2. Faeces were colored yellow-brownish, indicating oxidized sediment. Feeding pits occurred only occasionally and if so, only for a limited time. A change of individual positions of feeding pits and casts was observed in all mesocosms every 1 - 3 days, indicating a constant relocation of feeding pockets and tail shafts of the polychaete burrows. Neither during visual observation or smoothing of faecal casts any MP particles were detected in the faeces. However, few days after the start of the experiment, faeces in most mesocosms exhibited a reddish hue, suggesting that luminophores have reached feeding layers and were ingested. Faeces containing luminophores were noticed in regular intervals in all active AM mesocosms until the end of the experiment. The ceasing of faecal cast production in mesocosm AM5 suggested successive death of both individuals 2 and 4 weeks after beginning of the experiment, respectively. Another individual died in AM2. All other polychaetes were retrieved alive during sediment slicing, equaling an overall recovery rate of 83.3%. The sediment depth where polychaetes were found was assumed to be their respective feeding layer. During slicing all sediment layers displayed the same yellowish color pattern as the faeces, no change in sediment coloring was observed with increasing depth."

### 3.4.3. Mortality and biomass change

Polychaete recovery during mesocosm sectioning was 81.25% (13 individuals). Mortality occurred in AM2 (one individual) and AM5 (both individuals), hence no net biomass change could be determined for those mesocosms. A loss of biomass was detected in three mesocosms (AM1, AM6,

[1] The denoted passage is cited according to Gebhardt & Forster (2018).

AM8) with a mean net loss of 1.74 ± 0.74 g (FM), another two showed a distinct net biomass gain of 1 g FM or more (AM4, AM7). No apparent biomass change was found in mesocosm AM3 (Table 7). Incubation time or mean sediment ingestion per mesocosm had no significant effect on biomass change, and neither had the interaction of those two factors (two-way ANOVA).

**Table 7: Individual and total biomasses added and recovered from each AM mesocosm.** Net biomass change is shown as difference between experiment start and termination. Biomass change for AM2 and AM5 could not be determined due to mortality.

| mesocosm | initial biomass (g FM) | | | terminal biomass (g FM) | | | net biomass change (g FM) | mortality (ind.) |
|---|---|---|---|---|---|---|---|---|
| | ind. 1 | ind. 2 | sum | ind. 1 | ind. 2 | sum | | |
| AM1 | 4.92 | 2.92 | 7.84 | 2.01 | 3.56 | 5.57 | - 2.28 | - |
| AM2 | 3.74 | 5.31 | 9.05 | 2.38 | | | | 1 |
| AM3 | 3.91 | 4.25 | 8.16 | 4.03 | 4.32 | 8.35 | 0.19 | - |
| AM4 | 3.39 | 3.08 | 6.47 | 4.94 | 4.07 | 9.01 | 2.54 | - |
| AM5 | 5.23 | 2.48 | 7.71 | | | | | 2 |
| AM6 | 7.57 | 2.96 | 10.53 | 6.83 | 2.81 | 9.64 | - 0.89 | - |
| AM7 | 5.31 | 3.53 | 8.84 | 5.24 | 4.60 | 9.84 | 1.00 | - |
| AM8 | 5.30 | 3.88 | 9.18 | 4.57 | 2.55 | 7.12 | - 2.06 | - |

### 3.4.4. Particle transport

[1]"Mean particle recovery rates were 82.75 ± 16.11% for luminophores (n = 11), 99.59 ± 1.75% for PS (n = 11) and 94.58 ± 2.36% for PA (n = 11; Appendix, Table A14). Particle concentrations in control and AM mesocosms differed significantly from each other in every depth and for every particle type except for 16 – 20 cm depth (luminophores), 2 – 4 and 16 – 20 cm depth (PS) and 18 – 20 cm (PA), (Mann Whitney U test, $p < 0.05$). In the control treatment, nearly all particle tracers recovered remained in the 0 – 2 cm surface layer (luminophores: 95.89 ± 3.90%, PS: 99.99 ± 0.01%, PA: 99.97 ± 0.03%, n = 3; Figure 28). No MPs were found in sediment layers deeper than 4 cm. However, uniform luminophore concentrations were detected in all layers beneath the surface in low concentrations (0.25 ± 0.26%, n = 9). In contrast, a distinct burial of MP particles and luminophores occurred in all mesocosms containing *A. marina*. Maximal burial depth was 14 to 20 cm in all mesocosms and never exceeded below the depth of the lowermost feeding layer. The observed particle distributions showed distinct patterns that differed considerably with respect to particle quantities that were transported below the surface layer (0 – 2 cm) and the depth layer of 6 – 8 cm (lowest position of

[1] The denoted passage is cited according to Gebhardt & Forster (2018).

the uppermost feeding layer recorded in all mesocosms). An exponential decrease of particle tracer concentration with increasing depth was determined for half of all mesocosms (AM1, AM2, AM3, AM5; Figure 29, 30). Particle concentrations in the surface layer remained comparably high (highest: AM2; luminophores: 42.81%, PS: 55.46%, PA: 48.15%; lowest: AM5; luminophores: 24.95%, PS: 20.73%, PA: 28.04%). Maximum penetration depth of particles was lowest for luminophores in AM1 (10 – 12 cm) and highest in AM5 (16 – 18 cm). For PS, MPD ranged between 10 – 12 cm (AM1) and 16 – 18 cm (AM3), for PA between 8 – 10 cm (AM2) and 14 – 16 cm (AM3) (Table 8). Subsurface peaks in MP concentrations were observed in AM1 (8 – 10 cm; PS: 42.29%, PA: 38.71%), AM3 (2 – 4 cm; PS: 50.10%, PA: 36.13%) and AM5 (2 – 4 cm; PS: 50.10%, PA: 36.13%).

In the remaining four mesocosms peaks of plastic particles were observed at 8 – 12 cm sediment depth. Luminophore distribution showed a peak at those depths as well, but in contrast exhibited low but uniform particle concentrations in the uppermost 8 – 10 cm in all mesocosms (6.26 ± 1.38%; n = 4), whereas these layers were almost completely free of MP particles (0.18 ± 0.21% (PS), 0.14 ± 0.15% (PA), n = 4; Figure 29, 30). The maximum penetration depth for all particle tracer types was between 14 cm (AM4) and 20 cm (AM6, AM7, AM8), showing that MPs were buried considerably deeper compared to mesocosms with exponential decreasing particle distribution patterns (Table 8).”

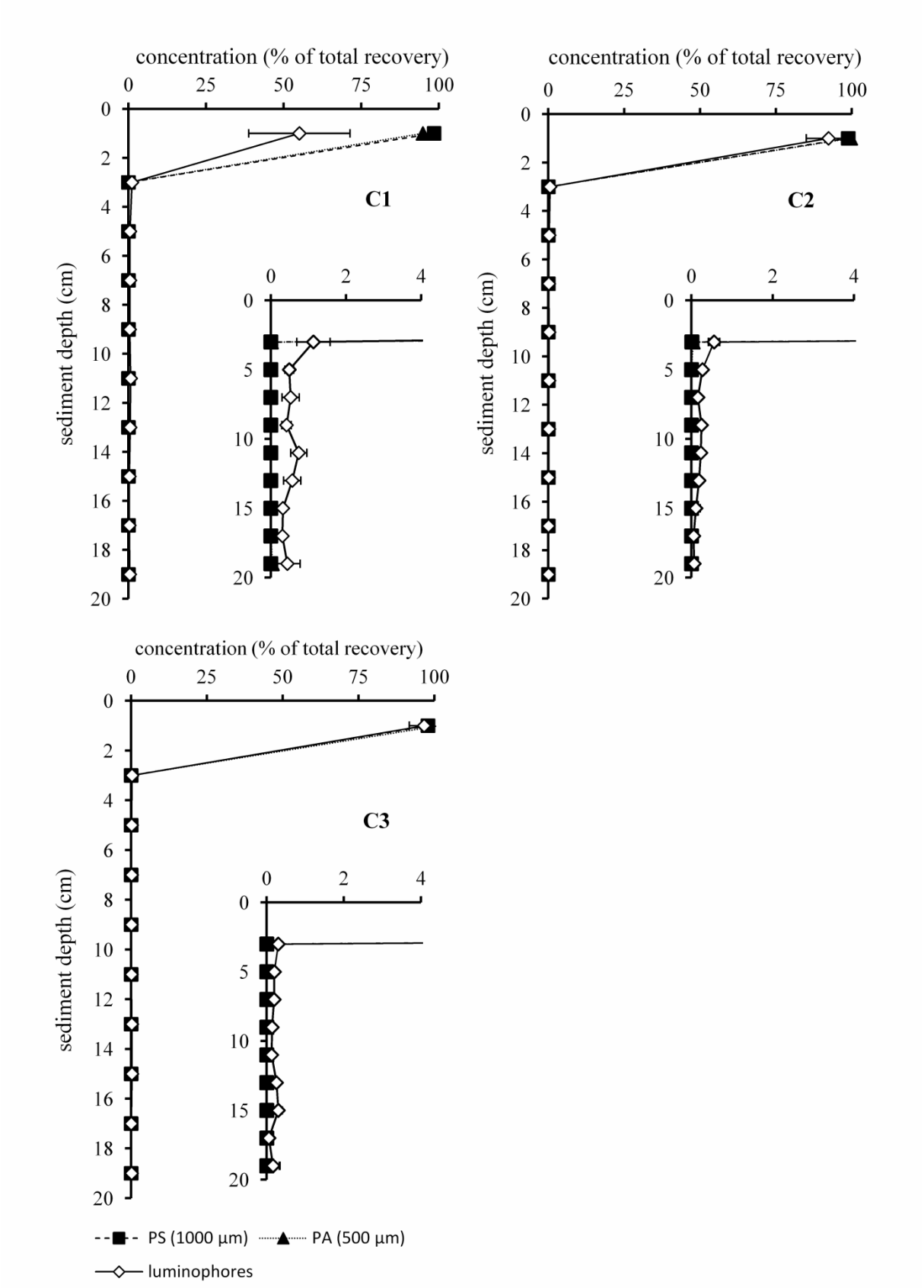


**Figure 28: Luminophore and microplastic particle profiles for AM control mesocosms.** Error bars represent analytical replicates for luminophore concentration determination (mean ± SD; n = 5). Inserts depict low concentration range (0 – 4%).

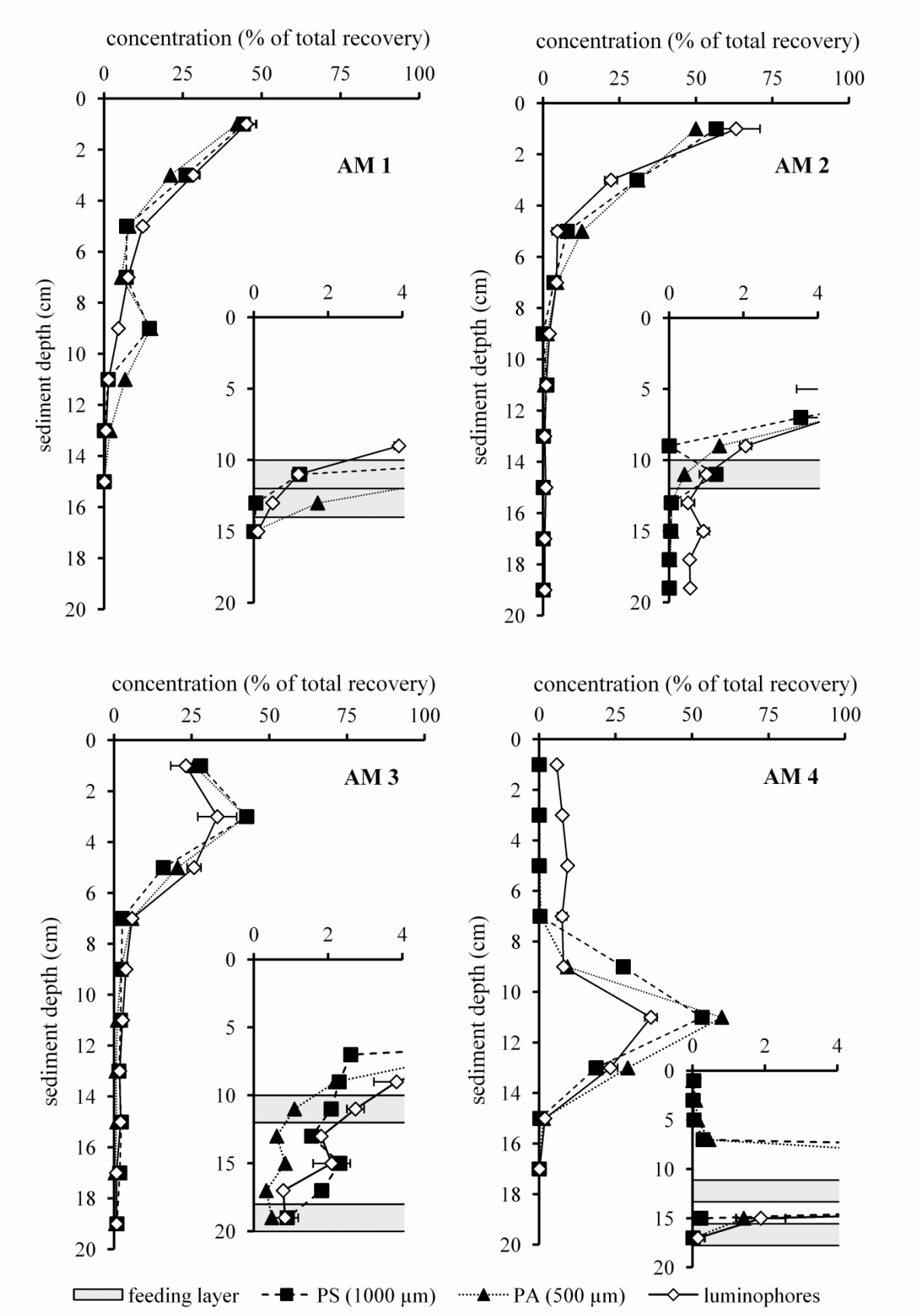


**Figure 29: Luminophore and microplastic particle profiles for mesocosms AM1 - 4.** Error bars represent analytical replicates for luminophore concentration determination (mean ± SD; n = 5). Inserts depict low concentration range (0 – 4%).

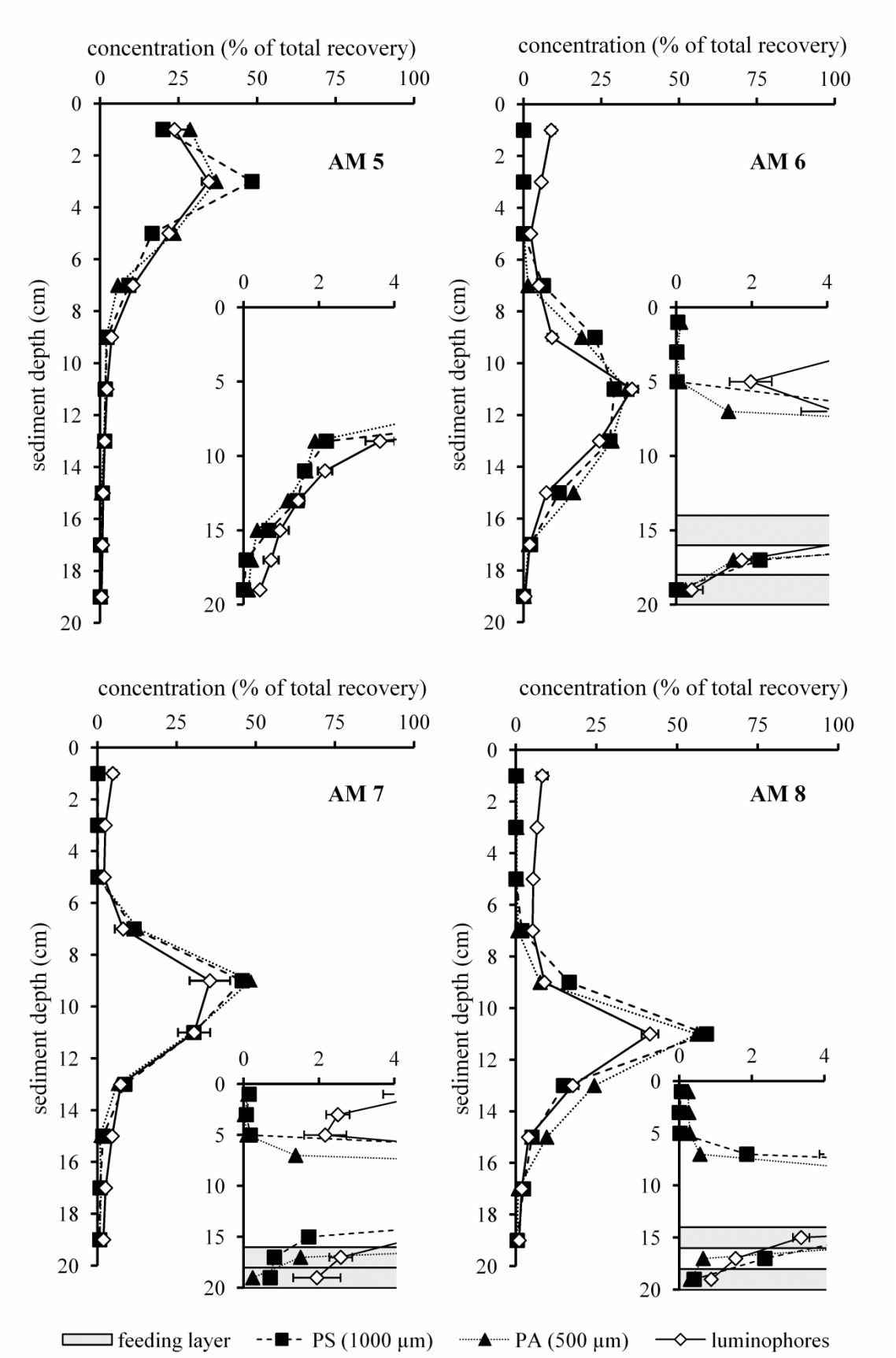


**Figure 30: Luminophore and microplastic particle profiles for mesocosms AM5 - 8.** Error bars represent analytical replicates for luminophore concentration determination (mean ± SD; n = 5). Inserts depict low concentration range (0 – 4%).

**Table 8: Maximum penetration depths (MPD) of all particle types used in the AM experiment.** MPD is defined as the depth of 99% recovery of each tracer, respectively.

| mesocosm | PS (cm) | PA (cm) | luminophores (cm) |
|---|---|---|---|
| C1 | 0 – 2 | 0 – 2 | 16 – 18 |
| C2 | 0 – 2 | 0 – 2 | 6 – 8 |
| C3 | 0 – 2 | 0 – 2 | 8 – 10 |
| AM1 | 10 – 12 | 10 – 12 | 10 – 12 |
| AM2 | 10 – 12 | 8 – 10 | 14 – 16 |
| AM3 | 16 – 18 | 14 – 16 | 16 – 18 |
| AM4 | 12 – 14 | 14 – 16 | 14 – 16 |
| AM5 | 12 – 14 | 12 – 14 | 14 – 16 |
| AM6 | 16 – 18 | 16 – 18 | 16 – 18 |
| AM7 | 16 – 18 | 16 – 18 | 18 – 20 |
| AM8 | 16 – 18 | 16 – 18 | 18 – 20 |

Incubation time (STI: short time interval, runtime ≤ 134 d; LTI: long time interval, runtime ≥ 239 d) did not significantly affect the concentration of luminophores, PS and PA at all depths (Mann Whitney U test). With respect to the amount of particle tracers transported below sediment depths of 2 and 8 cm the MDS analysis indicated the existence of two distinct groups with little variance among mesocosms in Group 1 (AM4, AM6, AM7, AM8) and larger differences between mesocosms in Group 2 (AM1, AM2, AM3, AM5; Figure 31).

Particle concentrations below 2 and 8 cm differed significantly between these two groups for all particle types (Mann Whitney U test, $p = 0.029$ for all tests). No significant differences between concentrations of luminophores, PS and PA at all depths could be detected in STI and LTI groups (Games Howell test, $p > 0.05$). However, when grouped according to the MDS, concentrations of luminophores differed significantly from MP concentrations at the depth range of 0 – 4 cm in Group 1 (AM4, AM6, AM7, AM8; Games Howell test, $p < 0.05$).

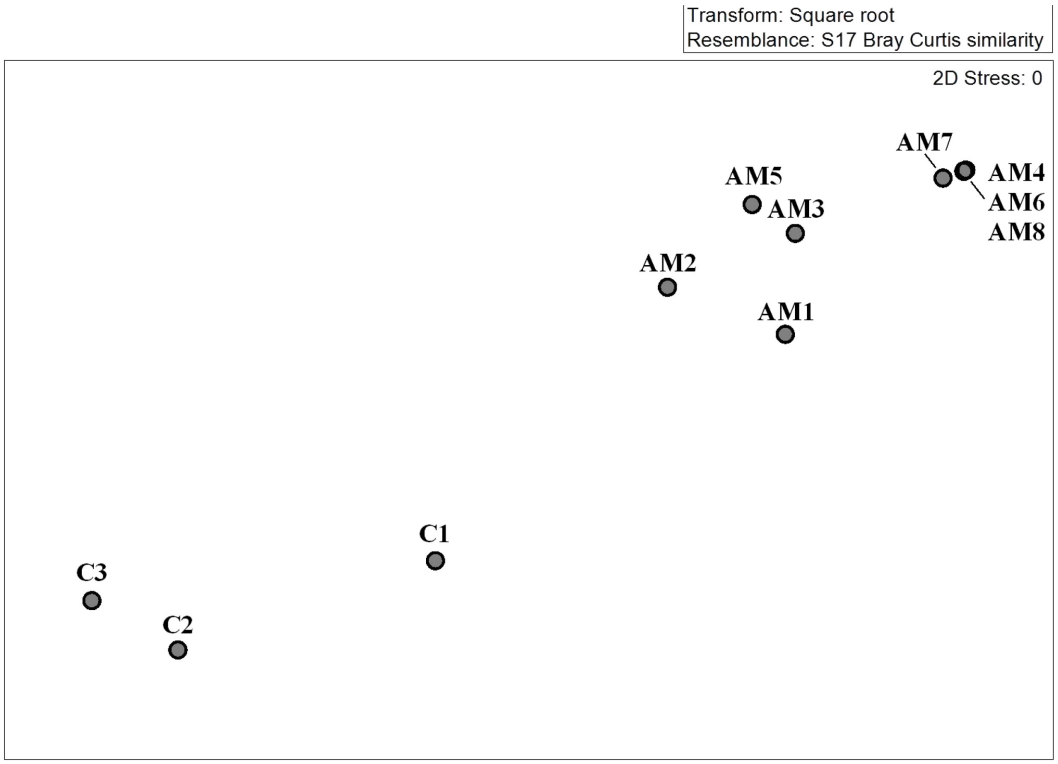


**Figure 31: Two-dimensional MDS plot of controls and AM mesocosms for luminophore and microplastic (PS, PA) concentrations below 2 cm and 8 cm sediment depth.**

### 3.4.5. Grain size distribution

After experiment termination, sediment grain size in control treatments showed a uniform distribution between the sediment surface (0 – 2 cm; 240 ± 33.51 µm, n = 3) and the bottom layer (18 – 20 cm; 233 ± 42.13 µm. n = 3; Figure 32). In contrast, polychaete bioturbation had profound effect on grain size in all AM mesocosms. Compared to controls, surface median grain size (0 – 2 cm) was slightly lowered in AM mesocosms (223 ± 18.35 µm, n = 8), but without rendering the difference statistically significant. A general increase of mean grain size was observed in feeding layers and was found to be less pronounced for upper feeding layers (UFL: residence depth of the uppermost specimen of *A. marina*, which was assumed to be its respective feeding layer; 234 ± 15.2 µm; n = 7; Figure 32) than for lower feeding layers (LFL: residence depth of the lowermost specimen of *A. marina*; 270 ± 30.65 µm; n = 7, Figure 32). Grain size changes for LFLs were significantly different from changes found in UFL and surface layers (Tukey HSD test, $p < 0.05$).

The factor incubation time (STI, LTI) had no significant effect on median grain size, there was, however, a significant influence of the factor sediment depth (surface, LFL, UFL; two-way ANOVA, $p < 0.05$). Interaction of incubation time and sediment depth had no significant effect on grain size distribution. Among LTI mesocosms, LFL sediment had significant higher median grain size (284 ± 20.81 µm, n = 4) than surface (222 ± 22.21 µm, n = 5; p = 0.003) and UFL sediments (230 ± 16.63 µm, n = 4; $p < 0.05$, Tukey HSD test). When results of the MDS analysis were

considered and mesocosms were grouped accordingly, the interaction of factors group (Group 1, Group 2) and sediment depth was found to be significant (two-way ANOVA, $p < 0.05$). In Group 1 a significant difference between median grain size at different sediment depths was found (ANOVA, $p < 0.001$). Grain size for LFL (281 ± 22.15 µm, n = 4) was significantly higher compared to surface (209 ± 13.25 µm, n = 4; p = 0.000) and UFL sediments (224 ± 12.45 µm, n = 4; 0.002; Tukey HSD test). No such difference was found in Group 2.

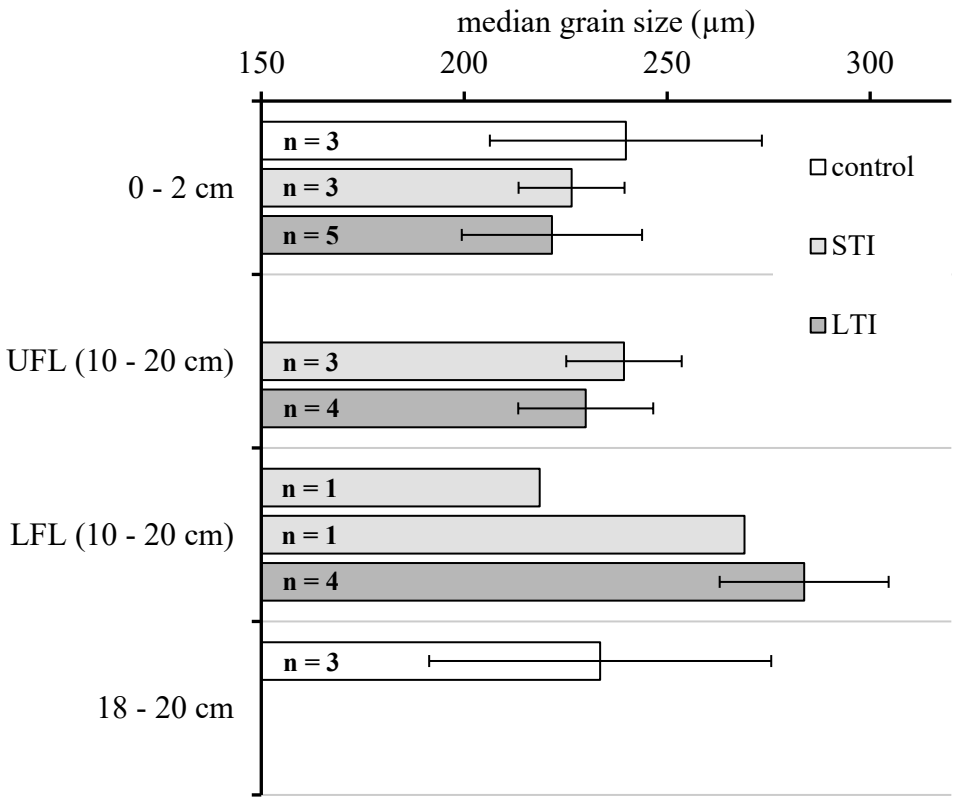


**Figure 32: Median grain size for all AM mesocosms after experiment termination, grouped as controls, STI (short time interval: runtime ≤134 d) and LTI (long time interval: runtime 239/240 d).** Median grain size is shown for surface layers, upper feeding layers (UFL: residence depth of the uppermost polychaete), lower feeding layers (LFL: residence depth of the lowermost polychaete) and bottom layers (controls only).

# 4. DISCUSSION

## 4.1. Particle and microplastic transport induced by *H. diversicolor*

### 4.1.1. Microplastic ingestion

No clear evidence of MP ingestion was found in the $HD_I$ experiment, as no faecal pellets could clearly be identified during sampling. Luminophores and PE particles visible on sample images (e.g. Figure 15) most likely originate from the initial particle tracer layer at the sediment surface and were sampled by accident. Gut contents of polychaetes recovered after experiment termination were not analyzed for MP, either. Hence, the ingestion and subsequent redistribution of MP particles by *H. diversicolor* cannot be verified by experimental data, but nevertheless can considered being plausible based on observations made in the $HD_I$ setup.

The frequent ingestion of MPs by benthic deposit feeders can be expected, since these organisms live in immediate proximity to an interface of marine MP accumulation. Hence, MP uptake is recognized to be common for benthic invertebrates and has been verified for various polychaete taxa both in the laboratory (Besseling et al., 2017; Setälä et al., 2016) and in the field (Mathalon and Hill, 2014; Van Cauwenberghe et al., 2015a). As many other sediment-dwellers, benthic deposit-feeding polychaetes are generally prone to the ingestion of small plastic particles – due to the need to process large sediment volumes to subsist from sediment-feeding (Lopez and Levinton, 1987) or the preferred ingestion of less dense particles, often carrying biofilms, which resemble organic particles or aggregates (Self and Jumars, 1988). Though, the potential of MP ingestion is strongly affected by individual feeding type (Setälä et al., 2016). As *H. diversicolor* is known to display a diverse feeding ecology, including surface deposit feeding (Reise, 1979), scavenging, predatory feeding (Fauchald and Jumars, 1979) and facultative suspension feeding (Riisgård, 1991), this versatility in food assembly might cause the increased uptake of MPs originating from various sources.

Based on its flexible diet, the gut content of *H. diversicolor* is mainly constituted by plant detritus, invertebrates and mucus (Costa et al., 2006). Sediment only accounts for a minor part of ingested material, as *H. diversicolor* does not conduct sediment feeding in a strict sense. Sediment uptake can rather be regarded a byproduct of feeding, causing ingestion of sediment grains adhering to food particles or mucus and hence might represent a pathway for the potential ingestion of similar-sized MP. In the context of the optimal foraging theory, the preferential uptake of low-density particles by many benthic invertebrates is hypothesized (Self and Jumars, 1988), which might promote MP ingestion as well. Active ingestion of man-made particles by *H. diversicolor* has been described repeatedly, including the uptake of paint particles (500 – 2000 µm diameter) in coastal zones of the southwest English coast (Muller-Karanassos et al., 2019) as well as the ingestion of PA particles (2000 µm diameter) in mesocosm experiments (Delefosse and Kristensen, 2012). Accordingly, PA

particles used in the HD and $HD_I$ experiment (diameter 500 µm) might be regularly ingested alongside much smaller PE particles.

While MP ingestion potentially occurs upon assembling food at the sediment surface, mucus, which is secreted to aid the collection of food particles, likely promotes the scavenging and subsequent uptake of MPs by *H. diversicolor*. The effect of mucus linings on MP immobilization at the sediment surface was clearly seen in some $HD_I$ samples and is very likely to provide an effective mechanism for MP ingestion, as ingested mucus often accounts for up to 50% of the total gut content found in *H. diversicolor* (Costa et al., 2006), illustrating the importance in obtaining food (mostly phytoplankton and bacteria) by the use of mucus trails or nets. Mucus linings found at the sediment water interface can serve as effective traps for MP either sinking down or transported laterally by bed load transport and might immobilize MP with particles diameters of a few µm (i.e. the size range of phytoplankton). Furthermore, mucus secretion allows *H. diversicolor* to establish a filter system to gain food by utilizing water flow during burrow ventilation. Particle retention rates close to 100% for particles larger than 7.5 µm (Riisgård, 1991) are indicating high efficiency in terms of capturing particles in the same size class as phytoplankton. Suspension feeding using mucus nets might hence represent an additional pathway for deposition and ingestion of small MPs usually found in the water column, resembling MP uptake mechanisms known from other filter feeders. Filtration activity of *H. diversicolor* can induce the turnover of substantial water volumes, and hence might exert considerable control over local phytoplankton biomass. In the Odense Fjord, the clearance rate of a local *H. diversicolor* population with a mean abundance of 2400 ind. $m^{-2}$ was calculated to be ~ 10 $m^3$ $d^{-1}$, equaling a tenfold turnover of the overlying water column (Riisgård, 1991), and might consequently represent an effective mechanism for the removal of floating MP in shallow waters. Suspension feeding intensity is mainly mediated by ambient temperature and phytoplankton productivity (Vedel et al., 1994), inducing strong seasonal patterns in clearance rates. While reaching an annual minimum in autumn, suspension feeding can account for 50 – 100% of the polychaete's total feeding activity during summer (Vedel et al., 1994), which is also reflected by increased mucus contents in the gut during this season (Costa et al., 2006). Thus, suspension feeding by *H. diversicolor* might be a relevant process for MP removal from the water column during summer months, reaching clearance rates comparable to those determined for other, obligate filter feeders as bivalves (Ward and Kach, 2009; Wegner et al., 2012). Nevertheless, MP uptake via deposit feeding will not lead to any net vertical particle translocation, as particles in question are deposited at the site of their ingestion (i.e. the sediment surface; Gunnarsson et al., 1999; Kulkarni and Panchang, 2015; Figure 2C).

Additionally, particles can be moved in the wake of the polychaete's food prospecting behavior or adhere to the animals themselves and food items and can consequently be transported into burrows, leading to a net burial of surficial material (Duport et al., 2006; Scaps, 2002). Deposition feeding of *H. diversicolor* is known to exhibit strong variability, affected by food presence (Murray et al., 2017; Nogaro et al., 2007), water inundation period (Esselink and Zwarts, 1989) and daily light cycle (Tang

and Kristensen, 2007; Wenzhöfer and Glud, 2004) and thus, can be expected to have a stronger influence on MP burial during summer months. Suspension feeding causes the immobilization, ingestion and defaecation of particles and hence, induces a net deposition of material originating from the water column at the sediment surface. Surficial deposition within faecal pellets or immobilization at mucus linings make MPs accessible to other benthic epi- or infauna, which subsequently might promote further transport or burial of those particles. With respect to absolute MP transport rates mediated by *H. diversicolor*, suspension feeding might represent an environmentally more relevant process than deposit feeding, as particle retention rates for small particles are high and known MP abundances in most habitats tend to strongly increase with decreasing particle size (Song et al., 2014).

### 4.1.2. Modeling

Uncertainties in modeling results might arise from the need to arbitrarily set the biodiffusive mixing depth when applying the biodiffuser model. Depth of biodiffusive mixing is mainly governed by burrow morphology, which is often difficult to assess, though. Particle distributions determined for both feeding treatments represent the sum of activities carried out by all polychaetes of the respective mesocosms, at which individual contributions to the community bioturbation performance might strongly differ. The best fit for determined concentration profiles was obtained for low biodiffusive layer depths of 1 cm (Figure 33), indicating biodiffusive transport to be restricted to the uppermost sediment cm. Biodiffusive mixing depths for *H. diversicolor* are known to extend in a range of 1 cm to 5 cm sediment depth (François et al., 2002; Hedman et al., 2011). Surface-near particle burial depths usually are associated with the feeding behavior of *H. diversicolor*, as particles were dragged into the gallery system for safe food ingestion in absence of potential intra- and interspecific competitors or predators as birds and fish (Rosa et al., 2008), resulting in burial depths of the captured material of ~ 0.5 – 1.5 cm (Delefosse and Kristensen, 2012; Murray et al., 2017).

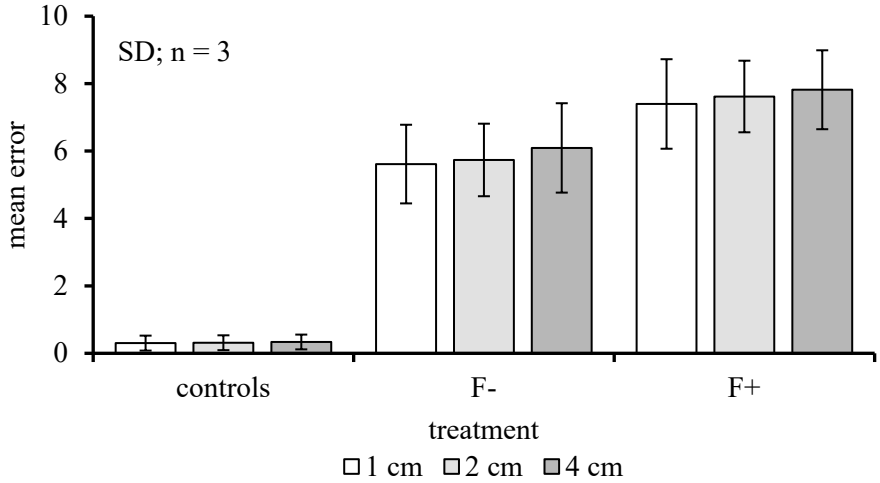


**Figure 33: Mean error, representing fit of the gallery-diffuser model to obtained particle distributions in the HD experiment.** Values shown for different biodiffusive mixing depths applied (1 cm, 2 cm, 4 cm).

In terms of local transport, modeled *Db*s showed a slight increase with increasing biodiffusive layer depth (applied depth thresholds: 1 cm, 2 cm, 4 cm), with results not being statistically significant due to overall variability (Figure 34), though. Non-local transport coefficients exhibited stronger dependency on biodiffusive mixing depth, resulting in stronger reduction of particle transport with increasing depth thresholds. Though *r* values for PE particles doubled for biodiffusive mixing depths of 1 cm compared to the 4 cm depth interval in the $F^+$ treatment, differences in particle transport between those depth thresholds were only statistically significant in the $F^-$ group ($p = 0.039$, Games Howell test; Figure 35). Considering observed particle distributions in both feeding treatments, which show no exponential decrease in particle concentrations below sediment depths of 2 – 3 cm, biodiffusive mixing depth was set to 2 cm in all mesocosms for modeling purposes, being in good accordance to literature data.

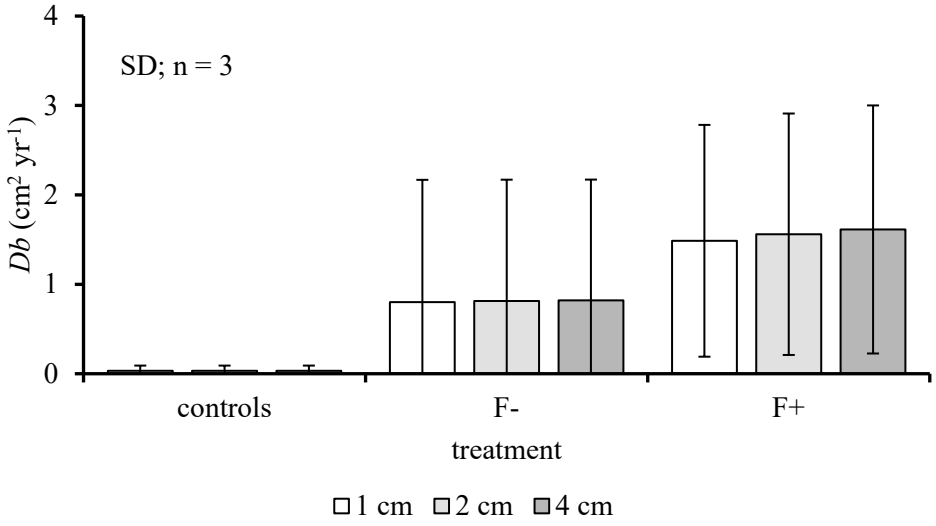


**Figure 34: Local transport coefficients (*Db*) of the HD experiment, shown for PE particles and modeled for different biodiffusive mixing depths (1 cm, 2 cm, 4 cm).** $F^-$: no feeding group (HD1 - HD3), $F^+$: feeding group (HD4 - HD6).

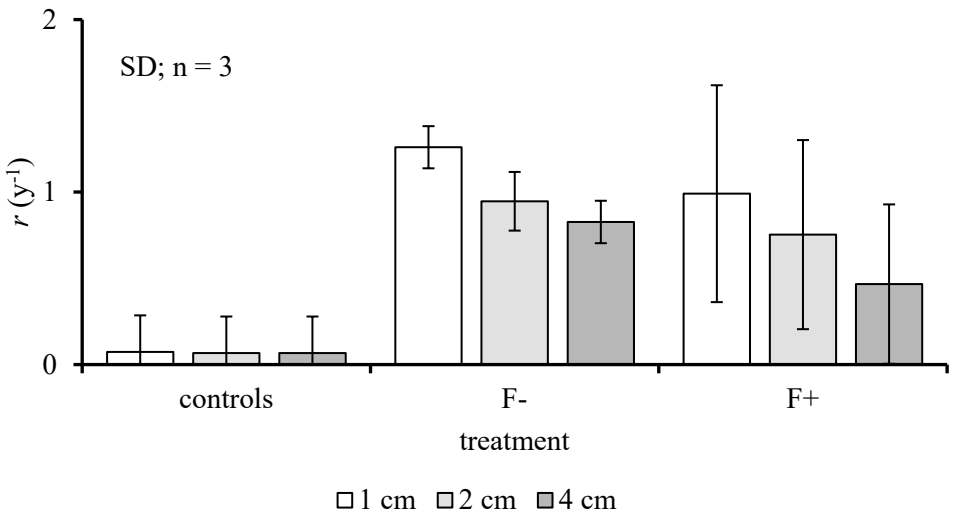


**Figure 35: Non-local transport coefficients (*r*) of the HD experiment, shown for PE particles and modeled for different biodiffusive mixing depths (1 cm, 2 cm, 4 cm).** $F^-$: no feeding group (HD1 - HD3), $F^+$: feeding group (HD4 - HD6).

### 4.1.3. Bioturbation of microplastic

Polychaete activity increased vertical particle export from the sediment surface compared to control mesocosms, as seen in lowered surficial particle tracer concentrations of 60 – 90% in both feeding groups. Observed particle distributions showed exponential decreases in concentration within the upper 4 cm in all mesocosms, representing diffusion-analogous particle transport. Particle concentrations in deeper sediment layers were uniformly low, but exceeded down to sediment depths > 10 cm. The increase of maximum burial depths below 10 cm in most $F^-$ and $F^+$ mesocosms indicates non-local particle transport, as well as the occurrence of faint particle peaks found in mesocosms HD2 and HD5. Simultaneous occurrence of local and non-local particle transport is characteristic for bioturbation of the gallery-diffusor *H. diversicolor* (Cournane et al., 2010; Duport et al., 2007). However, as particle concentrations within the biodiffusive layer exhibit strong variations and are uniformly low below biodiffusive layer depths (4 cm) in most mesocosms, no significant differences with respect to particle distribution between controls and $F^-/F^+$ treatments were found. MDS results (Figure 19) allow a rough distinction of control and $F^-/F^+$ mesocosms with respect to particle relocation, indicating a certain effect of polychaete activity on particle redistribution.

Modeled biodiffusion coefficients range between 0.59 $cm^2$ $yr^{-1}$ (PA; $F^-$ treatment) and 1.97 $cm^2$ $yr^{-1}$ (luminophores, $F^+$ treatment), and hence are well within the range of values obtained by other experiments using similar temperatures and abundances (Duport et al., 2007; Hedman et al., 2011). Contrasting *Db*, *r* values were increased compared to controls in $F^-/F^+$ mesocosms, but were generally low with minimum values of 0.27 $yr^{-1}$ (luminophores, $F^+$ treatment) and maximum values of 1.23 $yr^{-1}$ (PA, $F^-$ treatment), and thus, being lower compared to *r* values determined in other studies by

a factor of 3 – 10 (Duport et al., 2007; Lindqvist et al., 2013). However, comparable low biotransport values were assessed by Cournane et al. (2010), and notably, by Nogaro et al. (2007), who stimulated the bioturbation activity of *H. diversicolor* by food addition in a similar manner as it was done for the $F^+$ group, consequently suggesting high variability in the bioturbation performance of *H. diversicolor*. In the light of this observed variability, *Db* and *r* values are difficult to interpret, as different factors can affect the sediment reworking activity of *H. diversicolor*, of which abundance and burrow morphology might play the most pivotal roles (Duport et al., 2006; François et al., 2002).

Abundance in both feeding treatments was reduced by mortality ($F^-$: 17% in total; $F^+$: 43% in total), which was probably due to the onset of reproduction of some individuals. For Baltic Sea populations of *H. diversicolor*, spawning is known to occur during early spring (Dales, 1950), matching with the polychaete sampling date. Supporting the idea of reproduction-induced mortality, several individuals were found to exhibit a conspicuous greenish coloring during experimental incubation, indicating a recent spawning event. Following reproduction, polychaetes die due to histolysis (Dales, 1950; Smith, 1964). However, as *H. diversicolor* is known to show strong territorial behavior, including defense of burrows and burrow openings against intruders (Reise, 1979), observed mortality might be attributed to intraspecific competition as well. For long-term cultivation, mortality is known to significantly increase after ~ one month of incubation for a broad range of abundances (Nesto et al., 2012). Abundances in both feeding treatments were 200 ind. $m^{-2}$, and hence, far below maximum densities known from the field, which can reach several 1000 ind. $m^{-2}$ (Arndt, 1989; Davey and Watson, 1995). Long-term mortality under comparable abundances is reported to remain low (~ 5%; Nesto et al., 2012), suggesting that observed losses do not represent an effect of abundance and might be ascribed to other factors, as reproduction.

Due to territoriality, community bioturbation and abundance are not linearly linked. Individual contribution to overall bioturbation performance decreases with increasing abundances (Duport et al., 2006), reflecting changes in burrow morphology and the decrease of individual searching area at the sediment surface. Few polychaetes can cover comparably large sediment areas upon searching for food and thus mediate particle transport rates comparable to those accomplished by larger communities of *H. diversicolor* (Duport et al., 2007), potentially compensating for mortality effects in terms of local transport. As burrows established by different polychaetes are never in contact with each other (Davey, 1994), the individual sediment volume available for the construction of a dense gallery network in the upper burrow sections is much smaller under high abundances, causing galleries and burrows to be more vertical-oriented (Davey, 1994), eventually promoting non-local transport. Under lower abundances, gallery networks of single burrows with extended horizontal sections can spread farther, favoring local transport in upper sediment layers. Davey (1994) observed burrows established by *H. diversicolor* to extend more horizontally in laboratory experiments compared to burrows analyzed in the field, attributing this difference to the absence of juvenile polychaetes and other co-fauna in artificial mesocosm designs.

Lastly, burrowing performance is affected by the individual health state of the polychaetes, as stressed animals tend to generally establish less deep burrows compared to vital specimens (Esselink and Zwarts, 1989). Weakened polychaetes, which might have occurred in some mesocosms as a consequence of reproduction, create less deep burrows and exhibit an overall reduced bioturbation activity, potentially further impeding non-local particle transport. Nevertheless, only a faint correlation between local and non-local transport between all particle types and mortality (used as a measure of overall health state) in the respective mesocosms was found (*Db*: -0.137, $p > 0.05$, Spearman-Rho correlation; Figure 36A; *r*: -0.234, $p > 0.05$, Spearman-Rho correlation; Figure 36B), emphasizing the role of other factors as individual feeding behavior or burrow morphology on particle transport. However, the exact morphology of individual burrows is hard to determine and known to exhibit strong variances (Davey, 1994), which might be reflected by strong variability of particle transport observed in both feeding groups.

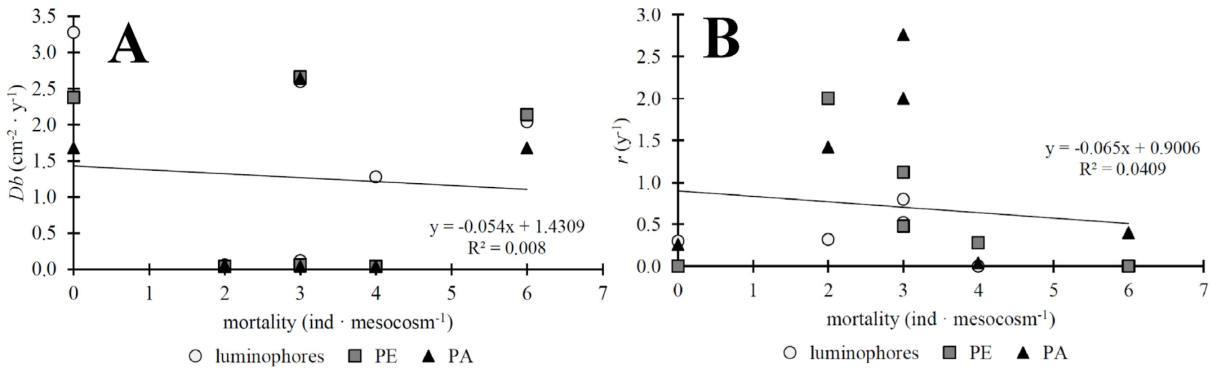


**Figure 36: Correlation of mortality determined for individual mesocosms and modeled bioturbation coefficients.** A: Db (local transport); B: r (non-local transport).

### 4.1.4. Feeding effect

The slight increase of *Db* in the $F^+$ treatment compared to $F^-$ mesocoms might hint towards an effect of food addition by inducing polychaete searching behavior, as an immediate response in surficial polychaete activity was seen in $F^+$ mesocosms during feeding. Increased food availability can significantly enhance particle transport mediated by *H. diversicolor*, as it was demonstrated in other studies (Murray et al., 2017; Nogaro et al., 2007). *H. diversicolor* is known to drag captured food into the gallery sections of its burrow for safe ingestion, causing a shallow net particle burial and thus, inducing local particle transport. However, no significant effect of feeding either on local or non-local particle transport was found in this experiment. As discussed above, the effect of food addition might be masked by strong observed individual variability among mesocosms. Murray et al. (2017) observed limited impact of enhanced food availability on bioturbation performance as well, with highest increases in particle transport for moderate food addition. However, enhanced food supply had strong

effects on local transport rates induced by polychaete activity at the sediment surface. Contrasting these findings, Nogaro et al. (2007) demonstrated that food addition caused no increase in local, but only in non-local transport, further emphasizing that particle burial rates might be governed by numerous factors.

Fast and selective uptake of potential food items, as it was observed in the $F^+$ treatment is known from other studies (Delefosse and Kristensen, 2012), and freshly deposited particles are reported to reach maximum burial depths in less than one day (Lindqvist et al., 2013), rendering feeding induced particle burial to be a process occurring over short time scales. Despite such fast responses on food addition, increase in food abundance or addition frequency was found to have no significant effect on particle transport (Murray et al., 2017; Nogaro et al., 2007), indicating that bioturbation activity cannot be linearly linked to food availability. Sediment consolidation by mucus secretion, creating mucus-lined trails at the sediment-water interface, might immobilize particulate material and hence, impede bioturbation-induced transport in spite of high polychaete activity. Selective ingestion of freshly added material (Delefosse and Kristensen, 2012) might minimize the individual sediment surface area that is prospected for food, further reducing particle transport. Consequently, those short-term responses represent a pathway for the rapid removal of freshly deposited material, especially in the context of larger food availability, e.g. the deposition of algal blooms, which are known to induce bioturbation activity on short time scales (Gerino et al., 1998). As floating MPs can be incorporated into marine aggregates (Long et al., 2017; Zhao et al., 2018), the deposition and selective uptake of deposited material might constitute an effective mechanism for removal of MPs from the water column and their fast burial within marine sediments.

### 4.1.5. Particle selective transport

Numerous benthic deposit feeders are known to exhibit selectivity in terms of particle transport or uptake. Size-dependent particle burial rates are reported for deep-sea communities of the eastern Pacific, were smaller particles are subjected to stronger vertical transport (Taghon, 1982; Wheatcroft, 1992). This dependency is assumed to be passively induced by differential gravitational forced migration patterns of small particles that might occur upon disturbance by animal locomotion. Furthermore, selective ingestion of smaller particles is hypothesized as well, as these particles exhibit greater surface area per volume unit and thus, provide more food per ingested volume in a habitat in which most available food is associated to particle surfaces. Besides particle size, many surficial deposit feeding animals tend to preferentially ingest particles of lower specific gravity, which also is explained in the context of the optimal foraging theory, as less dense particles are often associated with high nutritional value. According to latter considerations, the selective uptake of PS particles over ambient sediment grains could be shown for several taxa of surficial deposit feeding invertebrates (Self and Jumars, 1988).

As the particle tracers used in the HD experiment differed in size (PA vs. luminophores/PE) and specific gravity (luminophores vs. PE/PA), a potential differential transport of particle tracers is

considered plausible. PERMANOVA revealed a significant influence of particle type on tracer burial, as well as significant interactions between the factors particle type and treatment. Contrasting the findings of Wheatcroft (1992), large PA particles showed high vertical export rates in the HD experiment. High *r* values of PA particles found in all control mesocosms very likely represent artifacts that occurred during sediment sampling, causing the large particles to fall down from slicing instruments or mesocosm walls to deeper sediment layers due to their comparably high specific gravity. This size-dependent transport might be relevant in polychaete burrows as well, suggesting stronger vertical export of larger MPs along vertical burrow shafts. When corrected for this artifact, biological induced transport rates of PA particles are comparable to those observed for luminophores and PE particles, though. However, with respect to controls, PA particles displayed significant stronger vertical transport than luminophores/PE particles in the $F^-$ treatment, suggesting a certain size-selective particle export.

Regarding local transport rates, the pattern of transport intensity was determined as luminophores > PE > PA in both feeding treatments. As variabilities in bioturbation coefficients were high, it remains difficult to derive general principles of particle transport from those findings. As size- and density-driven differences in particle transport described by Wheatcroft (1992) and Taghon (1982) are mostly stochastic processes, governed by differential gravitational forcing or encounter probability of feeding appendages with sediment particles, active and directed ingestion of particles as it is known for *H. diversicolor* might counteract those processes. Ingestion of freshly deposited PA particles with several mm particle diameter is reported for *H. diversicolor* (Delefosse and Kristensen, 2012). Interestingly, in the same study polychaetes displayed preferential ingestion of natural eelgrass seedlings over PA particles of the same size and density, indicating the ability to distinguish between those particles, probably based on different surface properties, as the virgin PA particles used might have differed in biofilm composition from eelgrass seedlings obtained from natural sites. The uptake of comparably large particles of both natural (eelgrass seedlings) and anthropogenic origin (PA particles, paint fragments; Muller-Karanassos et al., 2019), suggests at least some influence of particle size on particle ingestion behavior of *H. diversicolor*. Based on size-selective particle uptake, it might be expected that local transport rates for PA particles are increased, as particles are dragged into the burrow gallery network for ingestion. PA particles did not exhibit any increased local transport in the HD experiment, though, indicating that particle burial might be canceled out by faecal pellet deposition at the sediment surface, causing no net transport of ingested particles.

After correction for artificial transport upon sediment slicing, PA particles still showed increased non-local transport along with PE particles compared to luminophores in $F^-/F^+$ treatments, with differences not being statistically significant, however. As vertical export of PA might be gravity-driven, the same might be true for PE particles in an opposite way. Based on the lowest specific gravity of all particle tracers used, PE might stronger adhere to polychaete bodies and thus might experience longer transport intervals, enabling those particles to be introduced to deeper burrow

sections, possibly explaining stronger non-local transport compared to similar-sized luminophores. Again, systematic differences in particle transport are difficult to derive due to observed strong variability. Differential transport of particles displaying different sizes and specific gravities might be governed by other factors as well, as feeding mode, mucus secretion and burrow morphology and thus, might display strong spatial and temporal variations for a given polychaete community.

## 4.2. Particle and microplastic transport induced by *A. marina*

### 4.2.1. Sediment feeding activity ($AM_{SI}$ experiment)

Overall rate of sediment defaecation (and thus, sediment ingestion) in the $AM_{SI}$ experiment was $1.94 \pm 2.91$ ml $day^{-1}$ $ind.^{-1}$ (n = 4), and therefore markedly lower than known in situ sediment ingestion rates of *A. marina* for similar ambient temperatures, which are reported to be 11.0 ml – 12.3 ml $day^{-1}$ $ind.^{-1}$ (Cadée, 1976; Rijken, 1979). As food availability is the most governing factor in terms of sediment ingestion (De Wilde and Berghuis, 1979), those conspicuously low feeding rates can be explained by the modalities of the $AM_{SI}$ experiment, e.g. sampling in late autumn, sediment sieving during sampling, incubation in the dark and lack of additional food; further reducing the already low food content and preventing the growth of microphytobenthos, which is acknowledged to represent a major food source for *A. marina* (Andresen and Kristensen, 2002). Organic matter content of the sediment used was determined with ~ 0.3% DM (~ 0.1% POC) prior to the experiment, rendering food scarcity the most likely explanation for the observed low sediment ingestion rates, since feeding activity of *A. marina* correlates positively with food availability (Jacobsen, 1967; Rijken, 1979). Low POC contents in the sediment represent conditions of food scarcity that are usually found in permeable, sandy sediments during late autumn and winter. For example, sedimentary organic matter contents from the German Wadden Sea are reported to be 0.1 – 1.0% (TOC) during autumn (Freese et al., 2008; Volkman et al., 2000). According to low food content, observed sediment ingestion rates in the $AM_{SI}$ experiment are well within the range of feeding activities determined in the Dutch Wadden Sea in winter (2.4 ml $day^{-1}$ $ind.^{-1}$; Cadée, 1976). In situ defaecation of *A. marina* exhibits an annual cycle with lowest rates in autumn (Riisgård and Banta, 1998), which might coincide with enhanced migration behavior during this season (Cadée, 1976; Flach and Beukema, 1994).

High variability in feeding of single polychaetes as well as among specimens was observed with respect to ingested sediment volume and frequency of feeding events. Both is well known for *A. marina* (Cadée, 1976), resting periods between phases of feeding activity are common and can extend up to several days. While most polychaetes in the $AM_{SI}$ experiment showed signs of sediment defaecation on a daily basis, some specimens were found to feed slower and with prolonged phases of inactivity compared to the other polychaetes ($AM_{SI}1$, $AM_{SI}5$), hinting towards factors influencing feeding rates on an individual level. Hence, it was hypothesized that individual metabolic states might

affect overall feeding activity (Retraubun et al., 1996b). Adaptation to different environments might play a role as well, as feeding rates of *A. marina* were found to differ for several regions of the Dutch Wadden Sea (Brey, 1991). Whether observed differential feeding behaviors can be ascribed to individual adaption cannot be verified, as the exact origin of single polychaetes used for the $AM_{SI}$ experiment will remain unknown.

Relocation of faeces deposition sites was common for most of all polychaetes with rhythms somewhat slower than usually observed for cycles of sediment ingestion and resting. In these cases, existing burrow openings were frequently used alongside newly established openings for defaecation, indicating the persistence of at least the burrow tail shaft over the course of the experiment (two periods of 14 d incubation). Burrow walls were most probably stabilized by mucus secretion. Migrations of *A. marina* within the sediment are commonly described, with the particular mode of burrow relocation changing with sediment quality. While for organic-rich, cohesive sediments which do not allow for the formation of a feeding funnel only the movement of the feeding pocket is reported (Rijken, 1979), the relocation of the complete burrow (and consequently, the polychaete) is frequently found in sediments low on organic matter content (Brey, 1991). Consistent with feeding rates, migration behavior differs for various sites in the field (Brey, 1991). The correlation of mean individual defaecation rate and relocation frequency might furthermore indicate that these parameters reflect mechanisms that occur on an individual level, which might be represented by metabolic conditions or adaptations to small-scale spatial heterogeneity (or both), even though this correlation is not significant, but close to significance (0.634, $p = 0.067$, Pearson's correlation; Figure 37A).

Net increase in biomass was observed for 6 of total 8 individuals upon experiment termination, illustrating that the sediment used was able to sustain net growth over the incubation period of the $AM_{SI}$ experiment (7 weeks) in spite of its food scarcity. According to the assumption that 1 ml $O_2$ is needed for combustion of 1 mg organic matter (Riisgård and Banta, 1998) and based on sedimentary OM content found in the $AM_{SI}$ experiment (0.26% DM), the amount of sediment that individual polychaetes need to ingest to cover their energetic demands can be determined. Respiration can be estimated based on individual fresh mass (FM) by using a temperature-dependent power law function exemplified by Krüger (1964). Hence, a polychaete with a FM of 1.4 g (the lowest individual biomass found in the $AM_{SI}$ experiment upon experiment start) respires 51.69 µl $h^{-1}$, equating a daily OM demand of 1.24 mg and, accordingly, a daily sediment uptake of ~ 0.5 g sediment $d^{-1}$. For a FM of 3.3 g (highest individual FM in the experiment), oxygen consumption results to 104.89 µl $h^{-1}$, corresponding to a daily uptake of 2.51 mg OM or ~ 1 g sediment, respectively. As not all organic matter taken up is assimilated, the actual amount of sediment that necessarily is ingested might be considerably higher. For deposit-feeding animals a general assimilation efficiency of 5 – 15% is estimated (Lopez and Levinton, 1987). If the assimilation efficiency of *A. marina* is conservatively assumed to be ~ 10%, the actual amount of sediment that is needed to be taken up by a polychaete of 1.4 g and 3.3 g DM is 5 g $ind.^{-1}$ $d^{-1}$ and 10 g $ind.^{-1}$ $d^{-1}$, respectively. These values correspond to a

sediment volume of 2.9 ml ind.$^{-1}$ d$^{-1}$ and 5.9 ml ind.$^{-1}$ d$^{-1}$, respectively, which is in good agreement with the overall mean ingestion rate found in the experiment, being 1.94 ± 2.91 ml ind.$^{-1}$ d$^{-1}$ (minimum: 0.10 ± 3.26 ml ind.$^{-1}$ d$^{-1}$; maximum: 5.36 ± 5.53 ml ind.$^{-1}$ d$^{-1}$). Albeit this calculation can only represent a crude estimation of polychaete energetic demand, the results suggest that despite of food scarcity conservation or increase in biomass can be attained for adequately high sediment ingestion rates (i.e. ≥ 3 – 5 ml ind.$^{-1}$ d$^{-1}$, depending on individual biomass).

Growth rates differed strongly between individuals and were found to correlate positively with individual sediment uptake. As no or very little spatial heterogeneity in organic matter content can be expected due to homogenized sediments, the observed variances in individual growth further suggest individual responses to low food availability. As *A. marina* usually relies on freshly grown microphytobenthos which is transported to the feeding pocket via the feeding funnel, enhanced mobility might be an advantage in a dark environment without algal growth. Frequent migrations might allow to optimize utilization of other, light-independent food sources, which can be more evenly distributed within the sediment body, such as bacteria (Andresen and Kristensen, 2002). Accordingly, there was a weak positive correlation between net biomass change and relocation frequency (0.192, $p > 0.05$, Pearson's correlation; Figure 37B), that was not significant, though. Probably this correlation represents the mere fact that mobile individuals tend to ingest more sediment due to their general level of activity, allowing them to scavenge more food. Furthermore, bacteria are acknowledged to only partially cover the energy demand of *A. marina* (Andresen and Kristensen, 2002; Riisgård and Banta, 1998) and likely do not provide enough energy for a net biomass gain over longer time scales. Ultimately, individual feeding and migration behavior must be regarded as intrinsic factors and cannot be interpreted as a general adaptation to food scarcity, as compensatory feeding (i.e. intensification of feeding activity to cope with low food supply) is not known for *A. marina*, which usually reduces feeding upon starving to minimize its energy demand (Lopez and Levinton, 1987).

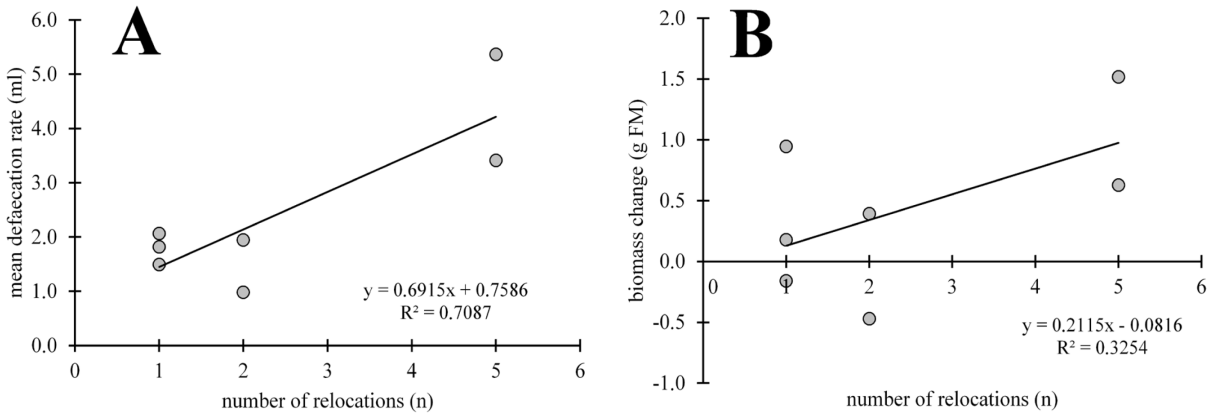


**Figure 37: Correlation of tail shaft relocation frequency and mean defaecation rate (A) and biomass change (B).**

### 4.2.2. Sediment feeding activity (AM experiment)

Though incubation times in the AM experiment varied by a factor of ~ 2, experiment duration had no significant effects on tracer burial below 2 or 8 cm. The steep, exponential decrease of particle concentrations with increasing depth and the subsequent formation of concentration maxima in various sediment depths in both the STI and LTI group suggest differing individual sediment ingestion rates as the driving process for the observed depth distribution of particle tracers. As no MP was detected in the faeces at any time during the experiment, sediment ingestion rates were estimated by the amount of MP-free sediment that was deposited on top of the initial particle tracer layer in each mesocosm. However, the presence of particle concentration maxima at a given sediment depth allows no conclusion about the modalities of their formation, as they can be created by subduction of the initial tracer layer as a consequence of constant sediment deposition or by discrimination of larger particles around the feeding layer (or a combination of these two processes). If formed by selective feeding of *A. marina*, those particle accumulation zones could have formed already at some time point before experiment termination, which might be true for mesocosms AM4, AM6, AM7 and AM8. Despite the existence of those similar-aged peaks, associated estimated sediment ingestion rates (representing the amount of deposited sediment per time interval) might strongly differ, as the mesocosms in question were incubated for different time spans (106 d vs. 239/240 d), rendering the ingestion rates depicted in Table 9 to be conservative estimates and likely underestimations for the respective mesocosms. Nevertheless, determined sediment ingestion rates match well to differences in particle tracer depth distribution detected by MDS (Figure 31). MDS data also indicate low particle burial rates coinciding with lower sediment ingestion and vice versa, suggesting individual feeding activity to be the driving factor for the observed differences in both MDS groups. Hence, mesocosms AM1, AM2, AM3 and AM5 are hereafter referred to as the "low bioturbation" group (LB) and AM4, AM6, AM7 and AM8 as the "high bioturbation" group (HB) (Table 9).

Corresponding to findings from the $AM_{SI}$ experiment, LB ingestion rates were distinctly lower in the AM experiment (2.88 ± 2.38 ml $d^{-1}$ $ind.^{-1}$; n = 4) as it can be expected for *A. marina* under similar in situ conditions. Thus, observed low feeding activity is most likely a consequence of poor food supply. Conversely, sediment ingestion determined for the HB group was 8.92 ± 4.96 ml $d^{-1}$ $ind.^{-1}$ (n= 4) and hence, in good accordance with field values determined by Cadée (1976) and Rijken (1979) (11.0 ml – 12.3 ml $d^{-1}$ $ind.^{-1}$). Similar to results found in the $AM_{SI}$ experiment, the presence of those considerably high ingestion rates in the HB group suggests that individual sediment reworking activity is not solely governed by low food availability. Individual activity levels might be driven by metabolic conditions or adaptations to local environments and therefore might have caused differences in feeding activity among the LB and HB group, as discussed in section 4.2.1.

Net loss of biomass in mesocosms AM1, AM6 and AM8 can most likely be ascribed to food scarcity, since for AM6 and AM8 a reduction of biomass was found while exhibiting high feeding rates at the same time. However, no net biomass change was determined for AM3 (LB), whereas AM4

and AM7 (HB) displayed a considerable increase in biomass at the end of the experiment. While with regard to sediment characteristics (mean grain size, OM content, sediment homogeneity) all AM mesocosms displayed similar conditions, the strongly differing net growth rates found in each mesocosm resemble the pattern found in the $AM_{SI}$ experiment and thus, can be explained best with individual activity levels. For conditions of low food supply, a net loss in average biomass is known to be common for *A. marina*. During winter, a mean biomass loss of 25% is reported for a Balgzand population (Beukema and De Vlas, 1979), illustrating the ability of *A. marina* to endure enhanced periods of starvation with subsequent biomass stagnation or even loss (De Wilde and Berghuis, 1979). This adaptation to seasonal occurring food scarcity might be reflected by low overall mortality observed in both the $AM_{SI}$ and AM experiment.

**Table 9: Mean individual sediment reworking shown as individual sediment ingestion rate derived from particle concentration profiles.** Bioturbation classification is based on MDS (Figure 29).

| mesocosm | mean sediment ingestion rate (ml sed. $day^{-1}$ $ind.^{-1}$) | bioturbation classification |
|---|---|---|
| AM1 | 2.08 | low |
| AM2 | 2.05 | low |
| AM3 | 1.03 | low |
| AM4 | 16.21 | high |
| AM5 | 6.37 | low [a] |
| AM6 | 7.19 | high |
| AM7 | 7.16 | high |
| AM8 | 5.11 | high |

[a] Classification as low bioturbation despite of high sediment ingestion rates is due to mortality within the first 14 d of the experiment.

### 4.2.3. Bioturbation of microplastic particles

Particle tracer distributions determined for the LB and HB group significantly differed from those found in control mesocosms, indicating that the sediment reworking activity of *A. marina* constitutes an effective pathway for MP burial and accumulation of particles ≥ 500 µm. Variation of sediment reworking activity resulted in substantial differences in burial efficiency with regard to the amount of buried particles and maximum burial depth. Even for low feeding rates, which represent in situ minimum values found during winter, a considerable MP transport into the upper 4 cm of the sediment was detected.

Particle redistribution patterns for PS and PA and visual observation of mesocosms indicate that plastic particles were not ingested by polychaetes upon reaching feeding layer depth. Contrasting MP, uniform concentrations of smaller-sized luminophores above MP accumulation layers indicate the

ingestion and subsequent deposition of ambient sediment particles atop of the surficial particle tracer layer in the HB group. Luminophore concentrations in control mesocosms were low (~ 0.25%) and exhibited uniform concentration levels below 2 cm sediment depth, which most likely represent artifacts that can be associated with sediment smearing during sampling. Discrimination of larger particles in the feeding process is widely reported for *A. marina*; upper size thresholds for ingestion are known to range between 1000 µm (Baumfalk, 1979) and 2000 µm (Krüger, 1971), strongly depending in individual polychaete size. As the MP used in the AM experiment was below or at the very edge of the reported size limits, the ingestion of at least the smaller PA particles was expected, but not observed in any case, though. Furthermore, the general coarsening of feeding layer sediment with a significant increase in mean grain size for lower feeding layers (10 – 20 cm depth) can be interpreted as a consequence of discriminatory sediment ingestion. Such an increase was observed in situ and could be mimicked in experiments (Cadée, 1976), generally resulting in the formation of so-called graded bedding, i.e. the occurrence of one or several layers of shell debris and/or coarse sediment in varying sediment depths. Hence, it can be concluded that the discriminatory feeding of *A. marina* represents the driving force for the observed accumulation of particles ≥ 500 µm in several AM mesocosms. Particle rejection depends on individual polychaete size, causing the threshold for particle discrimination to shift towards larger particle sizes with individual growth. Despite being smaller in diameter than discrimination thresholds reported by Baumfalk (1979) and Krüger (1971), PA particles used in the experiment were not found to be ingested. Feeding of *A. marina* is a process mainly governed by physical adhesion of particles to the polychaete's proboscis (Baumfalk, 1979), determined by a particle's shape, specific gravity and surface properties. Adhesion of the used PS particles to feeding appendages might be reduced by the regular, non-spherical shape of the particles or specific surface properties of the polymer. However, MP in diameters similar to ambient sediment grains tend to be ingested (Van Cauwenberghe et al., 2015a), and will be redistributed similarly as seen for luminophores in the AM experiment, including burial via subduction and exhibition of uniform particle distributions in upper sediment depths.

[1]"Even though overall feeding activity was impaired by food scarcity, the observed particle distributions were significantly different from the controls for the LB and HB group. Greatly varying sediment ingestion induced depth distribution patterns that resembled more or less diffusion analogous particle bioturbation (LB group) as well as patterns with a distinct burial of the initial particle tracer layer, resulting in conspicuous MP peaks in particle concentrations in several cm depth (HB group). Since there is no effect of incubation time on concentration of particle tracers below 2 or 8 cm, these differences can be explained with individual sediment feeding performance. As individual feeding rates differ with season, the potential of *A. marina* for MP burial might exhibit great annual fluctuations with minimum MP subduction rates of ~ 0.01 mm $day^{-1}$ in winter and ~ 1 mm $day^{-1}$ as

[1] The denoted passage is cited according to Gebhardt & Forster (2018).

annual average. Export rates via feeding funnel transport might be considerably higher but are restricted to small areas.

The progressing subduction of particle tracer layers in sediments with time is known for many conveyor belt feeders and often accompanied with the generation of a second peak of ingested material at the sediment surface and an overall broadening of particle peaks over time (Robbins et al., 1979). The reappearance of ingested luminophores at the sediment surface was observed in the HB group, but without the formation of concentration maxima. The homogenous luminophore concentrations above MP peaks in all HB mesocosms suggest a uniform rate of luminophore ingestion and upward transport. According to Robbins et al. (1979), particle peaks tend to get smoothed, rendering particle depth distribution to become more uniform over time. However, despite the long experimental duration, this broadening of MP peaks did not occur in the AM experiment. Within the HB group, pronounced particle maxima were located 1 – 2 cm above the uppermost feeding layer with a vertical extension of 4 – 6 cm and with very low abundances or absence of MP in the remaining sediment layers. Most probably due to the particle discrimination of *A. marina*, large MPs cannot penetrate through the feeding layer and consequently accumulate in a narrow particle horizon. In LB mesocosms, distinct particle peaks are recognizable as well, but MP particles were detected in all sediment horizons above the feeding layer, indicating slight vertical particle export from the uppermost sediment layers. A broadening of particle peaks is ascribed to variable sediment feeding rates or bioturbation activities penetrating through the accumulation layer (Robbins et al., 1979). Particle transport via the feeding funnel, which connects the sediment surface with the feeding pocket of *A. marina*, can explain this small but observable particle transport of MPs and luminophores in the LB group (Fig. 1, AM2). This MP export via the feeding funnel might cause differential mixing of MP particles as smaller PA particles (500 µm) could enter the funnel more easily and are able to descend faster than larger PS particles (1000 µm). However, no evidence of such differential mixing processes was found, as differences between PA and PS concentrations were non-significant for all sediment depths. Furthermore, for a given size-dependent particle discrimination, the existence of permanent feeding funnels would suggest the quick formation of a second MP concentration peak right above the feeding layer, since sediment transported via the funnel is transported into the feeding pocket in a relatively short time of several hours (Rijken, 1979). However, existing funnels are often abandoned after several days due to migration movements of *A. marina* within the sediment (Brey, 1991; Rijken, 1979). Redistribution of faecal casts was observed after 2 – 3 days for most of the polychaetes as well, suggesting a similar migration behavior. Actual particle concentrations within the feeding funnel cannot be determined with the sampling method used, since particle concentrations were averaged over the whole depth interval of each sediment layer. Thus, the observed particle profiles likely represent a mixture of two different particle distributions with high particle concentrations and transport within the feeding funnel and surrounding sediment unaffected by sediment transport (Timmermann et al., 2003). The exponential decrease of particle concentrations with increasing depth

and the lack of MP accumulation zones near the feeding layer in the LB group might be explained by a combination of non-permanent burrows and overall low feeding rates that cause initial burrowing of particles but do not allow them to reach the feeding layer."

Based on experimental findings, the mechanism of MP redistribution induced by *A. marina* can be regarded as a combined particle transport realized by burial via both the feeding funnel and sediment subduction. The exact contribution of both transport mechanisms to particle burial cannot be resolved with the sampling strategies applied, causing horizontal averaging of particle concentrations. Bioturbation intensity represents the main driver for the relative impact of those two modes of transport on vertical particle distribution. As seen in the HB group, high feeding activities will favor sediment subduction as the prevailing process of particle burial, which is not constrained to small-scale sediment areas as feeding funnel transport. The exact contribution of these two processes to net particle burial may be hard to determine though, as it can differ with site, depending on local sediment characteristics. Based on sediment cohesiveness, feeding funnels can form broad, conical-shaped structures, which spread over an enlarged surface area, increasing overall vertical particle export (Rijken, 1979). In sediments with high OM content frequent relocation of the feeding pocket is common, causing surficial sediment to sink down at once over larger areas without the formation of any feeding funnel (Rijken, 1979), eventually promoting particle transport via subduction processes. The potential for MP burial at a given site might be governed by hydrodynamic conditions as well, as local flow regimes affect particle settling behavior and accordingly, particle deposition or erosion rates. The formation of feeding pits at the sediment surface as a consequence of funnel feeding might enhance local MP burial rates by acting as particle traps under low turbulence conditions which induce bedload transport (Valdemarsen et al., 2011; Yager et al., 1993). However, pits as well as faecal casts might be smoothed under high hydrodynamic forcing, effectively impeding any vertical particle export. Furthermore, stronger current events can induce long-distance bedload transport or resuspension of already buried MPs (Ballent et al., 2013). In the Wadden Sea, current and wave driven sediment erosion rates are known to reach down to 2 cm sediment depth during heavy wind forcing (Christiansen et al., 2006; Christie et al., 1999). In winter months, net sediment export can add up to 3.5 cm, representing an overall stronger wind influence (Christie et al., 1999), which might cause the enhanced net release of deposited MPs from sediments during this season. During winter, the feeding activity of *A. marina* reaches an annual minimum while concurring with simultaneously present high wind-induced sediment erosion rates. Hence, the burial of MPs in tidal flat habitats is very likely to exhibit a distinct annual pattern, with no burial or even release of MPs from sediments during autumn/winter and promotion of MP burial in summer, at least for areas high in abundance of *A. marina*. As the impact of lugworm bioturbation on MP transport might strongly differ with time and space, the potential for MP burial needs to separately evaluated for different habitats, considering population density, local sediment characteristics and prevailing hydrodynamic conditions. As MPs tend to accumulate in shallow and sheltered systems (Castañeda et al., 2014; Hengstmann et al., 2018),

an increased MP burial can be expected in those habitats. In an attempt to mimic the burial of eelgrass seedlings by using PA particles under conditions that are found in the shallow Danish Odense Fjord, a substantial transport of particles below sediment depths of 6 cm was found (Valdemarsen et al., 2011). Subduction of particles as a consequence of sediment deposition was found to represent the major mode of burial, reflecting high polychaete abundances used in the experiment. With water temperature set to represent late spring/early summer conditions (15°C) and flow velocities corresponding to moderate wind influence (max. 20 cm $s^{-1}$), the work of Valdemarsen et al. (2011) illustrates the ability of *A. marina* to induce MP transport into considerable sediment depths in these habitats under conditions common in the summer months.

## 4.3. Potential toxicity of microplastic particles

MP concentrations used for the experiments were high (HD experiment: PE: ~14 000 particles $kg^{-1}$ sediment; PA: ~900 particles $kg^{-1}$; AM experiment: PS: ~800 particles $kg^{-1}$; PA: ~5000 particles $kg^{-1}$), exceeding most in situ concentrations found by one or two orders of magnitude. Comparably high MP counts with several thousand particles per kg sediment were determined at heavily anthropogenic influenced sites as harbors (Norén, 2008) or regions adjacent to large urban areas (Matsuguma et al., 2017; Vianello et al., 2013), rendering the conducted experiments to represent the scenario of maximum sediment MP contamination that is presently observable in the marine realm. Those high concentrations were chosen in favor of particle quantification and visualization of possible long term transport processes. However, the used concentrations fall within a range which is known to potentially induce stress responses in polychaetes and therefore might have affected experimental results, especially with regard to high mortality (HD experiment) and low sediment reworking rates (AM experiment).

While MPs are known to inflict gut blockage and consequently lead to internal injuries or starvation in numerous vertebrate taxa (Gregory, 2009; Laist, 1987), this scenario presumably has minor relevance for deposit-feeding organisms, as these organisms are well adapted to ingestion and defaecation of particulate material and additionally, often are able to effectively discriminate particles in diameters not appropriate for digestion by size-selective feeding mechanisms (Baumfalk, 1979; Self and Jumars, 1988). Ingestion of MP particles is known for *H. diversicolor* and *A. marina* and MPs were found in digestive tracts of both species and faeces of *A. marina* in laboratory experiments (Besseling et al., 2017; Gomiero et al., 2018). However, evidence for MP ingestion by polychaetes from the field is scarce. MP concentrations found in faecal casts along the Nova Scotia shoreline originating from undetermined polychaete species showed no concentration difference to surrounding sediments, indicating MPs were not retained within the digestive tract after ingestion (Mathalon and Hill, 2014).

Besides effects of physical damage, MP ingestion is often hypothesized to represent a potential pathway of exposure to plastic additives, which often are persistent organic pollutants (POPs) as polybrominated diphenyl ethers (PBDE), phthalates, nonylphenol (NP) or bisphenol A (BPA) (Hermabessiere et al., 2017; Hirai et al., 2011). Desorption of those substances might occur in the digestive tract due to changing pH regimes, potentially leading to bioaccumulation and subsequently, harmful effects on health and fitness of organisms in question. However, desorption rates of plastic additives are highly variable and depending on numerous factors as salinity, UV radiation, turbulence or adsorption strength to organic matter (Besseling et al., 2017; Suhrhoff and Scholz-Böttcher, 2016). Furthermore, the qualitative and quantitative additive composition of purchased plastics often remains unknown and can strongly differ between manufacturers. Of all polymers used in the experiment, PS might have the most toxic effect on marine invertebrates. The release of styrene monomers from PS is reported for environmental conditions (Suhrhoff and Scholz-Böttcher, 2016) and the exposure to PS is known to impair fertility and larval growth of sea urchin larvae (Martínez-Gómez et al., 2017). For PE and PA polymers, the addition of bioactive substances as antioxidants or plasticizers is uncommon, for both plastic types the most used additives are colorants (Hansen et al., 2013). The exact toxicity of those substances on invertebrates is hard to determine, though.

The observed high mortality and low overall sediment reworking rates in the respective HD and AM experiment might hint to toxic additive effects as a consequence of exposition to high MP concentrations, as these effects were determined in other experiments as well. Biological effects of benzo(a)pyrene on *H. diversicolor* include the induction of immunological responses, oxidative stress as well as enhanced genotoxicity (Gomiero et al., 2018), but no increase in mortality. Exposure to nonylphenol is known to trigger phagocytic responses in *A. marina*, while contamination of Triclosan or polychlorinated biphenyls (PCBs) can lead to a reduction of bioturbation activity (Besseling et al., 2013; Browne et al., 2013). However, exposure to other additives and pollutants as PBDE or phenantrene was found to have no significant effect on sediment reworking of *A. marina* (Browne et al., 2013). Furthermore, as these results are mostly obtained by using sediments and MP particles artificially spiked with additives, they might not represent conditions found in the environment or established in the HD and AM experiment. In both the HD and AM experiment, MP ingestion did not occur for particles $\geq 500$ µm in diameter; uptake of PE particles and subsequent exposure to potentially desorbed additives could yet have occurred in the HD experiment. However, due to slow diffusion rates in combination with comparably low gut residence times in deposit feeders, the uptake of plastic additives upon digestion is assumed to represent a negligible process of pollutant exposure (Lohmann, 2017). Conversely, uptake via ambient sediment pore water might constitute a major pathway for POP contamination in benthic organisms (Besseling et al., 2017; Browne et al., 2013). In both experiments, additives released from the MP deposit layer might be transported into polychaete residence depths by burrow ventilation. However, since there are no clean (i.e. contaminant-free) habitats in situ, animals are constantly accumulating pollutants originating from their environment by

feeding and respiration. Sediments and polychaetes used in the experiments are likely to already exhibit a certain contaminant burden upon sampling, which is in equilibrium with their environment (Lohmann, 2017). The same might be true for the MPs used, which were incubated in sea water prior to the experiment, allowing MP and water additive concentrations to align over time. This MP incubation might decrease their potential for a net additive release during the experiment. Furthermore, the use of pre-contaminated specimens from the field might further reduce the ability to accumulate present pollutants over short time scales.

Consequently, a negative impact of MP additives on polychaete health in both experiments cannot be ruled out completely but appears to be unlikely, since the observed phenomena as low bioturbation activity or elevated mortality can be explained by other factors as well. Low rates of sediment reworking activity in the AM experiment are most probably a consequence of low temperature and food scarcity, as observed feeding rates represent typical values that are found in situ during winter. Furthermore, feeding rates were similar to those determined in the $AM_{SI}$ experiment without any MP addition. Mortality observed in the HD experiment might be due to seasonal effects and cannot be unambiguously ascribed to high MP and contaminant loads, as even the use of comparably high concentrations of MPs spiked with benzo(a)pyrene did not lead to a significant increase in mortality in *H. diversicolor* (Gomiero et al., 2018).

# 5. SYNTHESIS: implications for the field

Results obtained from both the HD and AM experiment demonstrate that (1) benthic macrofauna can mediate MP burial into considerable sediment depths; (2) intensity of particle transport and burial depth crucially depend on bioturbation types considered; (3) MPs are generally buried in a similar manner than ambient sediment grains, despite of potential differences in particle size or specific gravity. The very finding that benthic MP distribution is affected by bioturbation processes might not surprise, as marine sediments represent important accumulation sites for the majority of marine plastic litter. Despite being a comparably young topic of interest, the redistribution of MPs in bioturbated sediments has been systematically analyzed in several environmental studies over the past decades. Plastic particle tracers were used to address various questions, aiding to improve quantitative descriptions of bioturbation processes, such as determining in situ horizontal bioturbation rates (Wheatcroft, 1991). Additionally, MPs were used to investigate mixing of particles exhibiting lower densities than ambient sediment grains, determining preferential ingestion and burial of organic matter (Delefosse and Kristensen, 2012; Self and Jumars, 1988; Valdemarsen et al., 2011). Due to these works, some aspects of the differential mixing of MPs in marine sediments had been revealed so far. Random, stochastic mixing processes (e.g. in the context of biodiffusive transport) can cause systematic differences in particle mixing, driven by different ratios of particle size and specific gravity (Wheatcroft, 1992), a phenomenon which is also known in the context of the so-called brazil nut problem (Hong et al., 2001; Möbius et al., 2001). In contrast, mixing phenomena that occur over larger spatial scales as ingestion/defaecation by benthic organisms or non-local transport induced by burrow morphology can be governed by particle selection as well, counteracting these random mixing patterns. Particle ingestion of benthic deposit feeders is known to be driven by size or density, causing preferential uptake of smaller (Wheatcroft, 1992) or less dense particles (Self and Jumars, 1988; Taghon, 1982). Furthermore, MPs are known to be subject of biofilm formation comparable to other surfaces in the marine environment (Harrison et al., 2014), which also can promote their ingestion by marine organisms, as it was shown for uptake by plankton species (Vroom et al., 2017), rendering surface properties of a given particle potentially crucial for its ingestion potential. Thus, organism-specific interaction renders particular properties of a MP particle relevant for their further transport, as seen for PA particles that were subjected to different size-dependent transport rates in the HD and AM experiment, respectively. Those observed differences in particle burial demonstrate the importance of species-specific responses in MP transport and might define potential key species that are able to induce strong non-local transport of MP particles.

Nonetheless, some local transport processes can be characterized by non-local features as well, as deposit feeding-induced transport usually occurs across large transport step lengths or over short time intervals as a consequence of particle ingestion or burrow construction. Hence, strong horizontal mixing in upper sediment layers can resemble local (i.e. diffusion-analogous) particle distributions,

especially in combination with a vertical advection component (Wheatcroft et al., 1990). Due to the inherent non-local nature of numerous diffusion-analogous mixing mechanisms, the differentiation between local and non-local patterns often solely reflects the time scales considered for interpretation. With increasing number of transport events that are taken into account, particle distributions in question often gradually adjust to diffusion-analogous mixing patterns (Maire et al., 2007), leveling out particle peaks that are associated with discrete transport events. This is especially true if bioturbation performance is regarded at community levels, which are constituted by different mixing types and display different burial step lengths or frequencies, interfering with each other. Despite frequently affected by non-local transport, many depth-dependent particle distributions found in situ can be well described by solely applying biodiffusion models – a phenomenon hereupon coined the "biodiffusion paradox" (Maire et al., 2010; Meysman et al., 2003). As the underlying mechanisms of the paradox might be true for MP burial as well, the impact of potential key species on MP redistribution might be restricted to short time effects, as non-local particle transport might be mitigated over time, resulting in an overall biodiffusive MP distribution within marine sediments. Hence, the impacts of potential key species on MP burial possibly vary with time, as non-local transport might induce a short-term burial of MPs, but local transport processes might smooth given particle peaks in depth over time. In contrast, particle accumulation layers within the sediment might persist on longer time scales if non-local transport is linked with a mechanism of particle selectivity, actively preserving particle peaks in the sediment, as seen in the HB group of the AM experiment.

Data on MP depth distributions from the field are scarce, but known particle patterns roughly follow diffusion-analogy (Corcoran et al., 2015; Martin et al., 2017; Matsuguma et al., 2017; Wang et al., 2019), with absolute MP concentrations decreasing as sediment depth increases. This consistency in diffusion-analogous particle mixing for MPs as well as for established particle tracers (Boudreau, 1986; Soetaert et al., 1996) might allow for the derivation of MP burial potentials from already existing bioturbation data in given habitats. Consequently, the biodiffusion paradox might render non-local bioturbators key species for MP transport only in habitats where these organisms represent dominant elements of the faunal community, generating local hot spots of deep or fast MP burial. For example, the lugworm *Arenicola marina*, which was found to profoundly affect MP distributions in the AM experiment, is known to exhibit high abundances at the European Wadden Sea and to be the dominant faunal element of some local benthic assemblages (Beukema, 1976), suggesting high burial of larger MPs at those sites. However, main distribution of this species is confined to a zone between the 40 m depth mark and the mean high water line (Retraubun et al., 1996b), probably rendering the impact of lugworm-induced MP burial at tidal flats negligible relative to MP mediated by benthic assemblages abundant in deeper parts of the North Sea. Furthermore, sediment reworking activity of *A. marina* is mainly driven by temperature and food availability, and thus, showing strong fluctuations with season (Retraubun et al., 1996b), with summer activities exceeding winter values by one order of

magnitude (Cadée, 1976). Hence, a distinct MP burial mediated by *A. marina* might only occur during spring/summer months and is distinctly hampered during winter.

Significant non-local transport of MPs might furthermore occur in fresh water ecosystems, as lacustrine sediments bear MP concentrations comparable to those found in marine systems (Castañeda et al., 2014; Corcoran et al., 2015). Conveyor-belt feeder as oligochaetes or chironomid larva often represent dominant faunal elements in those systems, facilitating particle transport in sediment depths down to 7 – 10 cm (Fisher et al., 1980; Matisoff and Wang, 2000). According to findings of the AM experiment, the potential accumulation of larger MPs at the base of oligochaete and chironomid burrows can be expected. However, as smaller particles are introduced into the burrows, ingested and defaecated at the sediment surface, the constant repetition of those feeding cycles generates particle concentration peaks at the sediment surface, which are slowly subduced by sediment deposition (Matisoff and Wang, 2000). Those emerging multi-peak patterns are often homogenized to uniform particle concentrations, extending over the whole sediment depth affected by bioturbation (Robbins et al., 1979). For these cases, strong non-local transport can promote a fast and deep burial of MPs, creating homogeneous particle distributions that strongly differ from biodiffusive mixing processes.

Considering their vast extension, continental shelf regions and abyssal plains of the world's oceans probably represent the most relevant ecosystem in terms of MP burial. Overall sedimentation in this systems is low, causing bioturbation to have a stronger impact on particle redistribution, as a given sediment layer can be subject to bioturbation processes for several 1000 years before it is subduced below mixed layer depths due to sedimentation (Guinasso and Schink, 1975). Food input into deep sea habitats is known to be pulsed (Levin et al., 1997), causing non-local transport to show strong responses to organic matter input, causing the burial of deposited material into considerable depths within short time scales (e.g. several days; Blair et al., 1996; Smith et al., 1993, 1986). Conveyor belt-feeders as maldanid polychaetes are known to mediate short-term transports into depths of 10 cm, but exhibit spatially patchy distributions as well, creating local hot spots of intense particle burial (Levin et al., 1997). Hence, the potential of MP burial in deep sea sediments might display considerable spatial differences and is probably confined to areas of high food input (e.g. sedimentation). Non-local burial of deposited particles might represent a pathway for the fast removal of MPs from the sediment surface. However, high concentrations of MP particles found in shallow depths or at the surface of deep sea sediments (Reed et al., 2018; Woodall et al., 2014) might indicate that this transport is selective and only relevant for MPs incorporated into potential food particles such as marine aggregates or faecal pellets.

Patchy macrofauna distributions, seasonal patterns of bioturbation intensity as well as fluctuating food input events therefore might cause strong variations in short-term bioturbation activity at a given site. As bioturbation may be considered a dynamic process, representing individual responses to different stimuli over variable time scales (Queirós et al., 2015), the evaluation of the exact MP burial potential for a given site based on local community composition might be rather

difficult. MP burial depths derived from abundances of three abundant polychaetes for the Danish Odense Fjord show considerable differences in MP transport on spatial scales of several 100 m (Delefosse and Kristensen, 2012), demonstrating high spatial variabilities solely caused by macrofauna distribution patterns. Additionally, hydrodynamic forcing can further enhance spatial differences in MP burial potential by generating local zones of net MP export or import, causing the formation of small- (Delefosse and Kristensen, 2012) and large-scale (Cluzard et al., 2015; Fang et al., 2018) accumulation zones for MP, which are governed by wind- or current-induced particle transport. Hydrodynamic forcing tends to show changes with season, further adding a temporal component to this complex issue.

Despite the presently observed diffusion-analogous distribution of MPs in marine sediments, distinct differences in maximal MP burial depths might reflect those differential impacts of community structure, food availability or hydrodynamic regime, causing strong local differences is maximum MP burial depths, ranging from 3.5 cm at the Irish Shelf (Martin et al., 2017) to depths of 20 cm in sediments of the Yellow Sea (Wang et al., 2019) or even 40 cm in moat sediments sampled in inner Tokyo (Matsuguma et al., 2017). Whereas some particle burial can completely be ascribed to sedimentation (Matsuguma et al., 2017), MP distributions at the Irish Shelf were found to exceed below sediment layers that date to the onset of plastic production in the 1940s, suggesting bioturbation to represent the driving factor of this particle export. Nevertheless, particle transport was found to be weak, possibly caused by the absence of large bioturbation events, which are commonly observed at the Irish Shelf (Coughlan et al., 2015). In contrast, observed high MP burial depths in Yellow Sea sediments might be associated with the presence of non-local particle translocation, mediated by several abundant conveyor belt feeders, representing terebellid or maldanid taxa (Zhang et al., 2012). Hence, variable biodiffusive MP mixing depths probably suggest that MP burial depths can vary with site based on varying local community structures.

The highly variable nature of bioturbation processes on temporal and spatial scales renders the transfer of experimental findings made in this study to actual processes of MP burial in the field extraordinary difficult. As data on vertical MP distributions in marine sediments are scarce, many species-specific responses to MP deposition need to be hypothesized. Hence, the sampling of deeper sediment strata in the context of future monitoring campaigns is strongly recommended based on the present study and previous investigations (Martin et al., 2017). This will allow comparing obtained MP distributions to already existing data on bioturbation for a correct evaluation of MP burial at a given site. However, due to inconsistent sampling and monitoring protocols recent findings are often biased and hard to compare (Van Cauwenberghe et al., 2015b). This is especially true for MPs < 1 µm, so called nanoplastics, as existing methods show low extraction efficiencies for this particle class, which might therefore be underrepresented in present data sets (da Costa et al., 2016; Gigault et al., 2016).

A refined knowledge of macrofauna impact on benthic MP transport can be crucial for a correct assessment of habitat MP contamination, helping to identify accumulation zones and to understand the behavior of this particle class in the marine environment. As MP concentrations in marine sediments are comparably low and usually are not exceeding concentrations of 10 – 100 particles $l^{-1}$ $sediment^{-1}$, MP bioturbation and ingestion solely affects particle redistribution, having no harmful effects on organisms in question. However, global plastic production and MP formation rates are estimated to keep rising during the coming decades, and will probably have profound effects on export functions of bioturbation and on potential toxicity to marine organisms in the future. By 2100, the global amount of floating MPs is assumed to have increased by a factor of 50 compared to MP levels observed in 2010 (Everaert et al., 2018). With regard to strong vertical export of floating MPs to the seafloor, bioturbation might become a pivotal process in mediating MP transport to sediment matrices, preventing further transport or resuspension, and thus, strongly reducing the amount of MP that is accessible to other marine organisms. Potential toxic effects of MPs on benthic invertebrates are known to occur under high MP concentration exposures (Browne et al., 2013; Wright et al., 2013) that might be reached during the second half of the 21st century in marine sediments (Everaert et al., 2018). Hence, MP burial by bioturbation potentially represents an important mechanism to prevent adverse effects of MP exposure from other benthic organisms in the future. However, trends of plastic inputs into marine waters are difficult to estimate, as they are governed by numerous socio-economic and technical factors such as population density and growth, sewage water treatment efficiency and ultimately, future societal developments and environmental management plans. For two different scenarios of the further progression of global technical advance and environmental conservation strategies, slightly decreased plastic inputs in the year 2050 compared to the present were found, exhibiting only minor differences between both scenarios (Everaert et al., 2018). Efforts to remediate the global plastic pollution, e.g. by collection of plastic litter, are proven to have little impact on a global scale, as they are limited to terrestrial habitats or beaches. Hence, the most effective tool for remediation lies within an overall reduction of plastic inputs into marine ecosystems. This concept can only be accomplished by a global orchestration of technical and socio-economic advances, both reducing general plastic production rates and improving recycling efficiencies of these materials and hence, minimizing losses to the environment. Plastic once introduced to marine systems might remain there for elongated times scales in the range of several hundred years (Barnes et al., 2009) until its complete disintegration due to fragmentation. Bioturbation thus will represent a key process for the removal of MP particles from marine ecosystems for a long time and might also support a long-term conservation of these already hardly degradable materials under absence of light and oxygen within the sediment body, preventing further MP fragmentation.

# REFERENCES


Aller, R.C., 1980. Quantifying solute distributions in the bioturbated zone of marine sediments by defining an average microenvironment. Geochim. Cosmochim. Acta **44**, 1955–1965.

Andersen, F.Ø., Kristensen, E., 1988. The influence of macrofauna on estuarine benthic community metabolism: a microcosm study. Mar. Biol. **99**, 591–603.

Anderson, M.J., 2017. Permutational Multivariate Analysis of Variance (PERMANOVA), Wiley StatsRef: Statistics Reference Online, Major Reference Works.

Andrady, A.L., 2011. Microplastics in the marine environment. Mar. Pollut. Bull. **62**, 1596–1605.

Andrady, A.L., Neal, M.A., 2009. Applications and societal benefits of plastics. Philos. Trans. R. Soc. Lond. B Biol. Sci. **364**, 1977–1984.

Andresen, M., Kristensen, E., 2002. The importance of bacteria and microalgae in the diet of the deposit-feeding polychaete *Arenicola marina*. Ophelia **56**, 179–196.

Arndt, E.A., 1989. Ecological, physiological and historical aspects of brackish water fauna distribution, in: Ryland, J.S., Tyler, P.A. (Eds.), Reproduction, Genetics and Distributions of Marine Organisms. Olsen & Olsen, Swansea, UK, pp. 327–338.

Arthur, C., Baker, J., Bamford, H., Barnea, N., Lohmann, R., McElwee, K., Morishige, C., Thompson, R., 2009. Summary of the international research workshop on the occurrence, effects, and fate of microplastic marine debris, in: Arthur, C., Baker, J., Bamford, H. (Eds.), Proceedings of the International Research Workshop on the Occurrence, Effects, and Fate of Microplastic Marine Debris. NOAA Technical Memorandum NOS-OR & R-30, University of Washington Tacoma, Tacoma, WA, USA, pp. 7–17.

Bale, A.J., Kenny, A.J., 2005. Sediment analysis and seabed characterization, in: Eleftheriou, A., McIntyre, A. (Eds.), Methods for the Study of Marine Benthos. Blackwell Science Ltd, pp. 43–86.

Ballent, A., Pando, S., Purser, A., Juliano, M.F., Thomsen, L., 2013. Modelled transport of benthic marine microplastic pollution in the Nazaré Canyon. Biogeosciences **10**, 7957–7970.

Banta, G.T., Holmer, M., Jensen, M.J., Kristensen, E., 1999. Effects of two polychaete worms, *Nereis diversicolor* and *Arenicola marina*, on aerobic and anaerobic decomposition in a sandy marine sediment. Aquat. Microb. Ecol. **19**, 189–204.

Barnes, D.K.A., Galgani, F., Thompson, R.C., Barlaz, M., 2009. Accumulation and fragmentation of plastic debris in global environments. Philos. Trans. R. Soc. Lond. B. Biol. Sci. 364, 1985–98.

Baumfalk, Y.A., 1979. Heterogeneous grain size distribution in tidal flat sediment caused by bioturbation activity of *Arenicola marina* (Polychaeta). Netherlands J. Sea Res. **13**, 428–440.

Baztan, J., Carrasco, A., Chouinard, O., Cleaud, M., Gabaldon, J.E., Huck, T., Jaffrès, L., Jørgensen, B.B., Miguelez, A., Paillard, C., Vanderlinden, J.P., 2014. Protected areas in the Atlantic facing the hazards of micro-plastic pollution: First diagnosis of three islands in the Canary Current. Mar. Pollut. Bull. **80**, 302–311.

Bergmann, M., Wirzberger, V., Krumpen, T., Lorenz, C., Primpke, S., Tekman, M.B., Gerdts, G., 2017. High Quantities of Microplastic in Arctic Deep-Sea Sediments from the HAUSGARTEN Observatory. Environ. Sci. Technol. **51**, 11000–11010.

Berner, R.A., 1980. Early diagenesis: A theoretical approach. Princeton University Press, Princeton, N.J.

Besseling, E., Foekema, E.M., van den Heuvel-Greve, M.J., Koelmans, A.A., 2017. The Effect of Microplastic on the Uptake of Chemicals by the Lugworm *Arenicola marina* (L.) under Environmentally Relevant Exposure Conditions. Environ. Sci. Technol. **51**, 8795–8804.

Besseling, E., Wegner, A., Foekema, E.M., van den Heuvel-Greve, M.J., Koelmans, A.A., 2013. Effects of microplastic on fitness and PCB bioaccumulation by the lugworm *Arenicola marina* (L.). Environ. Sci. Technol. **47**, 593–600.

Beukema, J.J., 1976. Biomass and species richness of the macro-benthic animals living on the tidal flats of the Dutch Wadden Sea. Netherlands J. Sea Res. **48**, 111–125.

Beukema, J.J., De Vlas, J., 1979. Population parameters of the lugworm, *Arenicola marina*, living on tidal flats in the Dutch Wadden Sea. Netherlands J. Sea Res. **13**, 331–353.

Blair, N.E., Levin, L.A., DeMaster, D.J., Plaia, G., 1996. The short-term fate of fresh algal carbon in continental slope sediments. Limnol. Oceanogr. **41**, 1208–1219.

Blumenröder, J., Sechet, P., Kakkonen, J.E., Hartl, M.G.J., 2017. Microplastic contamination of intertidal sediments of Scapa Flow, Orkney: A first assessment. Mar. Pollut. Bull. **124**, 112–120.

Boudreau, B.P., 1994. Is burial velocity a master parameter for bioturbation? Geochim. Cosmochim. Acta **58**, 1243–1249.

Boudreau, B.P., 1986. Mathematics of tracer mixing in sediments; I, Spatially-dependent, diffusive mixing. Am. J. Sci. **286**, 161–198.

Bravo Rebolledo, E.L., Van Franeker, J.A., Jansen, O.E., Brasseur, S.M.J.M., 2013. Plastic ingestion by harbour seals (*Phoca vitulina*) in The Netherlands. Mar. Pollut. Bull. **67**, 200–202.

Brey, T., 1991. The relative significance of biological and physical disturbance an example from intertidal and subtidal sandy bottom communities. Estuar. Coast. Shelf Sci. **33**, 339–360.

Browne, M.A., Crump, P., Niven, S.J., Teuten, E., Tonkin, A., Galloway, T., Thompson, R., 2011. Accumulation of microplastic on shorelines worldwide: sources and sinks. Environ. Sci. Technol. **45**, 9175–9179.

Browne, M.A., Dissanayake, A., Galloway, T.S., Lowe, D.M., Thompson, R.C., 2008. Ingested microscopic plastic translocates to the circulatory system of the mussel, *Mytilus edulis* (L). Environ. Sci. Technol. **42**, 5026–5031.

Browne, M.A., Niven, S.J., Galloway, T.S., Rowland, S.J., Thompson, R.C., 2013. Microplastic Moves Pollutants and Additives to Worms, Reducing Functions Linked to Health and Biodiversity. Curr. Biol. **23**, 2388–2392.

Cadée, G.C., 1976. Sediment reworking by *Arenicola marina* on tidal flats in the Dutch Wadden Sea. Netherlands J. Sea Res. **10**, 440–460.

Carpenter, E.J., Anderson, S.J., Harvey, G.R., 1972. Polystyrene spherules in coastal waters. Science (80-. ). **178**, 749–750.

Castañeda, R.A., Avlijas, S., Simard, M.A., Ricciardi, A., 2014. Microplastic pollution in St. Lawrence River sediments. Can. J. Fish. Aquat. Sci. **71**, 1767–1771.

Christiansen, C., Vølund, G., Lund-Hansen, L.C., Bartholdy, J., 2006. Wind influence on tidal flat sediment dynamics: Field investigations in the Ho Bugt, Danish Wadden Sea. Mar. Geol. **235**, 75–86.

Christie, M.C., Dyer, K.R., Turner, P., 1999. Sediment Flux and Bed Level Measurements from a Macro Tidal Mudflat. Estuar. Coast. Shelf Sci. **49**, 667–688.

Cluzard, M., Kazmiruk, T.N., Kazmiruk, V.D., Bendell, L.I., 2015. Intertidal Concentrations of Microplastics and Their Influence on Ammonium Cycling as Related to the Shellfish Industry. Arch. Environ. Contam. Toxicol. **69**, 310–319.

Cole, M., Lindeque, P., Fileman, E., Halsband, C., Goodhead, R., Moger, J., Galloway, T.S., 2013. Microplastic ingestion by zooplankton. Environ. Sci. Technol. **47**, 6646–55.

Cole, M., Lindeque, P.K., Fileman, E., Clark, J., Lewis, C., Halsband, C., Galloway, T.S., 2016. Microplastics Alter the Properties and Sinking Rates of Zooplankton Faecal Pellets. Environ. Sci. Technol. **50**, 3239–3246.

Corcoran, P., Moore, C., Jazvac, K., 2014. An anthropogenic marker horizon in the future rock record. GSA Today **24**, 4–8.

Corcoran, P.L., Norris, T., Ceccanese, T., Walzak, M.J., Helm, P.A., Marvin, C.H., 2015. Hidden plastics of Lake Ontario, Canada and their potential preservation in the sediment record. Environ. Pollut. **204**, 17–25.

Cospheric, 2014. Preparing Tween Solutions. Santa Barbara, CA. USA.

Costa, P.F., F., O.R., da Fonseca, L.C., 2006. Feeding Ecology of *Nereis diversicolor* ( O. F. Müller ) ( Annelida , Polychaeta ) on Estuarine and Lagoon Environments in the Southwest Coast of Portugal. Panam. J. Aquat. Sci. **1**, 114–126.

Coughlan, M., Wheeler, A.J., Dorschel, B., Lordan, C., Boer, W., Gaever, P. van, Haas, H. de, Mörz, T., 2015. Record of anthropogenic impact on the Western Irish Sea mud belt. Anthropocene **9**, 56–69.

Cournane, S., León Vintró, L., Mitchell, P.I., 2010. Modelling the reworking effects of bioturbation on the incorporation of radionuclides into the sediment column: implications for the fate of particle-reactive radionuclides in Irish Sea sediments. J. Environ. Radioact. **101**, 985–991.

da Costa, J.P., Santos, P.S.M., Duarte, A.C., Rocha-Santos, T., 2016. (Nano)plastics in the environment – Sources, fates and effects. Sci. Total Environ. **566–567**, 15–26.

Dales, R.P., 1950. The reproduction and larval development of *Nereis diversicolor* O. F. Müller. J. Mar. Biol. Assoc. United Kingdom **29**, 321–360.

Davey, J.T., 1994. The architecture of the burrow of *Nereis diversicolor* and its quantification in relation to sediment-water exchange. J. Exp. Mar. Bio. Ecol. **179**, 115–129.

Davey, J.T., Watson, P.G., 1995. The activity of *Nereis diversicolor* (Polychaeta) and its impact on nutrient fluxes in estuarine waters. Ophelia **41**, 57–70.

De Wilde, P.A.W.J., Berghuis, E.M., 1979. Laboratory experiments on growth of juvenile lugworms, *Arenicola marina*. Netherlands J. Sea Res. **13**, 487–502.

Delefosse, M., Kristensen, E., 2012. Burial of *Zostera marina* seeds in sediment inhabited by three polychaetes: Laboratory and field studies. J. Sea Res. **71**, 41–49.

Devriese, L.I., van der Meulen, M.D., Maes, T., Bekaert, K., Paul-Pont, I., Frère, L., Robbens, J., Vethaak, A.D., 2015. Microplastic contamination in brown shrimp (*Crangon crangon*, Linnaeus 1758) from coastal waters of the Southern North Sea and Channel area. Mar. Pollut. Bull. **98**, 179-187.

Duis, K., Coors, A., 2016. Microplastics in the aquatic and terrestrial environment: sources (with a specific focus on personal care products), fate and effects. Environ. Sci. Eur. **28**, 2.

Duport, E., Gilbert, F., Poggiale, J.-C., Dedieu, K., Rabouille, C., Stora, G., 2007. Benthic macrofauna and sediment reworking quantification in contrasted environments in the Thau Lagoon. Estuar. Coast. Shelf Sci. **72**, 522–533.

Duport, E., Stora, G., Tremblay, P., Gilbert, F., 2006. Effects of population density on the sediment mixing induced by the gallery-diffusor *Hediste* (*Nereis*) *diversicolor* O. F. Müller, 1776. J. Exp. Mar. Bio. Ecol. **336**, 33–41.

Einstein, A., 1905. Über die von der molekularkinetischen Theorie der Wärme geforderte Bewegung von in ruhenden Flüssigkeiten suspendierten Teilchen. Ann. Phys. **322**, 549–560.

Esselink, P., Zwarts, L., 1989. Seasonal trend in burrow depth and tidal variation in feeding activity of *Nereis diversicolor*. Mar. Ecol. Prog. Ser. **56**, 243–254.

Everaert, G., Van Cauwenberghe, L., De Rijcke, M., Koelmans, A.A., Mees, J., Vandegehuchte, M., Janssen, C.R., 2018. Risk assessment of microplastics in the ocean: Modelling approach and first conclusions. Environ. Pollut. **242**, 1930–1938.

Fang, C., Zheng, R., Zhang, Y., Hong, F., Mu, J., Chen, M., Song, P., Lin, L., Lin, H., Le, F., Bo, J., 2018. Microplastic contamination in benthic organisms from the Arctic and sub-Arctic regions. Chemosphere **209**, 298–306.

Farrell, P., Nelson, K., 2013. Trophic level transfer of microplastic: *Mytilus edulis* (L.) to *Carcinus maenas* (L.). Environ. Pollut. **177**, 1–3.

Fauchald, K., Jumars, P.A., 1979. The Diet of Worms : A Study of Polychaete Feeding Guilds. Oceanogr. Mar. Biol. An Annu. Rev. **17**, 193–284.

Fendall, L.S., Sewell, M.A., 2009. Contributing to marine pollution by washing your face: microplastics in facial cleansers. Mar. Pollut. Bull. **58**, 1225–1228.

Fischer, V., Elsner, N.O., Brenke, N., Schwabe, E., Brandt, A., 2015. Plastic pollution of the Kuril–Kamchatka Trench area (NW pacific). Deep Sea Res. Part II Top. Stud. Oceanogr. **111**, 399–405.

Fisher, J.B., Lick, W.J., McCall, P.L., Robbins, J.A., 1980. Vertical mixing of lake sediments by tubificid oligochaetes. J. Geophys. Res. Ocean. **85**, 3997–4006.

Flach, E.C., Beukema, J.J., 1994. Density-governing mechanisms in populations of the lugworm *Arenicola marina* on tidal flats. Mar. Ecol. Prog. Ser. **115**, 139–149.

Folk, R.L., Ward, W.C., 1957. Brazos River bar ; a study in the significance of grain size parameters. J. Sediment. Res. **21**, 3–26.

Fossi, M.C., Panti, C., Guerranti, C., Coppola, D., Giannetti, M., Marsili, L., Minutoli, R., 2012. Are baleen whales exposed to the threat of microplastics? A case study of the Mediterranean fin whale (*Balaenoptera physalus*). Mar. Pollut. Bull. **64**, 2374–2379.

François, F., Gerino, M., Stora, G., Durbec, J.-P., Poggiale, J.-C., 2002. Functional approach to sediment reworking by gallery-forming macrobenthic organisms: modeling and application with the polychaete *Nereis diversicolor*. Mar. Ecol. Prog. Ser. **229**, 127–136.

François, F., Poggiale, J.-C., Durbec, J.-P., Stora, G., 1997. A New Approach for the Modelling of Sediment Reworking Induced by a Macrobenthic Community. Acta Biotheor. **45**, 295–319.

Freese, E., Köster, J., Rullkötter, J., 2008. Origin and composition of organic matter in tidal flat sediments from the German Wadden Sea. Org. Geochem. **39**, 820–829.

Gerino, M., Aller, R.C., Lee, C., Cochran, J.K., Aller, J.Y., Green, M.A., Hirschberg, D., 1998. Comparison of Different Tracers and Methods Used to Quantify Bioturbation During a Spring Bloom : 234-Thorium , Luminophores and Chlorophyll a. Estuar. Coast. Shelf Sci. **46**, 531–547.

Gewert, B., Plassmann, M.M., MacLeod, M., 2015. Pathways for degradation of plastic polymers floating in the marine environment. Environ. Sci. Process. Impacts **17**, 1513–1521.

Geyer, R., Jambeck, J.R., Law, K.L., 2017. Production, use, and fate of all plastics ever made. Sci. Adv. 3, e1700782.

Gigault, J., Pedrono, B., Maxit, B., Ter Halle, A., 2016. Marine plastic litter: the unanalyzed nano-fraction. Environ. Sci. Nano **3**, 346–350.

Gomiero, A., Strafella, P., Pellini, G., Salvalaggio, V., Fabi, G., 2018. Comparative Effects of Ingested PVC Micro Particles With and Without Adsorbed Benzo(a)pyrene vs. Spiked Sediments on the Cellular and Sub Cellular Processes of the Benthic Organism *Hediste diversicolor*. Front. Mar. Sci. **5**, 99.

Green, D.S., Boots, B., Sigwart, J., Jiang, S., Rocha, C., 2016. Effects of conventional and biodegradable microplastics on a marine ecosystem engineer (*Arenicola marina*) and sediment nutrient cycling. Environ. Pollut. **208**, 426–434.

Gregory, M.R., 2009. Environmental implications of plastic debris in marine settings—entanglement, ingestion, smothering, hangers-on, hitch-hiking and alien invasions. Philos. Trans. R. Soc. Lond. B Biol. Sci. **364**, 2013–2025.

Guinasso, N.L., Schink, D.R., 1975. Quantitative estimates of biological mixing rates in abyssal sediments. J. Geophys. Res. **80**, 3032–3043.

Gunnarsson, J.S., Hollertz, K., Rosenberg, R., 1999. Effects of organic enrichment and burrowing activity of the polychaete *Nereis diversicolor* on the fate of tetrachlorobiphenyl in marine sediments. Environ. Toxicol. Chem. **18**, 1149–1156.

Handy, R.D., Shaw, B.J., 2007. Toxic effects of nanoparticles and nanomaterials: Implications for public health, risk assessment and the public perception of nanotechnology. Health. Risk Soc. **9**, 125–144.

Hansen, E., Nilsson, N.H., Lithner, D., Lassen, C., 2013. Hazardous substances in plastic materials, Danish Technological Institute.

Harrison, J.P., Schratzberger, M., Sapp, M., Osborn, A.M., 2014. Rapid bacterial colonization of low-density polyethylene microplastics in coastal sediment microcosms. BMC Microbiol. **14**, 1–15.

Hedman, J.E., Gunnarsson, J.S., Samuelsson, G., Gilbert, F., 2011. Particle reworking and solute transport by the sediment-living polychaetes *Marenzelleria neglecta* and *Hediste diversicolor*. J. Exp. Mar. Bio. Ecol. **407**, 294–301.

Hengstmann, E., Tamminga, M., vom Bruch, C., Fischer, E.K., 2018. Microplastic in beach sediments of the Isle of Rügen (Baltic Sea) - Implementing a novel glass elutriation column. Mar. Pollut. Bull. **126**, 263–274.

Hermabessiere, L., Dehaut, A., Paul-Pont, I., Lacroix, C., Jezequel, R., Soudant, P., Duflos, G., 2017. Occurrence and effects of plastic additives on marine environments and organisms: A review. Chemosphere **182**, 781–793.

Hirai, H., Takada, H., Ogata, Y., Yamashita, R., Mizukawa, K., Saha, M., Kwan, C., Moore, C., Gray, H., Laursen, D., Zettler, E.R., Farrington, J.W., Reddy, C.M., Peacock, E.E., Ward, M.W., 2011. Organic micropollutants in marine plastics debris from the open ocean and remote and urban beaches. Mar. Pollut. Bull. **62**, 1683–1692.

Hong, D., Quinn, P., Luding, S., 2001. Reverse Brazil Nut Problem: Competition between Percolation and Condensation. Phys. Rev. Lett. **86**, 3423–3426.

Hoornweg, D., Bhada-Tata, P., 2012. What a waste: A Global Review of Solid Waste Management, Urban Development Series. Knowledge Papers. Washington, DC. USA.

Ivar do Sul, J.A., Spengler, A., Costa, M.F., 2009. Here, there and everywhere. Small plastic fragments and pellets on beaches of Fernando de Noronha (Equatorial Western Atlantic). Mar. Pollut. Bull. **58**, 1236–1238.

Jacobsen, V.H., 1967. The feeding of the lugworm, *Arenicola marina* (L.). Quantitative studies. Ophelia **4**, 91–109.

Jeong, C., Won, E., Kang, H., Lee, M., Hwang, D., Hwang, U., Zhou, B., Souissi, S., Lee, S., Lee, J., 2016. Microplastic Size-Dependent Toxicity, Oxidative Stress Induction, and p-JNK and p-p38 Activation in the Monogonont Rotifer (*Brachionus koreanus*). Environ. Sci. Technol. **50**, 8849–8857.

Josefson, A.B., Norkko, J., Norkko, A., 2012. Burial and decomposition of plant pigments in surface sediments of the Baltic Sea: role of oxygen and benthic fauna. Mar. Ecol. Prog. Ser. **455**, 33–49.

Koelmans, A.A., Kooi, K., Law, K.L., Sebille, E. van, 2017. All is not lost: deriving a top-down mass budget of plastic at sea. Environ. Res. Lett. **12**, 114028.

Kooi, M., Nes, E.H. van, Scheffer, M., Koelmans, A.A., 2017. Ups and Downs in the Ocean: Effects of Biofouling on Vertical Transport of Microplastics. Environ. Sci. Technol. **51**, 7963–7971.

Kowalski, N., Reichardt, A.M., Waniek, J.J., 2016. Sinking rates of microplastics and potential implications of their alteration by physical, biological, and chemical factors. Mar. Pollut. Bull. **109**, 310–319.

Kristensen, E., Hansen, T., Delefosse, M., Banta, G.T., Quintana, C.O., 2011. Contrasting effects of the polychaetes *Marenzelleria viridis* and *Nereis diversicolor* on benthic metabolism and solute transport in sandy coastal sediment. Mar. Ecol. Prog. Ser. **425**, 125–139.

Kristensen, E., Holmer, M., 2001. Decomposition of plant materials in marine sediment exposed to different electron acceptors ($O_2$, $NO_3^-$, and $SO_4^{2-}$), with emphasis on substrate origin, degradation kinetics, and the role of bioturbation. Geochim. Cosmochim. Acta **65**, 419–433.

Kristensen, E., Penha-Lopes, G., Delefosse, M., Valdemarsen, T., Quintana, C.O., Banta, G.T., 2012. What is bioturbation? The need for a precise definition for fauna in aquatic sciences. Mar. Ecol. Prog. Ser. **446**, 285–302.

Krüger, F., 1971. Bau und Leben des Wattwurmes *Arenicola marina*. Helgoländer Wissenschaftliche Meeresuntersuchungen **22**, 149–200.

Krüger, F., 1964. Versuche über die Abhängigkeit der Atmung von *Arenicola marina* (Annelida Polychaeta) von Größe und Temperatur. Helgoländer wissenschaftliche Meeresuntersuchungen **10**, 38–63.

Kukulka, T., Proskurowski, G., Morét-Ferguson, S., Meyer, D.W., Law, K.L., 2012. The effect of wind mixing on the vertical distribution of buoyant plastic debris. Geophys. Res. Lett. **39**, L07601.

Kulkarni, K.G., Panchang, R., 2015. New Insights into Polychaete Traces and Fecal Pellets: Another Complex Ichnotaxon? PLoS One **10**, e0139933.

Laist, D.W., 1997. Impacts of marine debris: entanglement of marine life in marine debris including a comprehensive list of species with entanglement and ingestion records, in: Coe, J.M., Rogers, D.B. (Eds.), Marine Debris, Sources, Impacts and Solutions. Springer-Verlag, New York, NY, pp. 99–139.

Laist, D.W., 1987. Overview of the biological effects of lost and discarded plastic debris in the marine environment. Mar. Pollut. Bull. **18**, 319–326.

Law, K.L., Morét-Ferguson, S., Maximenko, N.A., Proskurowski, G., Peacock, E.E., Hafner, J., Reddy, C.M., 2010. Plastic accumulation in the North Atlantic Subtropical Gyre. Science. **329**, 1185–1188.

Lebreton, L.C.-M., Greer, S.D., Borrero, J.C., 2012. Numerical modelling of floating debris in the world's oceans. Mar. Pollut. Bull. **64**, 653–661.

Lecroart, P., Maire, O., Schmidt, S., Grémare, A., Anschutz, P., Meysman, F.J.R., 2010. Bioturbation, short-lived radioisotopes, and the tracer-dependence of biodiffusion coefficients. Geochim. Cosmochim. Acta **74**, 6049–6063.

Lehtiniemi, M., Hartikainen, S., Näkki, P., Engström-Öst, J., Koistinen, A., Setälä, O., 2018. Size matters more than shape: Ingestion of primary and secondary microplastics by small predators. Food Webs **17**, e00097.

Leipe, T., Tauber, F., Vallius, H., Virtasalo, J., Uścinowicz, S., Kowalski, N., Hille, S., Lindgren, S., Myllyvirta, T., 2011. Particulate organic carbon (POC) in surface sediments of the Baltic Sea. Geo-Marine Lett. **31**, 175–188.

Levin, L., Blair, N., DeMaster, D., Plaia, G., Fornes, W., Martin, C., Thomas, C., 1997. Rapid subduction of organic matter by maldanid polychaetes on the North Carolina slope. J. Mar. Res. **55**, 595–611.

Lindqvist, S., Gilbert, F., Eriksson, S., Hulth, S., 2013. Activities by *Hediste diversicolor* under different light regimes: experimental quantification of particle reworking using time-resolved imaging. J. Exp. Mar. Bio. Ecol. **448**, 240–249.

Lobelle, D., Cunliffe, M., 2011. Early microbial biofilm formation on marine plastic debris. Mar. Pollut. Bull. **62**, 197–200.

Lohmann, R., 2017. Microplastics are not important for the cycling and bioaccumulation of organic pollutants in the oceans—but should microplastics be considered POPs themselves? Integr. Environ. Assess. Manag. **13**, 460–465.

Long, M., Moriceau, B., Gallinari, M., Lambert, C., Huvet, A., Raffray, J., Soudant, P., 2015. Interactions between microplastics and phytoplankton aggregates: Impact on their respective fates. Mar. Chem. **175**, 39–46.

Long, M., Paul-Pont, I., Hégaret, H., Moriceau, B., Lambert, C., Huvet, A., Soudant, P., 2017. Interactions between polystyrene microplastics and marine phytoplankton lead to species-specific hetero-aggregation. Environ. Pollut. **228**, 454–463.

Lopez, G.R., Levinton, J.S., 1987. Ecology of Deposit-Feeding Animals in Marine Sediments. Q. Rev. Biol. **62**, 235–260.

Lusher, A.L., McHugh, M., Thompson, R.C., 2013. Occurrence of microplastics in the gastrointestinal tract of pelagic and demersal fish from the English Channel. Mar. Pollut. Bull. **67**, 94–99.

Mahaut, M.-L., Graf, G., 1987. A luminophore tracer technique for bioturbation studies. Oceanol. Acta 10**,** 323–328.

Maire, O., Duchêne, J.. C., Grémare, A., Malyuga, V.S., Meysman, F.J.R., 2007. A comparison of sediment reworking rates by the surface deposit-feeding bivalve *Abra ovata* during summertime and wintertime, with a comparison between two models of sediment reworking. J. Exp. Mar. Bio. Ecol. **343**, 21–36.

Maire, O., Lecroart, P., Meysman, F., Rosenberg, R., Duchêne, J., Grémare, A., 2010. Quantification of sediment reworking rates in bioturbation research: A review. Aquat. Biol. **2**, 219–238.

Martin, J., Lusher, A., Thompson, R.C., Morley, A., 2017. The Deposition and Accumulation of Microplastics in Marine Sediments and Bottom Water from the Irish Continental Shelf. Sci. Rep. **7**, 10772.

Martínez-Gómez, C., León, V.M., Calles, S., Gomáriz-Olcina, M., Vethaak, A.D., 2017. The adverse effects of virgin microplastics on the fertilization and larval development of sea urchins. Mar. Environ. Res. **130**, 69–76.

Mathalon, A., Hill, P., 2014. Microplastic fibers in the intertidal ecosystem surrounding Halifax Harbor, Nova Scotia. Mar. Pollut. Bull. **81**, 69–79.

Matisoff, G., Wang, X., 2000. Particle Mixing by Freshwater Infaunal Bioirrigators: Midges (Chironomidae: Diptera) and Mayflies (Ephemeridae: Ephemeroptera). J. Great Lakes Res. **26**, 174–182.

Mato, Y., Isobe, T., Takada, H., Kanehiro, H., Ohtake, C., Kaminuma, T., 2001. Plastic Resin Pellets as a Transport Medium for Toxic Chemicals in the Marine Environment. Environ. Sci. Technol. **35**, 318–324.

Matsuguma, Y., Takada, H., Kumata, H., Kanke, H., Sakurai, S., Suzuki, T., Itoh, M., Okazaki, Y., Boonyatumanond, R., Zakaria, M.P., Weerts, S., Newman, B., 2017. Microplastics in Sediment Cores from Asia and Africa as Indicators of Temporal Trends in Plastic Pollution. Arch. Environ. Contam. Toxicol. **73**, 230–239.

Maximenko, N., Hafner, J., Niiler, P., 2012. Pathways of marine debris derived from trajectories of Lagrangian drifters. Mar. Pollut. Bull. **65**, 51–62.

Meysman, F.J.R., Boudreau, B.P., Middelburg, J.J., 2003. Relations between local, nonlocal, discrete and continuous models of bioturbation. J. Mar. Res. **61**, 391–410.

Miralles, L., Gomez-Agenjo, M., Rayon-Viña, F., Gyraitė, G., Garcia-Vazquez, E., 2018. Alert calling in port areas: Marine litter as possible secondary dispersal vector for hitchhiking invasive species. J. Nat. Conserv. **42**, 12–18.

Möbius, M.E., Lauderdale, B.E., Nagel, S.R., Jaeger, H.M., 2001. Size separation of granular particles. Nature **414**, 4646.

Muller-Karanassos, C., Turner, A., Arundel, W., Vance, T., Lindeque, P.K., Cole, M., 2019. Antifouling paint particles in intertidal estuarine sediments from southwest England and their ingestion by the harbour ragworm, *Hediste diversicolor*. Environ. Pollut. **249**, 163–170.

Murray, F., Solan, M., Douglas, A., 2017. Effects of algal enrichment and salinity on sediment particle reworking activity and associated nutrient generation mediated by the intertidal polychaete *Hediste diversicolor*. J. Exp. Mar. Bio. Ecol. **495**, 75–82.

Näkki, P., Setälä, O., Lehtiniemi, M., 2017. Bioturbation transports secondary microplastics to deeper layers in soft marine sediments of the northern Baltic Sea. Mar. Pollut. Bull. **119**, 255–261.

Nesto, N., Simonini, R., Prevedelli, D., Da Ros, L., 2012. Effects of diet and density on growth, survival and gametogenesis of *Hediste diversicolor* (O.F. Müller, 1776) (Nereididae, Polychaeta). Aquaculture **362–363**, 1–9.

Nogaro, G., Charles, F., Mendonça, J.B., Mermillod-Blondin, F., Stora, G., François-Carcaillet, F., 2007. Food supply impacts sediment reworking by *Nereis diversicolor*. Hydrobiologia **598**, 403–408.

Nor, N.H.M., Obbard, J.P., 2014. Microplastics in Singapore's coastal mangrove ecosystems. Mar. Pollut. Bull. **79**, 278–283.

Norén, F., 2008. Small plastic particles in Coastal Swedish waters. N-Research KIMO. Lysekil. Sweden 1–10.

Obbard, R.W., Sadri, S., Wong, Y.Q., Khitun, A.A., Baker, I., Thompson, R.C., 2014. Global warming releases microplastic legacy frozen in Arctic Sea ice. Earth's Futur. **2**, 315–320.

Ogonowski, M., Schür, C., Jarsén, Å., Gorokhova, E., 2016. The Effects of Natural and Anthropogenic Microparticles on Individual Fitness in *Daphnia magna*. PLoS One **11**, e0155063.

Papaspyrou, S., Thessalou-Legaki, M., Kristensen, E., 2010. The influence of infaunal (*Nereis diversicolor*) abundance on degradation of organic matter in sandy sediments. J. Exp. Mar. Bio. Ecol. **393**, 148–157.

PlasticsEurope, 2018. PlasticsEurope, 2018. Plastics - the Facts 2018. Frankfurt/Main. Germany.

Plotkin, P.T., Amos, A.F., 1988. Entanglement in and ingestion of marine debris by sea turtles stranded along the South Texas coast, in: Schroeder, B.A. (Ed.), Proceedings of the Eighth Annual Workshop on Sea Turtle Biology and Conservation. NOAA Technical Memorandum NMFS-SEFC-214, Forth Fisher, South Carolina, pp. 79–82.

Pruter, A.T., 1987. Sources, quantities and distribution of persistent plastics in the marine environment. Mar. Pollut. Bull. **18**, 305–310.

Queirós, A.M., Stephens, N., Cook, R., Ravaglioli, C., Nunes, J., Dashfield, S., Harris, C., Tilstone, G.H., Fishwick, J., Braeckman, U., Somerfield, P.J., Widdicombe, S., 2015. Can benthic community structure be used to predict the process of bioturbation in real ecosystems? Prog. Oceanogr. **137**, 559–569.

Rasband, W.S., 2014. ImageJ.

Reed, S., Clark, M., Thompson, R., Hughes, K.A., 2018. Microplastics in marine sediments near Rothera Research Station, Antarctica. Mar. Pollut. Bull. **133**, 460–463.

Reise, K., 1979. Spatial configurations generated by motile benthic polychaetes. Helgoländer wissenschaftliche Meeresuntersuchungen **32**, 55–72.

Retraubun, A.S.W., Dawson, M., and Evans, S.M., 1996a. The role of the burrow funnel in feeding processes in the lugworm *Arenicola marina* (L.). J. Exp. Mar. Bio. Ecol. **202**, 107–118.

Retraubun, A.S.W., Dawson, M., Evans, S.M., 1996b. Spatial and temporal factors affecting sediment turnover by the lugworm *Arenicola marina* (L.). J. Exp. Mar. Bio. Ecol. **201**, 23–35.

Ribeiro, F., Garcia, A.R., Pereira, B.P., Fonseca, M., Mestre, N.C., Fonseca, T.G., Ilharco, L.M., Bebianno, M.J., 2017. Microplastics effects in *Scrobicularia plana*. Mar. Pollut. Bull. **122**, 379–391.

Riisgård, H.U., 1991. Suspension feeding in the polychaete *Nereis diversicolor*. Mar. Ecol. Prog. Ser. **40**, 29–37.

Riisgård, H.U., Banta, G.T., 1998. Irrigation and deposit feeding by the lugworm *Arenicola marina*, characteristics and secondary effects on the environment: a review of current knowledge. Vie Milieu **48**, 243–257.

Rijken, M., 1979. Food and food uptake in *Arenicola marina*. Netherlands J. Sea Res. **13**, 406–421.

Robbins, J.A., McCall, P.L., Berton Fisher, J., Krezoski, J.R., 1979. Effect of deposit feeders on migration of $^{137}$Cs in lake sediments. Earth Planet. Sci. Lett. **42**, 277–287.

Rosa, S., Granadeiro, J.P., Vinagre, C., França, S., Cabral, H.N., Palmeirim, J.M., 2008. Impact of predation on the polychaete *Hediste diversicolor* in estuarine intertidal flats. Estuar. Coast. Shelf Sci. **78**, 655–664.

Ryan, P.G., 2015. Does size and buoyancy affect the long-distance transport of floating debris? Environ. Res. Lett. **10**, 84019.

Scaps, P., 2002. A review of the biology, ecology and potential use of the common ragworm *Hediste diversicolor* (OF Müller) (Annelida: Polychaeta). Hydrobiologia **470**, 203–218.

Self, R.F.L., Jumars, P.A., 1988. Cross-phyletic patterns of particle selection by deposit feeders. J. Mar. Res. **46**, 119–143.

Setälä, O., Fleming-Lehtinen, V., Lehtiniemi, M., 2014. Ingestion and transfer of microplastics in the planktonic food web. Environ. Pollut. **185**, 77–83.

Setälä, O., Norkko, J., Lehtiniemi, M., 2016. Feeding type affects microplastic ingestion in a coastal invertebrate community. Mar. Pollut. Bull. **102**, 95–101.

Smith, C.R., Pope, R.H., DeMaster, D.J., Magaard, L., 1993. Age-dependent mixing of deep-sea sediments. Geochim. Cosmochim. Acta **57**, 1473–1488.

Smith, J.N., Boudreau, B.P., Noshkin, V., 1986. Plutonium and $^{210}$Pb distributions in northeast Atlantic sediments: subsurface anomalies caused by non-local mixing. Earth Planet. Sci. Lett. **81**, 15–28.

Smith, R.I., 1964. On the early development of *Nereis diversicolor* in different salinities. J. Morphol. **114**, 437–463.

Snelgrove, P.V.R., 1998. The biodiversity of macrofaunal organisms in marine sediments. Biodivers. Conserv. **7**, 1123–1132.

Soetaert, K., Herman, P.M.J., Middelburg, J.J., 1996. A model of early diagenetic processes from the shelf to abyssal depths. Geochim. Cosmochim. Acta **60**, 1019–1040.

Song, Y.K., Hong, S.H., Jang, M., Kang, J.-H., Kwon, O.Y., Han, G.M., Shim, W.J., 2014. Large accumulation of micro-sized synthetic polymer particles in the sea surface microlayer. Environ. Sci. Technol. **48**, 9014–9021.

Stolte, A., Forster, S., Gerdts, G., Schubert, H., 2015. Microplastic concentrations in beach sediments along the German Baltic coast. Mar. Pollut. Bull. **99**, 216–229.

Suhrhoff, T.J., Scholz-Böttcher, B.M., 2016. Qualitative impact of salinity, UV radiation and turbulence on leaching of organic plastic additives from four common plastics - A lab experiment. Mar. Pollut. Bull. **102**, 84–94.

Taghon, G.L., 1982. Optimal foraging by deposit-feeding invertebrates: Roles of particle size and organic coating. Oecologia **52**, 295–304.

Tang, M., Kristensen, E., 2007. Impact of microphytobenthos and macroinfauna on temporal variation of benthic metabolism in shallow coastal sediments. J. Exp. Mar. Bio. Ecol. **349**, 99–112.

Teal, L.R., Bulling, M.T., Parker, E.R., Solan, M., 2008. Global patterns of bioturbation intensity and mixed depth of marine soft sediments. Aquat. Biol. **2**, 207–218.

Ter Halle, A., Jeanneau, L., Martignac, M., Jardé, E., Pedrono, B., Brach, L., Gigault, J., 2017. Nanoplastic in the North Atlantic Subtropical Gyre. Environ. Sci. Technol. **51**, 13689–13697.

Thompson, R.C., Olsen, Y., Mitchell, R.P., Davis, A., Rowland, S.J., John, A.W.G., McGonigle, D., Russell, A.E., 2004. Lost at sea: where is all the plastic? Science. **304**, 838.

Timmermann, K., Banta, G.T., Larsen, J., Andersen, O., 2003. Modelling particle and solute transport in sediments inhabited by *Arenicola marina*. Effects of pyrene on transport processes. Vie milieu **53**, 187–200.

Valdemarsen, T., Wendelboe, K., Egelund, J.T., Kristensen, E., Flindt, M.R., 2011. Burial of seeds and seedlings by the lugworm *Arenicola marina* hampers eelgrass (*Zostera marina*) recovery. J. Exp. Mar. Bio. Ecol. **410**, 45–52.

Van Cauwenberghe, L., Claessens, M., Vandegehuchte, M.B., Janssen, C.R., 2015a. Microplastics are taken up by mussels (*Mytilus edulis*) and lugworms (*Arenicola marina*) living in natural habitats. Environ. Pollut. 199, 10–17.

Van Cauwenberghe, L., Claessens, M., Vandegehuchte, M.B., Mees, J., Janssen, C.R., 2013. Assessment of marine debris on the Belgian Continental Shelf. Mar. Pollut. Bull. **73**, 161–169.

Van Cauwenberghe, L., Devriese, L., Galgani, F., Robbens, J., Janssen, C.R., 2015b. Microplastics in sediments: A review of techniques, occurrence and effects. Mar. Environ. Res. **111**, 1–13.

van der Meer, J., Heip, C.H.R., Herman, P.M.J., Moens, T., van Oevelen, D., 2005. Measuring the Flow of Energy and Matter in Marine Benthic Animal Populations, in: Eleftheriou, A., McIntyre, A. (Eds.), Methods for the Study of Marine Benthos. Blackwell Science Ltd, pp. 326–408.

Vedel, A., Andersen, B.B., Riisgård, H.U., 1994. Field investigations of pumping activity of the facultatively filter-feeding polychaete *Nereis diversicolor* using an improved infrared phototransducer system. Mar. Ecol. Prog. Ser. **103**, 91–101.

Vianello, A., Boldrin, A., Guerriero, P., Moschino, V., Rella, R., Sturaro, A., Da Ros, L., 2013. Microplastic particles in sediments of Lagoon of Venice, Italy: First observations on occurrence, spatial patterns and identification. Estuar. Coast. Shelf Sci. **130**, 54–61.

Volkenborn, N., Polerecky, L., Hedtkamp, S.I.C., van Beusekom, J.E.E., de Beer, D., 2007. Bioturbation and bioirrigation extend the open exchange regions in permeable sediments. Limnol. Oceanogr. **52**, 1898–1909.

Volkenborn, N., Woodin, S.A., Wethey, D.S., Polerecky, L., 2016. Bioirrigation in Marine Sediments, in: Elias, S. A. (Ed.), Reference Module in Earth Systems And Environmental Sciences. Elsevier.

Volkman, J.K., Rohjans, D., Rullkötter, J., Scholz-Böttcher, B.M., Liebezeit, G., 2000. Sources and diagenesis of organic matter in tidal flat sediments from the German Wadden Sea. Cont. Shelf Res. **20**, 1139–1158.

von Smoluchowski, M., 1906. Zur kinetischen Theorie der Brownschen Molekularbewegung und der Suspensionen. Ann. Phys. **326**, 756–780.

Vroom, R.J.E., Koelmans, A.A., Besseling, E., Halsband, C., 2017. Aging of microplastics promotes their ingestion by marine zooplankton. Environ. Pollut. **231**, 987–996.

Wang, J., Wang, M., Ru, S., Liu, X., 2019. High levels of microplastic pollution in the sediments and benthic organisms of the South Yellow Sea, China. Sci. Total Environ. **651**, 1661–1669.

Ward, J.E., Kach, D.J., 2009. Marine aggregates facilitate ingestion of nanoparticles by suspension-feeding bivalves. Mar. Environ. Res. **68**, 137–142.

Watts, A.J.R., Lewis, C., Goodhead, R.M., Beckett, S.J., Moger, J., Tyler, C.R., Galloway, T.S., 2014. Uptake and retention of microplastics by the shore crab *Carcinus maenas*. Environ. Sci. Technol. **48**, 8823–8830.

Wegner, A., Besseling, E., Foekema, E.M., Kamermans, P., Koelmans, A.A., 2012. Effects of nanopolystyrene on the feeding behavior of the blue mussel (*Mytilus edulis* L.). Environ. Toxicol. Chem. **31**, 2490–2497.

Welden, N.A.C., Cowie, P.R., 2016. Long-term microplastic retention causes reduced body condition in the langoustine, *Nephrops norvegicus*. Environ. Pollut. **218**, 895–900.

Welsh, D.T., 2003. It's a dirty job but someone has to do it: The role of marine benthic macrofauna in organic matter turnover and nutrient recycling to the water column. Chem. Ecol. **19**, 321–342.

Wenzhöfer, F., Glud, R.N., 2004. Small-scale spatial and temporal variability in coastal benthic $O_2$ dynamics: Effects of fauna activity. Limnol. Oceanogr. **49**, 1471–1481.

Wheatcroft, R.A., 1992. Experimental tests for particle size-dependent bioturbation in the deep ocean. Limnol. Oceanogr. **37**, 90–104.

Wheatcroft, R.A., 1991. Conservative tracer study of horizontal sediment mixing rates in a bathyal basin, California borderland. J. Mar. Res. **49**, 565–588.

Wheatcroft, R.A., Jumars, P.A., Smith, C.R., Nowell, A.R.M., 1990. A mechanistic view of the particulate biodiffusion coefficient: Step lengths, rest periods and transport directions. J. Mar. Res. **48**, 177–207.

Woodall, L.C., Sanchez-Vidal, A., Canals, M., Paterson, G.L.J., Coppock, R., Sleight, V., Calafat, A., Rogers, A.D., Narayanaswamy, B.E., Thompson, R.C., 2014. The deep sea is a major sink for microplastic debris. R. Soc. Open Sci. **1**, 140317.

Wright, S.L., Rowe, D., Thompson, R.C., Galloway, T.S., 2013. Microplastic ingestion decreases energy reserves in marine worms. Curr. Biol. **23**, 1031–1033.

Yager, P.L., Nowell, A.R.M., Jumars, P.A., 1993. Enhanced deposition to pits: A local food source for benthos. J. Mar. Res. **51**, 209–236.

Ye, S., Andrady, A.L., 1991. Fouling of floating plastic debris under Biscayne Bay exposure conditions. Mar. Pollut. Bull. **22**, 608–613.

Zalasiewicz, J., Waters, C.N., Ivar do Sul, J.A., Corcoran, P.L., Barnosky, A.D., Cearreta, A., Edgeworth, M., Gałuszka, A., Jeandel, C., Leinfelder, R., McNeill, J.R., Steffen, W., Summerhayes, C., Wagreich, M., Williams, M., Wolfe, A.P., Yonan, Y., 2016. The geological cycle of plastics and their use as a stratigraphic indicator of the Anthropocene. Anthropocene **13**, 4–17.

Zhang, J., Xu, F., Liu, R., 2012. Community structure changes of macrobenthos in the South Yellow Sea. Chinese J. Oceanol. Limnol. **30**, 248–255.

Zhao, S., Ward, J.E., Danley, M., Mincer, T.J., 2018. Field-Based Evidence for Microplastic in Marine Aggregates and Mussels: Implications for Trophic Transfer. Environ. Sci. Technol. **52**, 11038–11048.

# APPENDIX

**Table A1: Camera settings used for sample imaging.** EV: exposure value

| parameter | setting | |
|---|---|---|
| object - sensor distance | 20 cm | |
| resolution | 1 pixel ~ 6 x 6 µm | |
| picture mode | programmed auto | |
| exposure time | 2.5 s[1] | 1/13 s[2] |
| exposure compensation | - 3 EV[1] | - 1.7 EV[2] |
| exposure delay time | 5 sec | |
| ISO speed | 100[1] | 6 400[2] |

[1] HD experiment
[2] AM experiment

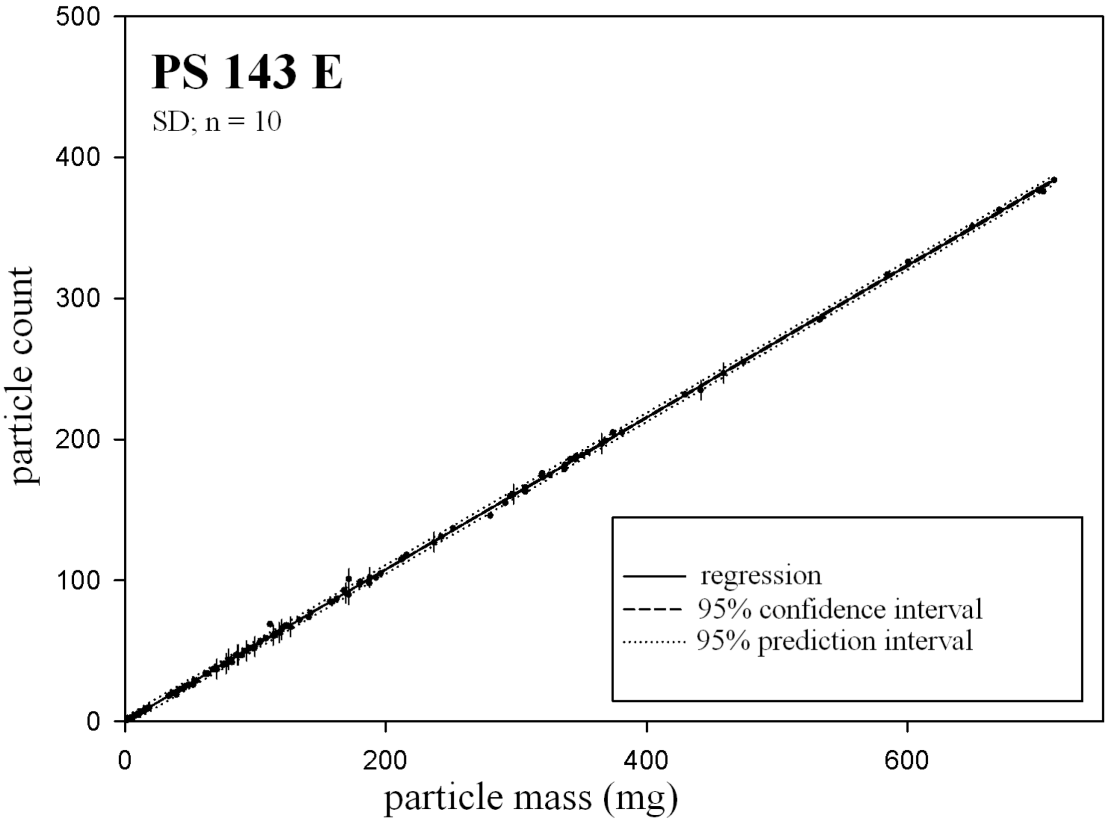


**Figure A1: Linear regression of particle mass and particle number, shown for PS particles used in the AM experiment.**

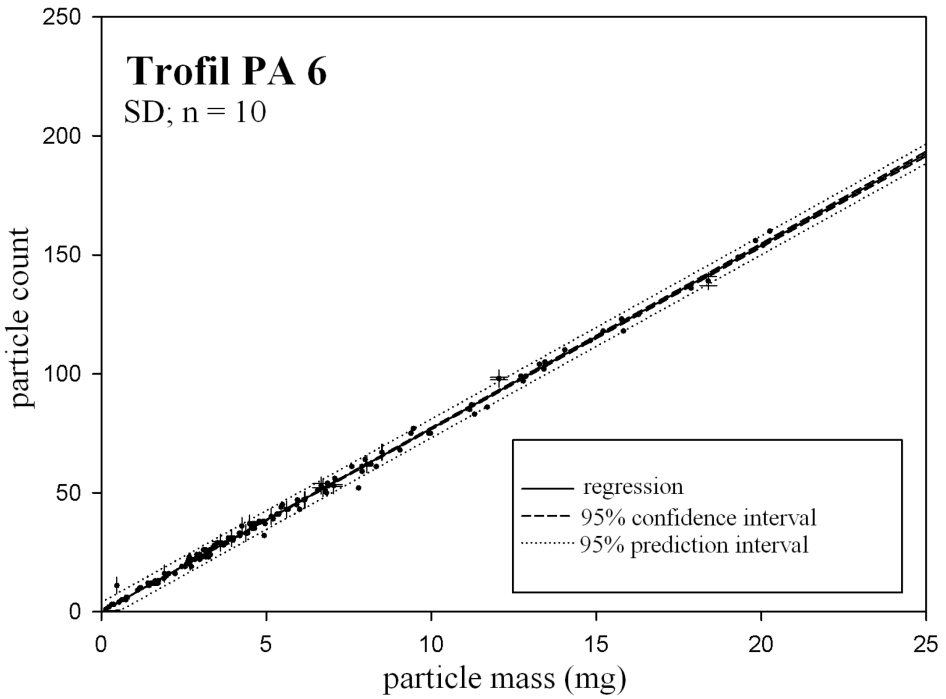


**Figure A2: Linear regression of particle mass and particle number, shown for PA particles used in the AM and HD experiment.**

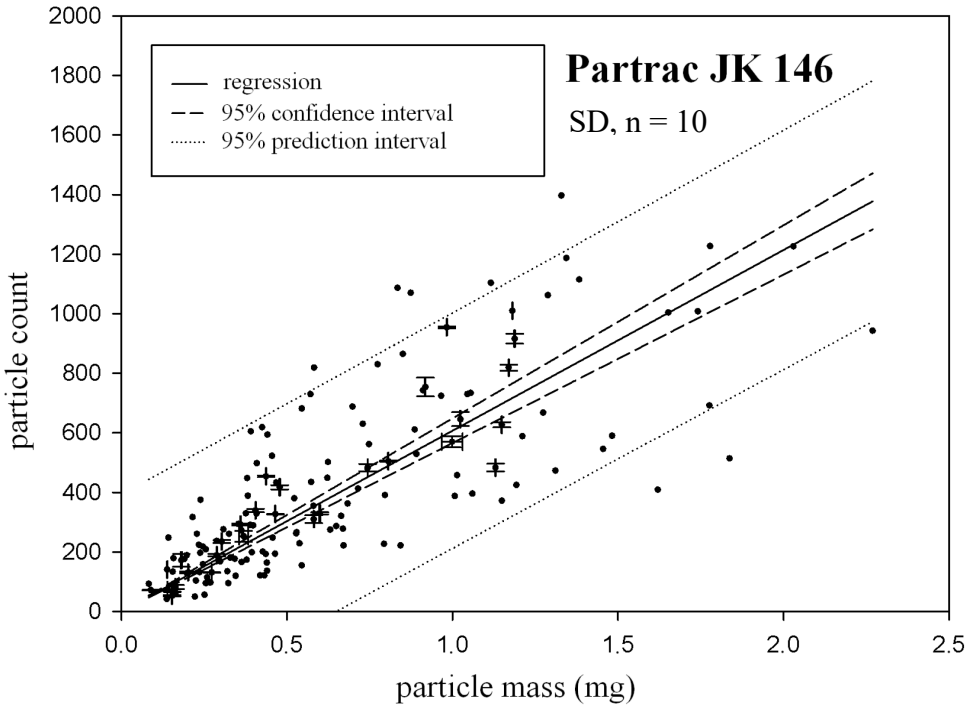


**Figure A3: Linear regression of particle mass and particle number, shown for luminophores used in the AM, HD and $HD_I$ experiment.**

**Table A2: Individual biomass (FM) of all polychaetes added to the HD experiment.** Net biomass change per mesocosm is shown as difference between experiment start and termination.

| mesocosm | initial biomass (g FM) | terminal biomass (g FM) | terminal biomass (g DM) | terminal biomass (g AFDM) | net biomass change (g FM) |
|---|---|---|---|---|---|
| HD1 | 3,95 | 3,97 | 0,18 | 0,012 | 0.02 |
| HD2 | 3,84 | 2,63 | 0,17 | 0,010 | - 1.21 |
| HD3 | 4,10 | 3,41 | 0,23 | 0,013 | - 0.69 |
| HD4 | 3,75 | 0,73 | 0,07 | 0,039 | - 3.02 |
| HD5 | 3,85 | 2,46 | 0,16 | 0,041 | - 1.39 |
| HD6 | 4,17 | 2,74 | 0,13 | 0,051 | - 1.43 |

**Table A3: Recovery rates (% of total amount of added tracers) for all particles types and mesocosms of the HD experiment.**

| mesocosm | luminophores | PE (150 µm) | PA (500 µm) |
|---|---|---|---|
| C1 | 97.94 | 86.85 | 99.85 |
| C2 | 104.93 | 100.78 | 100.57 |
| C3 | 88.24 | 99.04 | 99.85 |
| HD1 | 99.93 | 95.75 | 97.96 |
| HD2 | 93.55 | 97.58 | 99.98 |
| HD3 | 98.34 | 98.98 | 96.95 |
| HD4 | 98.32 | 98.43 | 93.25 |
| HD5 | 96.00 | 96.27 | 83.01 |
| HD6 | 85.17 | 100.29 | 93.13 |

**Table A4: Depth-dependent particle tracer concentrations determined for the first control mesocosm (C1) of the HD experiment.** Values are shown as percentages of total amount of added particle tracer type. Standard deviations (SD) depict analytical controls for luminophores and PE particles.

| **HD-C1** depth (cm) | c luminophores (%) | c PE (%) | c PA (%) | c PE (SD, n = 3) | c luminophores (SD, n = 3) |
|---|---|---|---|---|---|
| 0 - 1 | 96.73 | 86.56 | 95.44 | 7.97 | 5.65 |
| 1 - 2 | 0.08 | 0.01 | 0.30 | 0.04 | 0.01 |
| 2 - 3 | 0.05 | 0.00 | 0.19 | 0.02 | 0.00 |
| 3 - 4 | 0.07 | 0.06 | 0.37 | 0.01 | 0.01 |
| 4 - 5 | 0.15 | 0.00 | 0.38 | 0.06 | 0.00 |
| 5 - 6 | 0.16 | 0.00 | 0.34 | 0.09 | 0.00 |
| 6 - 7 | 0.06 | 0.03 | 0.37 | 0.01 | 0.03 |
| 7 - 8 | 0.14 | 0.08 | 0.33 | 0.07 | 0.07 |
| 8 - 9 | 0.06 | 0.01 | 0.28 | 0.02 | 0.01 |
| 9 - 10 | 0.06 | 0.01 | 0.32 | 0.02 | 0.01 |
| 10 - 11 | 0.05 | 0.02 | 0.29 | 0.00 | 0.01 |
| 11 - 12 | 0.09 | 0.01 | 0.33 | 0.03 | 0.02 |
| 12 - 13 | 0.07 | 0.01 | 0.26 | 0.03 | 0.01 |
| 13 - 14 | 0.07 | 0.02 | 0.18 | 0.03 | 0.02 |
| 14 - 15 | 0.06 | 0.01 | 0.27 | 0.02 | 0.02 |
| 15 - 16 | 0.05 | 0.04 | 0.20 | 0.00 | 0.04 |

**Table A5: Depth-dependent particle tracer concentrations determined for the second control mesocosm (C2) of the HD experiment.** Values are shown as percentages of total amount of added particle tracer type. Standard deviations (SD) depict analytical controls for luminophores and PE particles.

| **HD-C2** depth (cm) | c luminophores (%) | c PE (%) | c PA (%) | c PE (SD, n = 3) | c luminophores (SD, n = 3) |
|---|---|---|---|---|---|
| 0 - 1 | 104.27 | 100.53 | 95.24 | 4.61 | 2.45 |
| 1 - 2 | 0.05 | 0.07 | 0.41 | 0.01 | 0.00 |
| 2 - 3 | 0.04 | 0.03 | 0.37 | 0.00 | 0.03 |
| 3 - 4 | 0.05 | 0.00 | 0.40 | 0.00 | 0.00 |
| 4 - 5 | 0.04 | 0.06 | 0.41 | 0.00 | 0.04 |
| 5 - 6 | 0.04 | 0.02 | 0.27 | 0.00 | 0.02 |
| 6 - 7 | 0.04 | 0.00 | 0.35 | 0.01 | 0.00 |
| 7 - 8 | 0.05 | 0.04 | 0.35 | 0.02 | 0.04 |
| 8 - 9 | 0.04 | 0.00 | 0.34 | 0.00 | 0.00 |
| 9 - 10 | 0.04 | 0.02 | 0.38 | 0.00 | 0.01 |
| 10 - 11 | 0.04 | 0.01 | 0.38 | 0.00 | 0.01 |
| 11 - 12 | 0.06 | 0.00 | 0.31 | 0.00 | 0.00 |
| 12 - 13 | 0.04 | 0.00 | 0.41 | 0.00 | 0.00 |
| 13 - 14 | 0.04 | 0.00 | 0.31 | 0.00 | 0.00 |
| 14 - 15 | 0.04 | 0.00 | 0.31 | 0.00 | 0.00 |
| 15 - 16 | 0.03 | 0.00 | 0.33 | 0.00 | 0.00 |

**Table A6: Depth-dependent particle tracer concentrations determined for the third control mesocosm (C3) of the HD experiment.** Values are shown as percentages of total amount of added particle tracer type. Standard deviations (SD) depict analytical controls for luminophores and PE particles.

| **HD-C3** depth (cm) | c luminophores (%) | c PE (%) | c PA (%) | c PE (SD, n = 3) | c luminophores (SD, n = 3) |
|---|---|---|---|---|---|
| 0 - 1 | 86.77 | 98.49 | 95.83 | 2.52 | 3.62 |
| 1 - 2 | 0.06 | 0.09 | 0.23 | 0.04 | 0.03 |
| 2 - 3 | 0.07 | 0.09 | 0.27 | 0.02 | 0.03 |
| 3 - 4 | 0.08 | 0.07 | 0.27 | 0.03 | 0.02 |
| 4 - 5 | 0.09 | 0.03 | 0.24 | 0.05 | 0.01 |
| 5 - 6 | 0.09 | 0.03 | 0.22 | 0.08 | 0.03 |
| 6 - 7 | 0.13 | 0.03 | 0.24 | 0.06 | 0.01 |
| 7 - 8 | 0.06 | 0.00 | 0.27 | 0.02 | 0.00 |
| 8 - 9 | 0.08 | 0.02 | 0.24 | 0.04 | 0.02 |
| 9 - 10 | 0.05 | 0.02 | 0.31 | 0.01 | 0.01 |
| 10 - 11 | 0.24 | 0.02 | 0.38 | 0.21 | 0.02 |
| 11 - 12 | 0.06 | 0.05 | 0.29 | 0.01 | 0.03 |
| 12 - 13 | 0.06 | 0.01 | 0.22 | 0.04 | 0.01 |
| 13 - 14 | 0.22 | 0.06 | 0.17 | 0.17 | 0.01 |
| 14 - 15 | 0.11 | 0.00 | 0.33 | 0.11 | 0.00 |
| 15 - 16 | 0.05 | 0.02 | 0.34 | 0.00 | 0.02 |

**Table A7: Depth-dependent particle tracer concentrations determined for the HD1 mesocosm.** Values are shown as percentages of total amount of added particle tracer type. Standard deviations (SD) depict analytical controls for luminophores and PE particles.

| **HD1** depth (cm) | c luminophores (%) | c PE (%) | c PA (%) | c PE (SD, n = 3) | c luminophores (SD, n = 3) |
|---|---|---|---|---|---|
| 0 - 1 | 64.12 | 71.04 | 73.03 | 2.43 | 0.78 |
| 1 - 2 | 12.92 | 9.60 | 5.28 | 1.37 | 0.48 |
| 2 - 3 | 5.82 | 4.09 | 3.22 | 0.26 | 0.41 |
| 3 - 4 | 3.85 | 3.23 | 3.03 | 0.34 | 0.62 |
| 4 - 5 | 2.75 | 1.53 | 1.51 | 0.83 | 0.01 |
| 5 - 6 | 3.50 | 1.09 | 1.54 | 0.41 | 0.13 |
| 6 - 7 | 2.84 | 1.38 | 0.89 | 1.45 | 0.19 |
| 7 - 8 | 1.21 | 1.14 | 1.42 | 0.08 | 0.20 |
| 8 - 9 | 0.35 | 0.36 | 1.14 | 0.07 | 0.02 |
| 9 - 10 | 0.30 | 0.21 | 0.94 | 0.03 | 0.05 |
| 10 - 11 | 0.53 | 0.31 | 0.64 | 0.20 | 0.12 |
| 11 - 12 | 0.25 | 0.25 | 0.88 | 0.11 | 0.13 |
| 12 - 13 | 0.46 | 0.33 | 1.16 | 0.05 | 0.18 |
| 13 - 14 | 0.50 | 0.51 | 0.86 | 0.10 | 0.04 |
| 14 - 15 | 0.24 | 0.27 | 0.84 | 0.04 | 0.09 |
| 15 - 16 | 0.29 | 0.41 | 1.60 | 0.12 | 0.11 |

**Table A8: Depth-dependent particle tracer concentrations determined for the HD2 mesocosm.** Values are shown as percentages of total amount of added particle tracer type. Standard deviations (SD) depict analytical controls for luminophores and PE particles.

| **HD2** depth (cm) | c luminophores (%) | c PE (%) | c PA (%) | c PE (SD, n = 3) | c luminophores (SD, n = 3) |
|---|---|---|---|---|---|
| 0 - 1 | 82.30 | 86.45 | 78.76 | 4.01 | 2.47 |
| 1 - 2 | 4.33 | 4.24 | 4.41 | 0.86 | 0.29 |
| 2 - 3 | 1.65 | 1.79 | 2.28 | 0.24 | 0.08 |
| 3 - 4 | 1.15 | 0.98 | 1.45 | 0.17 | 0.04 |
| 4 - 5 | 1.04 | 1.11 | 1.59 | 0.14 | 0.06 |
| 5 - 6 | 0.35 | 0.49 | 2.85 | 0.08 | 0.08 |
| 6 - 7 | 0.14 | 0.08 | 1.17 | 0.05 | 0.07 |
| 7 - 8 | 0.15 | 0.13 | 1.15 | 0.02 | 0.09 |
| 8 - 9 | 0.22 | 0.23 | 1.13 | 0.02 | 0.05 |
| 9 - 10 | 0.46 | 0.44 | 0.94 | 0.00 | 0.08 |
| 10 - 11 | 0.35 | 0.41 | 1.16 | 0.04 | 0.08 |
| 11 - 12 | 0.23 | 0.23 | 0.69 | 0.07 | 0.04 |
| 12 - 13 | 0.35 | 0.32 | 0.63 | 0.06 | 0.05 |
| 13 - 14 | 0.60 | 0.51 | 0.54 | 0.25 | 0.08 |
| 14 - 15 | 0.18 | 0.13 | 0.90 | 0.06 | 0.05 |
| 15 - 16 | 0.04 | 0.01 | 0.35 | 0.00 | 0.01 |

**Table A9: Depth-dependent particle tracer concentrations determined for the HD3 mesocosm.** Values are shown as percentages of total amount of added particle tracer type. Standard deviations (SD) depict analytical controls for luminophores and PE particles.

| **HD3** depth (cm) | c luminophores (%) | c PE (%) | c PA (%) | c PE (SD, n = 3) | c luminophores (SD, n = 3) |
|---|---|---|---|---|---|
| 0 - 1 | 87.43 | 83.15 | 80.35 | 4.23 | 2.63 |
| 1 - 2 | 3.89 | 5.53 | 1.99 | 0.00 | 0.86 |
| 2 - 3 | 2.40 | 3.24 | 1.03 | 0.00 | 0.13 |
| 3 - 4 | 1.29 | 1.97 | 0.93 | 0.00 | 0.22 |
| 4 - 5 | 1.26 | 1.62 | 1.13 | 0.00 | 0.21 |
| 5 - 6 | 0.60 | 1.03 | 1.45 | 0.00 | 0.16 |
| 6 - 7 | 0.32 | 0.68 | 1.37 | 0.00 | 0.02 |
| 7 - 8 | 0.25 | 0.52 | 1.23 | 0.00 | 0.17 |
| 8 - 9 | 0.19 | 0.22 | 1.23 | 0.00 | 0.06 |
| 9 - 10 | 0.21 | 0.19 | 1.17 | 0.00 | 0.01 |
| 10 - 11 | 0.08 | 0.13 | 0.85 | 0.00 | 0.05 |
| 11 - 12 | 0.10 | 0.09 | 0.92 | 0.00 | 0.00 |
| 12 - 13 | 0.12 | 0.12 | 1.38 | 0.00 | 0.03 |
| 13 - 14 | 0.06 | 0.15 | 1.14 | 0.00 | 0.02 |
| 14 - 15 | 0.13 | 0.33 | 0.80 | 0.00 | 0.00 |
| 15 - 16 | | | | | |

**Table A10: Depth-dependent particle tracer concentrations determined for the HD4 mesocosm.** Values are shown as percentages of total amount of added particle tracer type. Standard deviations (SD) depict analytical controls for luminophores and PE particles.

| **HD4** depth (cm) | c luminophores (%) | c PE (%) | c PA (%) | c PE (SD, n = 3) | c luminophores (SD, n = 3) |
|---|---|---|---|---|---|
| 0 - 1 | 72.67 | 72.26 | 72.16 | 2.63 | 2.84 |
| 1 - 2 | 7.49 | 8.19 | 4.98 | 0.00 | 0.00 |
| 2 - 3 | 5.59 | 4.90 | 2.41 | 0.00 | 0.00 |
| 3 - 4 | 4.26 | 4.39 | 1.75 | 0.00 | 0.00 |
| 4 - 5 | 3.50 | 3.71 | 2.04 | 0.00 | 0.00 |
| 5 - 6 | 1.74 | 2.17 | 2.07 | 0.00 | 0.00 |
| 6 - 7 | 1.16 | 1.50 | 1.24 | 0.00 | 0.00 |
| 7 - 8 | 0.67 | 0.79 | 1.19 | 0.00 | 0.00 |
| 8 - 9 | 0.55 | 0.32 | 1.33 | 0.00 | 0.00 |
| 9 - 10 | 0.10 | 0.08 | 0.72 | 0.00 | 0.00 |
| 10 - 11 | 0.09 | 0.03 | 0.69 | 0.00 | 0.00 |
| 11 - 12 | 0.05 | 0.02 | 0.65 | 0.00 | 0.00 |
| 12 - 13 | 0.13 | 0.02 | 0.62 | 0.00 | 0.00 |
| 13 - 14 | 0.06 | 0.02 | 0.67 | 0.00 | 0.00 |
| 14 - 15 | 0.08 | 0.03 | 0.39 | 0.00 | 0.00 |
| 15 - 16 | 0.18 | 0.01 | 0.36 | 0.00 | 0.00 |

**Table A11: Depth-dependent particle tracer concentrations determined for the HD5 mesocosm.** Values are shown as percentages of total amount of added particle tracer type. Standard deviations (SD) depict analytical controls for luminophores and PE particles.

| **HD5** depth (cm) | c luminophores (%) | c PE (%) | c PA (%) | c PE (SD, n = 3) | c luminophores (SD, n = 3) |
|---|---|---|---|---|---|
| 0 - 1 | 64.77 | 63.02 | 54.08 | 1.87 | 2.75 |
| 1 - 2 | 9.48 | 9.44 | 6.72 | 0.00 | 0.00 |
| 2 - 3 | 4.58 | 4.55 | 3.49 | 0.00 | 0.00 |
| 3 - 4 | 4.03 | 4.05 | 3.22 | 0.00 | 0.00 |
| 4 - 5 | 3.99 | 4.10 | 2.45 | 0.00 | 0.00 |
| 5 - 6 | 6.02 | 6.01 | 5.44 | 0.00 | 0.00 |
| 6 - 7 | 0.81 | 0.83 | 1.21 | 0.00 | 0.00 |
| 7 - 8 | 0.50 | 0.46 | 1.08 | 0.00 | 0.00 |
| 8 - 9 | 0.42 | 0.85 | 0.83 | 0.00 | 0.00 |
| 9 - 10 | 0.57 | 1.09 | 1.31 | 0.00 | 0.00 |
| 10 - 11 | 0.56 | 0.90 | 0.62 | 0.00 | 0.00 |
| 11 - 12 | 0.10 | 0.39 | 0.70 | 0.00 | 0.00 |
| 12 - 13 | 0.04 | 0.16 | 0.49 | 0.00 | 0.00 |
| 13 - 14 | 0.04 | 0.07 | 0.63 | 0.00 | 0.00 |
| 14 - 15 | 0.09 | 0.36 | 0.75 | 0.00 | 0.00 |
| 15 - 16 | 64.77 | 63.02 | 54.08 | 1.87 | 2.75 |

**Table A12: Depth-dependent particle tracer concentrations determined for the HD6 mesocosm.** Values are shown as percentages of total amount of added particle tracer type. Standard deviations (SD) depict analytical controls for luminophores and PE particles.

| **HD6** depth (cm) | c luminophores (%) | c PE (%) | c PA (%) | c PE (SD, n = 3) | c luminophores (SD, n = 3) |
|---|---|---|---|---|---|
| 0 - 1 | 77.38 | 90.13 | 84.65 | 6.03 | 1.43 |
| 1 - 2 | 3.88 | 6.08 | 2.45 | 0.00 | 0.00 |
| 2 - 3 | 1.29 | 2.07 | 1.35 | 0.00 | 0.00 |
| 3 - 4 | 0.46 | 0.95 | 0.87 | 0.00 | 0.00 |
| 4 - 5 | 0.46 | 0.49 | 0.47 | 0.00 | 0.00 |
| 5 - 6 | 0.15 | 0.38 | 0.34 | 0.00 | 0.00 |
| 6 - 7 | 0.06 | 0.05 | 0.29 | 0.00 | 0.00 |
| 7 - 8 | 0.05 | 0.01 | 0.23 | 0.00 | 0.00 |
| 8 - 9 | 0.05 | 0.00 | 0.26 | 0.00 | 0.00 |
| 9 - 10 | 0.05 | 0.00 | 0.22 | 0.00 | 0.00 |
| 10 - 11 | 0.05 | 0.00 | 0.31 | 0.00 | 0.00 |
| 11 - 12 | 0.06 | 0.00 | 0.14 | 0.00 | 0.00 |
| 12 - 13 | 0.05 | 0.00 | 0.24 | 0.00 | 0.00 |
| 13 - 14 | 0.07 | 0.01 | 0.25 | 0.00 | 0.00 |
| 14 - 15 | 0.40 | 0.01 | 0.31 | 0.00 | 0.00 |
| 15 - 16 | 0.71 | 0.13 | 0.76 | 0.00 | 0.00 |

**Table A13: PERMANOVA results comparing particle tracer depth distribution using the factors particle type (luminophores, PE, PA), treatment (controls, $F^-$, $F^+$) and sediment depth.** Significant effects ($p < 0.05$) are indicated by asterisks.

| Source | df | SS | MS | Pseudo-F | P(perm) | Unique Perms |
|---|---|---|---|---|---|---|
| Particle type | 2 | 58 088 | 29 044 | 79.929 | 0.001* | 997 |
| Treatment | 2 | 100 530 | 50 266 | 138.33 | 0.001* | 998 |
| Depth | 15 | 226 240 | 15 083 | 41.508 | 0.001* | 998 |
| Particle type × treatment | 4 | 18 579 | 4 644.7 | 12.782 | 0.001* | 999 |
| Particle type × Depth | 30 | 16 338 | 544.6 | 1.4987 | 0.006* | 998 |
| Treatment × Depth | 30 | 49 647 | 1 654.9 | 4.5543 | 0.001* | 999 |
| Particle type × Treatment × Depth | 60 | 17 025 | 283.75 | 0.78087 | 0.968* | 998 |
| Residuals | 265 | 96 294 | 363.37 | | | |

**Table A14: Recovery rates (% of total amount of added tracers) for all particles types and mesocosms of the AM experiment.**

| mesocosm | luminophores | PS (1000 µm) | PA (500 µm) |
|---|---|---|---|
| C1 | 58.17 | 98,47 | 94,91 |
| C2 | 94.21 | 98,83 | 99,72 |
| C3 | 98.33 | 97,89 | 101,36 |
| AM1 | 86,02 | 99,18 | 92,44 |
| AM2 | 69.74 | 98,02 | 96,38 |
| AM3 | 64.23 | 98,99 | 91,08 |
| AM4 | 87.47 | 99,31 | 96,92 |
| AM5 | 105.41 | 103,65 | 97,99 |
| AM6 | 86.41 | 99,11 | 95,64 |
| AM7 | 101.86 | 98,51 | 93,45 |
| AM8 | 85.88 | 101,11 | 92,39 |

**Table A15: Depth-dependent particle tracer concentrations determined for first control mesocosm (C1) of the AM experiment.** Values are shown as percentages of total amount of added particle tracer type. Standard deviations (SD) depict analytical controls for luminophores.

| **AM-C1** depth (cm) | c PS (%) | c PA (%) | c luminophores (%) | c luminophores (SD, n = 3) |
|---|---|---|---|---|
| 0 - 2 | 98.47 | 94.86 | 53.16 | 1.54 |
| 2 - 4 | 0.00 | 0.01 | 1.12 | 0.44 |
| 4 - 6 | 0.00 | 0.00 | 0.55 | 0.11 |
| 6 - 8 | 0.00 | 0.00 | 0.52 | 0.20 |
| 8 - 10 | 0.00 | 0.00 | 0.49 | 0.12 |
| 10 - 12 | 0.00 | 0.00 | 0.75 | 0.21 |
| 12 - 14 | 0.00 | 0.00 | 0.59 | 0.23 |
| 14 - 16 | 0.00 | 0.00 | 0.33 | 0.08 |
| 16 - 18 | 0.00 | 0.00 | 0.34 | 0.05 |
| 18 - 20 | 0.00 | 0.04 | 0.32 | 0.34 |

**Table A16: Depth-dependent particle tracer concentrations determined for the second control mesocosm (C2) of the AM experiment.** Values are shown as percentages of total amount of added particle tracer type. Standard deviations (SD) depict analytical controls for luminophores.

| **AM-C2** depth (cm) | c PS (%) | c PA (%) | c luminophores (%) | c luminophores (SD, n = 3) |
|---|---|---|---|---|
| 0 - 2 | 98.83 | 99.68 | 92.34 | 7.34 |
| 2 - 4 | 0.01 | 0.04 | 0.56 | 0.13 |
| 4 - 6 | 0.00 | 0.00 | 0.27 | 0.08 |
| 6 - 8 | 0.00 | 0.00 | 0.16 | 0.07 |
| 8 - 10 | 0.00 | 0.00 | 0.25 | 0.05 |
| 10 - 12 | 0.00 | 0.00 | 0.23 | 0.01 |
| 12 - 14 | 0.00 | 0.00 | 0.18 | 0.03 |
| 14 - 16 | 0.00 | 0.00 | 0.11 | 0.10 |
| 16 - 18 | 0.00 | 0.00 | 0.05 | 0.05 |
| 18 - 20 | 0.00 | 0.00 | 0.06 | 0.07 |

**Table A17: Depth-dependent particle tracer concentrations determined for the third control mesocosm (C3) of the AM experiment.** Values are shown as percentages of total amount of added particle tracer type. Standard deviations (SD) depict analytical controls for luminophores.

| **AM-C3** depth (cm) | c PS (%) | c PA (%) | c luminophores (%) | c luminophores (SD, n = 3) |
|---|---|---|---|---|
| 0 - 2 | 97.89 | 101.36 | 96.62 | 4.88 |
| 2 - 4 | 0.00 | 0.00 | 0.30 | 0.07 |
| 4 - 6 | 0.00 | 0.00 | 0.20 | 0.04 |
| 6 - 8 | 0.00 | 0.00 | 0.19 | 0.05 |
| 8 - 10 | 0.00 | 0.00 | 0.14 | 0.05 |
| 10 - 12 | 0.00 | 0.00 | 0.13 | 0.07 |
| 12 - 14 | 0.00 | 0.00 | 0.25 | 0.05 |
| 14 - 16 | 0.00 | 0.00 | 0.30 | 0.10 |
| 16 - 18 | 0.00 | 0.00 | 0.06 | 0.08 |
| 18 - 20 | 0.00 | 0.00 | 0.16 | 0.17 |

**Table A18: Depth-dependent particle tracer concentrations determined for the AM1 mesocosm.** Values are shown as percentages of total amount of added particle tracer type. Standard deviations (SD) depict analytical controls for luminophores and PE particles.

| **AM1** depth (cm) | c PS (%) | c PA (%) | c luminophores (%) | c luminophores (SD, n = 3) |
|---|---|---|---|---|
| 0 - 2 | 43.85 | 39.05 | 38.87 | 43.85 |
| 2 - 4 | 25.78 | 19.49 | 24.35 | 25.78 |
| 4 - 6 | 7.08 | 7.28 | 10.53 | 7.08 |
| 6 - 8 | 6.93 | 5.07 | 6.54 | 6.93 |
| 8 - 10 | 14.25 | 13.67 | 3.90 | 14.25 |
| 10 - 12 | 1.23 | 6.15 | 1.20 | 1.23 |
| 12 - 14 | 0.06 | 1.72 | 0.51 | 0.06 |
| 14 - 16 | 0.00 | 0.00 | 0.11 | 0.00 |
| 16 - 18 | | | | |
| 18 - 20 | | | | |

**Table A19: Depth-dependent particle tracer concentrations determined for the AM2 mesocosm.** Values are shown as percentages of total amount of added particle tracer type. Standard deviations (SD) depict analytical controls for luminophores and PE particles.

| **AM2** depth (cm) | c PS (%) | c PA (%) | c luminophores (%) | c luminophores (SD, n = 3) |
|---|---|---|---|---|
| 0 - 2 | 55.46 | 48.15 | 42.81 | 2.65 |
| 2 - 4 | 30.08 | 29.87 | 16.02 | 1.47 |
| 4 - 6 | 7.69 | 12.22 | 3.38 | 1.25 |
| 6 - 8 | 3.47 | 4.31 | 3.50 | 0.52 |
| 8 - 10 | 0.00 | 1.30 | 1.48 | 0.16 |
| 10 - 12 | 1.23 | 0.40 | 0.72 | 0.19 |
| 12 - 14 | 0.06 | 0.05 | 0.36 | 0.18 |
| 14 - 16 | 0.04 | 0.06 | 0.67 | 0.15 |
| 16 - 18 | 0.00 | 0.01 | 0.39 | 0.05 |
| 18 - 20 | 0.00 | 0.00 | 0.41 | 0.02 |

**Table A20: Depth-dependent particle tracer concentrations determined for the AM3 mesocosm.** Values are shown as percentages of total amount of added particle tracer type. Standard deviations (SD) depict analytical controls for luminophores and PE particles.

| **AM3** depth (cm) | c PS (%) | c PA (%) | c luminophores (%) | c luminophores (SD, n = 3) |
|---|---|---|---|---|
| 0 - 2 | 27.55 | 23.47 | 14.00 | 1.94 |
| 2 - 4 | 42.29 | 38.71 | 21.58 | 4.06 |
| 4 - 6 | 15.71 | 18.61 | 16.72 | 1.46 |
| 6 - 8 | 2.58 | 5.21 | 4.06 | 0.62 |
| 8 - 10 | 2.27 | 2.00 | 2.49 | 0.40 |
| 10 - 12 | 2.06 | 1.00 | 1.78 | 0.15 |
| 12 - 14 | 1.54 | 0.56 | 1.18 | 0.03 |
| 14 - 16 | 2.29 | 0.77 | 1.36 | 0.32 |
| 16 - 18 | 1.81 | 0.31 | 0.51 | 0.04 |
| 18 - 20 | 0.89 | 0.44 | 0.55 | 0.23 |

**Table A21: Depth-dependent particle tracer concentrations determined for the AM4 mesocosm.** Values are shown as percentages of total amount of added particle tracer type. Standard deviations (SD) depict analytical controls for luminophores and PE particles.

| **AM4** depth (cm) | c PS (%) | c PA (%) | c luminophores (%) | c luminophores (SD, n = 3) |
|---|---|---|---|---|
| 0 - 2 | 0.03 | 0.00 | 4.72 | 0.56 |
| 2 - 4 | 0.01 | 0.08 | 6.61 | 0.40 |
| 4 - 6 | 0.04 | 0.13 | 8.14 | 0.56 |
| 6 - 8 | 0.29 | 0.44 | 6.98 | 1.16 |
| 8 - 10 | 27.30 | 8.97 | 6.98 | 0.39 |
| 10 - 12 | 52.90 | 57.83 | 31.92 | 1.75 |
| 12 - 14 | 18.51 | 28.07 | 20.34 | 2.10 |
| 14 - 16 | 0.22 | 1.37 | 1.65 | 0.60 |
| 16 - 18 | 0.01 | 0.02 | 0.13 | 0.16 |
| 18 - 20 | | | | |

**Table A22: Depth-dependent particle tracer concentrations determined for the AM5 mesocosm.** Values are shown as percentages of total amount of added particle tracer type. Standard deviations (SD) depict analytical controls for luminophores and PE particles.

| **AM5** depth (cm) | c PS (%) | c PA (%) | c luminophores (%) | c luminophores (SD, n = 3) |
|---|---|---|---|---|
| 0 - 2 | 20.73 | 28.04 | 24.95 | 4.51 |
| 2 - 4 | 50.10 | 36.13 | 36.45 | 2.32 |
| 4 - 6 | 17.15 | 23.03 | 23.09 | 0.61 |
| 6 - 8 | 9.47 | 5.48 | 11.06 | 0.62 |
| 8 - 10 | 2.27 | 1.86 | 3.81 | 0.41 |
| 10 - 12 | 1.68 | 1.62 | 2.28 | 0.20 |
| 12 - 14 | 1.47 | 1.15 | 1.53 | 0.17 |
| 14 - 16 | 0.70 | 0.35 | 1.02 | 0.24 |
| 16 - 18 | 0.07 | 0.21 | 0.77 | 0.21 |
| 18 - 20 | 0.00 | 0.12 | 0.46 | 0.07 |

**Table A23: Depth-dependent particle tracer concentrations determined for the AM6 mesocosm.** Values are shown as percentages of total amount of added particle tracer type. Standard deviations (SD) depict analytical controls for luminophores and PE particles.

| **AM6** depth (cm) | c PS (%) | c PA (%) | c luminophores (%) | c luminophores (SD, n = 3) |
|---|---|---|---|---|
| 0 - 2 | 0.04 | 0.11 | 7.32 | 0.46 |
| 2 - 4 | 0.01 | 0.02 | 4.94 | 0.22 |
| 4 - 6 | 0.02 | 0.09 | 1.97 | 0.56 |
| 6 - 8 | 6.31 | 1.38 | 4.64 | 0.69 |
| 8 - 10 | 22.76 | 17.88 | 7.92 | 1.29 |
| 10 - 12 | 28.91 | 31.84 | 30.09 | 1.67 |
| 12 - 14 | 27.49 | 27.18 | 21.07 | 0.54 |
| 14 - 16 | 11.37 | 15.38 | 6.32 | 0.57 |
| 16 - 18 | 2.22 | 1.51 | 1.73 | 0.25 |
| 18 - 20 | 0.00 | 0.24 | 0.41 | 0.29 |

**Table A24: Depth-dependent particle tracer concentrations determined for the AM7 mesocosm.** Values are shown as percentages of total amount of added particle tracer type. Standard deviations (SD) depict analytical controls for luminophores and PE particles.

| **AM7** depth (cm) | c PS (%) | c PA (%) | c luminophores (%) | c luminophores (SD, n = 3) |
|---|---|---|---|---|
| 0 - 2 | 0.15 | 0.05 | 4.77 | 1.16 |
| 2 - 4 | 0.07 | 0.05 | 2.50 | 0.31 |
| 4 - 6 | 0.18 | 0.04 | 2.16 | 0.56 |
| 6 - 8 | 11.37 | 11.93 | 8.74 | 1.86 |
| 8 - 10 | 45.02 | 45.31 | 36.03 | 6.50 |
| 10 - 12 | 29.99 | 27.82 | 30.98 | 5.16 |
| 12 - 14 | 8.49 | 5.79 | 7.45 | 1.01 |
| 14 - 16 | 1.73 | 0.71 | 4.70 | 0.68 |
| 16 - 18 | 0.82 | 1.09 | 2.58 | 0.30 |
| 18 - 20 | 0.70 | 0.65 | 1.94 | 0.63 |

**Table A25: Depth-dependent particle tracer concentrations determined for the AM8 mesocosm.** Values are shown as percentages of total amount of added particle tracer type. Standard deviations (SD) depict analytical controls for luminophores and PE particles.

| **AM8** depth (cm) | c PS (%) | c PA (%) | c luminophores (%) | c luminophores (SD, n = 3) |
|---|---|---|---|---|
| 0 - 2 | 0.06 | 0.24 | 6.56 | 0.51 |
| 2 - 4 | 0.00 | 0.26 | 5.62 | 0.69 |
| 4 - 6 | 0.02 | 0.28 | 4.61 | 0.57 |
| 6 - 8 | 1.85 | 0.57 | 4.76 | 0.17 |
| 8 - 10 | 16.70 | 6.93 | 7.61 | 0.61 |
| 10 - 12 | 59.76 | 51.88 | 35.77 | 2.23 |
| 12 - 14 | 14.94 | 22.45 | 15.17 | 1.52 |
| 14 - 16 | 5.02 | 8.82 | 3.35 | 0.23 |
| 16 - 18 | 2.36 | 0.66 | 1.55 | 0.05 |
| 18 - 20 | 0.41 | 0.30 | 0.88 | 0.09 |